bioRxiv preprint doi: https://doi.org/10.1101/050203; this version posted October 5, 2017. The copyright holder for this preprint (which was not certified by peer review) is the author/funder, who has granted bioRxiv a license to display the preprint in perpetuity. It is made available under aCC-BY-NC-ND 4.0 International license.

1 2 # The rate and potential relevance of new mutations in a colonizing plant lineage

3 Moises Exposito-Alonso[1,2†], Claude Becker[1†], Verena J. Schuenemann[3,4], Ella Reiter[3], Claudia Setzer[5],
4 Radka Slovak[5], Benjamin Brachi[6§], Jörg Hagmann[1§], Dominik G. Grimm[1§], Jiahui Chen[6,7], Wolfgang
5 Busch[5§], Joy Bergelson[6], Rob W. Ness[8], Johannes Krause[3,4,9], Hernán A. Burbano[2,*], Detlef Weigel[1,*]

6 [1]Department of Molecular Biology, Max Planck Institute for Developmental Biology, 72076 Tübingen,
7 Germany

8 [2]Research Group for Ancient Genomics and Evolution, Max Planck Institute for Developmental Biology,
9 72076 Tübingen, Germany

10 [3]Institute of Archaeological Sciences, University of Tübingen, 72070 Tübingen, Germany

11 [4]Senckenberg Center for Human Evolution and Paleoenvironment, University of Tübingen, 72070
12 Tübingen, Germany

13 [5]Gregor Mendel Institute, Austrian Academy of Sciences, 1030 Vienna, Austria

14 [6]Department of Ecology and Evolution, University of Chicago, Chicago, Illinois 60637, USA

15 [7]Institute of Tibet Plateau Research, Chinese Academy of Sciences, Beijing 100101, China

16 [8]Department of Biology, University of Toronto Mississauga, Mississauga, Ontario L5L IC6, Canada.

17 [9]Max Planck Institute for the Science of Human History, 07743 Jena, Germany

18 [†]Co-first authors

19 [§]Current addresses: INRA, UMR 1202 Biodiversité Gènes & Communautés, 33610 CESTAS, France
20 (B.B.); Computomics, 72072 Tübingen, Germany (J.H.); Department of Biosystems Science and
21 Engineering, ETH Zurich, 4058 Basel, Switzerland (D.G.G); Salk Institute for Biological Studies, La Jolla,
22 CA 92037, USA (W.B.).

23 *Correspondence to: hernan.burbano@tuebingen.mpg.de, weigel@weigelworld.org

24 Running title: *de novo* mutation rate in *A. thaliana*

25 Keywords: colonization, mutation, selection, herbarium genomes, aDNA, phylogenomics, population
26 genomics, association mapping, *Arabidopsis thaliana*

bioRxiv preprint doi: https://doi.org/10.1101/050203; this version posted October 5, 2017. The copyright holder for this preprint (which was not certified by peer review) is the author/funder, who has granted bioRxiv a license to display the preprint in perpetuity. It is made available under aCC-BY-NC-ND 4.0 International license.

27 **ABSTRACT**

28 **By following the evolution of populations that are initially genetically homogeneous, much**
29 **can be learned about core biological principles. For example, it allows for detailed studies**
30 **of the rate of emergence of *de novo* mutations and their change in frequency due to drift**
31 **and selection. Unfortunately, in multicellular organisms with generation times of months**
32 **or years, it is difficult to set up and carry out such experiments over many generations. An**
33 **alternative is provided by "natural evolution experiments" that started from colonizations**
34 **or invasions of new habitats by selfing lineages. With limited or missing gene flow from**
35 **other lineages, new mutations and their effects can be easily detected. North America has**
36 **been colonized in historic times by the plant *Arabidopsis thaliana*, and although multiple**
37 **intercrossing lineages are found today, many of the individuals belong to a single lineage,**
38 **HPG1. To determine in this lineage the rate of substitutions – the subset of mutations that**
39 **survived natural selection and drift –, we have sequenced genomes from plants collected**
40 **between 1863 and 2006. We identified 73 modern and 27 herbarium specimens that**
41 **belonged to HPG1. Using the estimated substitution rate, we infer that the last common**
42 **HPG1 ancestor lived in the early 17th century, when it was most likely introduced by**
43 **chance from Europe. Mutations in coding regions are depleted in frequency compared to**
44 **those in other portions of the genome, consistent with purifying selection. Nevertheless, a**
45 **handful of mutations is found at high frequency in present-day populations. We link these**
46 **to detectable phenotypic variance in traits of known ecological importance, life history and**
47 **growth, which could reflect their adaptive value. Our work showcases how, by applying**
48 **genomics methods to a combination of modern and historic samples from colonizing**
49 **lineages, we can directly study new mutations and their potential evolutionary relevance.**

bioRxiv preprint doi: https://doi.org/10.1101/050203; this version posted October 5, 2017. The copyright holder for this preprint (which was not certified by peer review) is the author/funder, who has granted bioRxiv a license to display the preprint in perpetuity. It is made available under aCC-BY-NC-ND 4.0 International license.

50 ## SUMMARY

51 A consequence of an increasingly interconnected world is the spread of species outside their native
52 range — a phenomenon with potentially dramatic impacts on ecosystem services. Using population
53 genomics, we can robustly infer dynamics of colonization and successful population establishment. We
54 have compared hundred genomes of a single *Arabidopsis thaliana* lineage in North America, including
55 genomes of contemporary individuals as well as 19th century herbarium specimens. These differ by an
56 average of about 200 mutations, and calculation of the nuclear evolutionary rate enabled the dating of
57 the initial colonization event to about 400 years ago. We also found mutations associated with
58 differences in traits among modern individuals, suggesting a role of new mutations in recent adaptive
59 evolution.

60 ## INTRODUCTION

61 Colonizing or invasive populations sampled through time (1,2) constitute "natural experiments" where it
62 is possible to study evolutionary processes in action (3). Colonizations, which are dramatically increasing
63 in number (4,5), sometimes are characterized by strong bottlenecks and genetic isolation (6,7), and thus
64 greatly facilitate the observation of new mutations and potentially their effects under natural population
65 dynamics and selection (8). Colonizations thus offer a complementary approach to other studies of new
66 mutations, which often minimize natural selection, for example in laboratory mutation accumulation
67 experiments (9) and parent-offspring comparisons (10). The study of colonizations is also
68 complementary to the investigation of genetic divergence over long time scales, e.g., between distant
69 species (11), where the results are largely independent of short-term demographic fluctuations. There is

bioRxiv preprint doi: https://doi.org/10.1101/050203; this version posted October 5, 2017. The copyright holder for this preprint (which was not certified by peer review) is the author/funder, who has granted bioRxiv a license to display the preprint in perpetuity. It is made available under aCC-BY-NC-ND 4.0 International license.

70 broad interest in understanding how genetic diversity is generated (12),(12)and how new mutations can
71 provide a path for rapid adaptive evolution (13–15). Additionally, accurate evolutionary rates permit
72 dating historic population splits, which is fundamental to the study of population history (16).

73 The analysis of colonizing populations can also contribute to resolving the "genetic paradox of
74 invasion" (17). This paradox comes from the observation that colonizing populations can be surprisingly
75 successful and spread very widely even when strongly bottlenecked, suggesting some level of adaptation
76 to new environments that goes beyond the exploitation of unoccupied ecological niches (17). Much of
77 the work in plant ecology and evolution has focused on evidence that populations can rapidly adapt from
78 standing variation (18). In invasive lineages, initial standing variation may originate from incomplete
79 bottlenecks, multiple introductions, or admixture with local relatives (19). Much less work has been
80 done with respect to the role of *de novo* mutations as a solution to the genetic paradox of invasion,
81 although this has been proposed as an alternative explanation for rapid adaptation by colonizing lineages
82 (3,17,20).

83 The self-fertilizing plant *Arabidopsis thaliana* is native to Africa and Eurasia (21,22) but has
84 recently colonized N. America, where it likely experienced a strong founder effect (23). At nearly half of
85 N. American sites sampled during the 1990s and early 2000s, more than 80% of plants belong to a single
86 haplogroup, HPG1, as inferred from genotyping with 149 intermediate-frequency markers evenly spread
87 throughout the genome (23). The HPG1 lineage has been reported from many sites along the East Coast
88 and in the Midwest as well as at a few sites in the West (23) (Figure 1, Table S1). The great ubiquity of
89 HPG1 in comparison to any other haplogroup could be due to either some adaptive advantage, or, more
90 parsimoniously, be the result of HPG1 being derived from one of the first arrivals of *A. thaliana* in the
91 continent.

bioRxiv preprint doi: https://doi.org/10.1101/050203; this version posted October 5, 2017. The copyright holder for this preprint (which was not certified by peer review) is the author/funder, who has granted bioRxiv a license to display the preprint in perpetuity. It is made available under aCC-BY-NC-ND 4.0 International license.

92 Here, we focus on 100 HPG1 individuals that do not show any evidence of outcrossing with
93 other lineages. We combine genomes from herbarium specimens and live individuals, collectively
94 covering the time span from 1863 to 2006, to infer mutation rates, to date the birth of the HPG1
95 lineage, and to investigate the evolutionary forces that shape genetic diversity. Our analyses of this
96 lineage serves as a model for future studies of similar colonizing or otherwise recently bottlenecked
97 plant populations, in order to better understand how diversity is generated and to which extent it
98 contributes to adaptation in nature.

99 **RESULTS AND DISCUSSION**

100 **Historic and modern genomes**

101 In a self-fertilizing species, a single individual can give rise to an entire lineage of millions of offspring,
102 which then diversify through new mutations and eventually intra-lineage recombination. If
103 self-fertilization is much more common than outcrossing, the founder is likely to have been homozygous
104 throughout almost the entire genome. Because it is so wide spread, HPG1 presents an opportunity to
105 sample many natural populations that have been potentially derived from a common, very recent
106 ancestor with such characteristics. In the best possible case, this would allow for new mutations to be
107 directly observed through time. To test these assumptions and to better understand the evolution of
108 HPG1, we sequenced two different groups of plants. The first group were live descendants of 87 plants
109 that had been collected between 1993 and 2006 (Fig. 1; Table S1), and which had been identified as likely
110 members of the HPG1 lineage with 149 genome-wide markers spaced at roughly 1-Mb-intervals (23).
111 We aimed for broad geographic representation, with at least two accessions per collection site, where
112 available. The second group comprised 35 herbarium specimens, collected between 1863 and 1993, for
113 which we had no a priori information whether they may or may not belong to the HPG1 lineage, but

bioRxiv preprint doi: https://doi.org/10.1101/050203; this version posted October 5, 2017. The copyright holder for this preprint (which was not certified by peer review) is the author/funder, who has granted bioRxiv a license to display the preprint in perpetuity. It is made available under aCC-BY-NC-ND 4.0 International license.

114 which were selected from the herbarium records to cover the full historical geographic range and
115 overlap with modern samples when possible (Fig. 1).

116 The DNA from the herbarium specimens showed biochemical features typical of ancient DNA
117 (aDNA) from plants, which we have previously described in detail (24). Such DNA damage included a
118 median fragment length of 60 bp, an excess of C-to-T substitutions of about 2.5% at the first base of
119 sequencing reads and a 1.5 to 1.8 fold enrichment of purines at DNA breakpoints (Fig. S1**,**
120 Supplementary Text 2**).** To remove aDNA associated damage and produce high-quality genomes,
121 chemically-repaired libraries (see Methods) were later sequenced. These reads were mapped against an
122 HPG1 pseudo-reference genome (25), focusing on single nucleotide polymorphisms (SNPs) because the
123 short sequence reads of herbarium samples preclude accurate calling of structural variants. Genome
124 sequences were of high quality, with herbarium samples covering 96.8–107.2 Mb of the 119 Mb
125 reference, and modern samples covering 108.0–108.3 Mb (Table S1).

126 Genetic diversity of HPG1 and delineation from other lineages

127 We visualized the relationships between the sequenced historic and modern plants building a neighbor
128 joining tree of all 123 samples and confirmed that the majority fell within a almost-identical clade, the
129 HPG1 (Fig. 2A) (23). Because any degree of introgression from other non-HPG1 lineages would
130 confound the discovery of new mutations downstream, we removed all divergent samples and built a
131 neighbour joining tree (n=103 samples), which revealed that the HPG1 samples were very similar to
132 each other, with very little within-population structure (Fig. 2B). A parsimony network was used to
133 detect recombinant genomes within this HPG1 clade (Fig. 2C), which led us to remove three potential
134 intra-lineage recombinants. Repeating the parsimony network cleared all previously inferred reticulations
135 due to recombinations (Fig. 2D). After such stringent filtering, we kept 27 of the 35 herbarium samples,

bioRxiv preprint doi: https://doi.org/10.1101/050203; this version posted October 5, 2017. The copyright holder for this preprint (which was not certified by peer review) is the author/funder, who has granted bioRxiv a license to display the preprint in perpetuity. It is made available under aCC-BY-NC-ND 4.0 International license.

136 and 73 of the 87 modern samples (Table S1). These constitute a set of non-admixed, non-recombined
137 and quasi-identical HPG1 individuals.

138 Pairs of HPG1 herbarium genomes differed by 28-207 SNPs genome-wide, pairs of HPG1
139 modern genomes by 2-259 SNPs, and pairs of historic-modern HPG1 genomes by 56-244 SNPs. That is,
140 whole-genome identity was at least 99.9997% in any of pair-wise comparison. Of the approximately five
141 to six thousand segregating SNPs in the HPG1 population, the vast majority, about 95% (Supplementary
142 Text 3), have not been reported outside of this lineage (21). Importantly, the density of SNPs along the
143 genome was low and evenly distributed (typically fewer than 20 SNPs / 100 kb) with no peaks of much
144 higher frequency, which makes us confident that chunks of introgressions from other lineages do not
145 exist in this putatively pure HPG1 set (Fig. 4). As a reminder, random pairs of *A. thaliana* accessions
146 from the native range or pairs of non-HPG1 typically differ by about 500 SNPs / 100 kb (21) (see scale in
147 Fig. 2A).

148 There were no SNPs in mitochondrial nor chloroplast genomes, which already suggested a
149 recent common origin, and genome-wide nuclear diversity ($\pi = 0.000002$, $\theta_W = 0.00001$, with 5,013 full
150 informative segregating sites) was two orders of magnitude lower than in the native range of the species
151 ($\theta_W = 0.007$) (21) (Table S1) (Supplementary Text 6). The population recombination parameter was
152 also four orders of magnitude lower ($4N_e r = \varrho = 3.0\text{x}10^{-6}$ cM bp^{-1}) than in the native range ($\varrho =$
153 $7.5\text{x}10^{-2}$ cM bp^{-1}) (26) (Supplementary Text 6). While recombination occurs in every generation,
154 regardless of self-fertilization or outcrossing, it is only observable after outcrossing between genetically
155 non-identical individuals, and this is what the population recombination parameter reports. We must
156 stress that because *A. thaliana* can outcross at rates of several percent per generation (23,27), but
157 because the HPG1 population is genetically so homogeneous, we are mostly "blind" to the
158 consequences of outcrossing in this special case. The lack of "observable recombination" in the genome

bioRxiv preprint doi: https://doi.org/10.1101/050203; this version posted October 5, 2017. The copyright holder for this preprint (which was not certified by peer review) is the author/funder, who has granted bioRxiv a license to display the preprint in perpetuity. It is made available under aCC-BY-NC-ND 4.0 International license.

159 is important, as it allows for the use of straightforward phylogenetic methods to calculate a mutation
160 rate. The enrichment of low frequency variants in the site frequency spectrum (Tajima's *D* = -2.84;
161 species mean = -2.04, (21)) and low levels of polymorphism are consistent with a recent bottleneck
162 followed by population expansion (Fig. 3). The obvious explanation is that the strong bottleneck
163 corresponds to a colonization founder event, likely by very few closely related individuals, or perhaps
164 only a single plant.

165 Altogether these patterns indicate that the collection of HPG1 plants we investigated constitute
166 a quasi-clonal and quasi-identical set of individual genomes, mostly devoid of observable recombination
167 and population structure, and thus eminently suited for the study of naturally arising *de novo* mutations.

168 The genome-wide substitution rate

169 It is important to distinguish between the *mutation rate*, which is the rate at which genomes change due
170 to DNA damage, faulty repair, gene conversion and replication errors, and *substitution rate*, which is the
171 rate at which mutations survive and accumulate under the influence of demographic processes and
172 natural selection (28,29). Under neutral evolution, mutation and substitution rates should be equal (29).
173 The simple evolutionary history of the HPG1 population enables direct estimates of substitution rates,
174 and the comparison of theses between different genome annotations, as well as with mutation rates
175 from controlled conditions experiments, could reveal the role played by both demographic and selective
176 forces.

177 To estimate the substitution rate in the HPG1 lineage, we used distance- and phylogeny-based
178 methods that take advantage of the known collection dates (Supplementary Text 7). The distance
179 method is independent of recombination and has been previously applied to viruses (30) and humans
180 (31). The substitution rate is calculated from correlation between differences in collection time in
181 historic-modern sample pairs, and the number of nucleotide differences between those pairs relative to

bioRxiv preprint doi: https://doi.org/10.1101/050203; this version posted October 5, 2017. The copyright holder for this preprint (which was not certified by peer review) is the author/funder, who has granted bioRxiv a license to display the preprint in perpetuity. It is made available under aCC-BY-NC-ND 4.0 International license.

182 a reference (Fig. 3C), scaled to the size of the genome accessible to Illumina sequencing. This method
183 resulted in an estimated rate of 2.11×10^{-9} substitutions site^{-1} year^{-1} (95% bootstrap Confidence Interval
184 [CI]: 1.88–2.33×10^{-9}) using rigorous SNP calling quality thresholds. Relaxing the thresholds for base
185 calling and minimum genotyped rate affects both the number of called SNPs and the length of the
186 interrogated reference sequence (32). These largely cancelled each other out, and the adjusted estimates
187 were relatively stable, between 2.1–3.2×10^{-9} substitutions site^{-1} year^{-1} (Table S3, Supplementary Text
188 3).

189 The second method, a Bayesian phylogenetic approach, uses the collection years for
190 tip-calibration and assumes a relaxed molecular clock. It summarizes thousands of plausible coalescent
191 trees, and it has been extensively used to calculate evolutionary rates in various organisms (33–35). This
192 method yielded a substitution rate of 4.0×10^{-9}, with confidence ranges overlapping the above estimates
193 (95% Highest Posterior Probability Density [HPPD]: 3.2–4.7×10^{-9}).

194 Based on the similar results obtained with two very different methods, we can confidently say
195 that the substitution rate in the wild populations of HPG1 is between 2 and 5 $\times10^{-9}$ site^{-1} year^{-1}.

196 To date the colonization of N. America by HPG1 *A. thaliana* and to improve the description of
197 intra-HPG1 relationships compared to that from a NJ tree, we further used a Bayesian phylogeny. At
198 first sight, the 73 modern samples appeared separated from the herbarium samples (Fig. 3B), but the
199 superimposition of thousands of possible trees showed that the apparent separation of samples was less
200 clear near the root (Fig. 3A). Long terminal branches reflected that the majority of the variants are
201 singletons, typical of populations that expand after bottlenecks.

202 The mean estimate of the last common HPG1 ancestor, the average tree root, was the year
203 1597 (HPPD 95%: 1519–1660) (Fig. 3A, B), and an alternative non-phylogenetic method gave a similar
204 estimate, 1625. Both estimates are older than a previously suggested date in the 19th century, using a

bioRxiv preprint doi: https://doi.org/10.1101/050203; this version posted October 5, 2017. The copyright holder for this preprint (which was not certified by peer review) is the author/funder, who has granted bioRxiv a license to display the preprint in perpetuity. It is made available under aCC-BY-NC-ND 4.0 International license.

205 laboratory mutation rate estimate and having no information from herbarium samples (25). Because
206 HPG1 appears to have been the most abundant lineage in N. America since the 1860s, we believe it
207 could have been one of the first, if not the first colonizer that could establish itself in N. America. If that
208 is true, the time of coalescence of the HPG1 diversity could be close to the time of HPG1 introduction
209 to N. America. During the colonial period, many European immigrants settled on the East coast,
210 consistent with N. American *A. thaliana* lineages being genetically closest to British and coastal West
211 European populations (21). Coincidentally, the oldest herbarium samples (12 out of the 27) were HPG1
212 and came from the East Coast, and we found a significant correlation between collection date and both
213 latitude and longitude (Fig. 1C). This could indicate that after the colonization they moved from the East
214 Coast to the Midwest – the other main area of the distribution that experienced an agricultural
215 expansion in the 19th century (36). Still, these conclusions need to be treated with caution, since
216 regardless of the robustness of the results and our attempts to sample evenly from available collections,
217 there could be unknown biases in the 19th century herbaria.

218 **Mutation spectra across genome annotations**

219 Although for dating divergence events a substitution rate expressed by years is ideal, in order to
220 compare substitution and mutation rates, both need to be expressed per generation. While *A. thaliana* is
221 an annual plant, seed bank dynamics generate a delay of average generation time at the population scale.
222 A comprehensive study of multiple *A. thaliana* populations in Scandinavia found that dormant seeds
223 could wait for longer than a year in the seed bank, generating overlapping generations and an delayed
224 average generation time of 1.3 years (37) with a notable variance across populations. Multiplication by
225 the mean generation time led to an adjusted rate of 2.7×10^{-9} substitutions site^{-1} generation^{-1} (95% CI
226 $2.4\text{-}3.0 \times 10^{-9}$) (Fig. 3E). To be able to compare this rate with a reference, we also re-sequenced mutation
227 accumulation (MA) lines in the Col-0 reference background grown under controlled conditions in the

bioRxiv preprint doi: https://doi.org/10.1101/050203; this version posted October 5, 2017. The copyright holder for this preprint (which was not certified by peer review) is the author/funder, who has granted bioRxiv a license to display the preprint in perpetuity. It is made available under aCC-BY-NC-ND 4.0 International license.

228 greenhouse that had been analyzed before with less advanced short read sequencing technology (38).
229 From the new re-sequencing data, we obtained an updated rate of 7.1×10^{-9} mutations site^{-1}
230 generation^{-1} (95% CI 6.3–7.9×10^{-9}) (Tables S2, S3, Supplementary Text 4 and 7). This is two- to
231 three-fold higher than the per-generation estimate in the wild, but within the same order of magnitude.
232 The same holds for rates in different genome annotations, i.e. genic, intronic and intergenic regions, but
233 the confidence intervals overlapped in many cases (Table S3).

234 Differences in per-generation rates between laboratory and wild populations could stem from
235 both methodological as well as biological causes. For instance, if the true average generation time was
236 actually over 3 years / generation, the differences would cancel out (Fig. 3E). Limitations in mapping
237 structural variation in non-reference samples could lower the substitution rate, what explains that we
238 calculated an atypically low substitution rate in regions with transposable elements (see Supplementary
239 Text 7.2.1). Environmentally-driven effects that are not yet well understood, such as variable
240 methylation status of cytosines, which account for much of the variation in local substitution rates (39),
241 could increase or decrease the rate (see Supplementary Text 7.2.3, Fig. S4).

242 An alternative evolutionary explanation to the aforementioned laboratory and wild populations'
243 rates differences is that purifying selection in the wild would slow down the accumulation of mutations
244 by removing deleterious mutations (Fig. 3E). This has been observed before and is one of the accepted
245 causes of the discrepancy between the so called long- and short-term substitution rates in a range of
246 organisms (40).

247 In order to provide evidence for negative purifying selection acting in the wild, we performed
248 three types of analyses involving comparisons across genomic annotations within the HPG1 dataset.
249 Firstly, by calculating contingency tables and computing a Fisher's exact test, we compared the deviation
250 of expected and observed SNPs between coding regions (more likely under purifying selection), with

bioRxiv preprint doi: https://doi.org/10.1101/050203; this version posted October 5, 2017. The copyright holder for this preprint (which was not certified by peer review) is the author/funder, who has granted bioRxiv a license to display the preprint in perpetuity. It is made available under aCC-BY-NC-ND 4.0 International license.

251 intergenic regions, intronic regions, and all non-coding regions of genome. All three pairwise
252 comparisons showed a depletion of coding SNPs and an enrichment of intergenic, intronic and
253 non-coding SNPs (odds ratio>2, $p<10^{-16}$). An obvious explanation is that in genome annotations where
254 a mutation is more likely to be deleterious, i.e. coding regions, the number of observed variants should
255 be lower due to selection having removed them from the population before we could sequence them.

256 Secondly, we studied the Site Frequency Spectrum (SFS) of genetic variants. The rationale was
257 that because purifying natural selection is more efficient at removing intermediate-frequency variants,
258 variants that tend to be deleterious or slightly deleterious should be found at lower frequency than
259 those that only suffer neutral drift (41). We built contingency tables of coding, intergenic, intronic and
260 non-coding variants segregating above and and below the conventional frequency cutoff of 5% to
261 separate low- and intermediate-frequency variants (42). We found that SNPs in coding regions were
262 more likely to be at low frequency than those in intergenic (odds ratio=2.34, $p=3.09\times10^{-11}$), intronic
263 (odds ratio=1.48, p=0.02), and all non-coding regions (odds ratio=2.05, $p=1.29\times10^{-8}$). We carried out
264 the same analysis using nonsynonymous and synonymous SNPs, which are easily interpretable in terms
265 of the selection regimes under which they evolve. We did not find an enrichment (p=0.67), perhaps a
266 consequence of the small number of such mutations (Table S3).

267 Thirdly, to verify that the full frequency spectrum of coding SNPs was shifted to lower
268 frequencies (i.e. the results were not dependent on the arbitrary 5% frequency cutoff), we used the
269 nonparametric Kolmogorov-Smirnov test for two samples. We found that the cumulative distribution of
270 the site frequency spectrum (CD_{SFS}) of coding regions is above (i.e., the frequency distribution is overall
271 skewed to lower values) both the intergenic CD_{SFS} ($p=3.25\times10^{-6}$) and the non-coding regions CD_{SFS}
272 (p=0.001), but not the intronic CD_{SFS} (p=0.60) (Fig. S5). As in our previous analysis, the comparison

bioRxiv preprint doi: https://doi.org/10.1101/050203; this version posted October 5, 2017. The copyright holder for this preprint (which was not certified by peer review) is the author/funder, who has granted bioRxiv a license to display the preprint in perpetuity. It is made available under aCC-BY-NC-ND 4.0 International license.

273 between the nonsynonymous and synonymous CD_{SFS} yielded, likely for similar reasons, no differences
274 (p=0.53).

275 All in all, these results support that purifying selection is a force shaping to some degree the
276 diversity across the HPG1 genome and might therefore as well contribute to the differences between
277 HPG1 and MA rates.

278 Potentially advantageous *de novo* mutations

279 Finally, having discovered over 5,000 *de novo* mutations in the HPG1 lineage, we wondered whether
280 there is any evidence for an adaptive role of these *de novo* mutations in the colonization of N. America
281 by HPG1. We noted that some new mutations had risen to intermediate or even high frequencies in the
282 HPG1 samples. This might have been the consequence of drift from stochastic demographic processes,
283 or it could have been caused by positive natural selection. To find direct evidence for the latter, we
284 grew the modern accessions in a common garden and studied phenotypes of known importance in
285 ecology of invasions (43), namely flowering time and root traits (see Supplementary Text 8). Using linear
286 mixed models, we calculated the proportion of variance explained (also called narrow sense heritability,
287 h^2) with a kinship matrix of all SNPs that had become common (>5%, n=391). We found significant
288 heritable variation for multiple traits including the growth rate in length (h^2=0.64) and the average root
289 gravitropic direction (h^2=0.54). As in our study mutations are the main source of genetic variants, these
290 mutations — or mutations linked to them — should be responsible for significant quantitative variation
291 in several traits (Table S4, Supplementary Text 10). The existence of mutation-driven phenotypic
292 variation at least indicates that natural selection could have acted upon such phenotypic variation.

293 Although linkage disequilibrium (LD) among SNPs is high, the fact that HPG1 genomes differ in
294 very few SNPs greatly reduces the list of candidate loci that might generate the observed phenotypic
295 variation (Fig. S6) (44). With this reasoning in mind and understanding the limitations imposed by LD, we

bioRxiv preprint doi: https://doi.org/10.1101/050203; this version posted October 5, 2017. The copyright holder for this preprint (which was not certified by peer review) is the author/funder, who has granted bioRxiv a license to display the preprint in perpetuity. It is made available under aCC-BY-NC-ND 4.0 International license.

296 carried out a genome-wide association (GWA) analysis and found 79 SNPs associated with one or more
297 root traits, mostly growth and directionality (Fig. 4). Twelve SNPs were in coding regions and seven
298 resulted in nonsynonymous changes — some producing non-conservative amino-acid changes and thus
299 likely to affect protein structure and/or function (Table 1, based on transition scores from (45)). Due to
300 the aforementioned LD, in some cases the results of associations could not be confidently assigned to a
301 specific SNP and thus we report the number of other associated mutations with $r^2 > 0.5$ (Table 1, Fig.
302 S6). For other cases, we were able to pinpoint clear candidates that were not in LD with other SNPs
303 and whose functional annotation had a strong connection to the phenotype (Table 1, Fig. S6). For
304 example, one SNP associated with root gravitropism was not linked to any other SNP hit and it was
305 found at 40% frequency (top 3% percentile). This SNP produces a cysteine to tryptophan change in
306 AT5G19330, which is involved in abscisic acid response and confers salt tolerance when overexpressed
307 (46). Another nonsynonymous SNP associated with root growth is located in AT2G38910, which
308 encodes a calcium-dependent kinase that is a factor regulating root hydraulic conductivity and
309 phytohormone response *in vitro* (47,48).

310 Nineteen other SNPs were associated with climate variables after correction for latitude and
311 longitude (www.worldclim.org, Table S4), and generally tended to coincide with top root-associated
312 SNPs (odds ratio = 3.9, Fisher's Exact test p = 0.002; Fig. 4, and Table S5). Specifically, this means that
313 alleles increasing root length and gravitropic growth were present in areas with lower precipitation, and
314 *vice versa* (Pearson's correlation r=0.85, p=0.003). This indicates that phenotypic variation generated by
315 mutations coincides with environmental (and not geographic) gradients along the colonized areas.
316 Compared to other mutations with matched allele frequencies, root-associated mutations are first found
317 in older herbarium samples nearer to Lake Michigan (Fig. S5), the area in US that seems to be most
318 populated by *A. thaliana* (21). This could be explained by natural selection having maintained mutations

bioRxiv preprint doi: https://doi.org/10.1101/050203; this version posted October 5, 2017. The copyright holder for this preprint (which was not certified by peer review) is the author/funder, who has granted bioRxiv a license to display the preprint in perpetuity. It is made available under aCC-BY-NC-ND 4.0 International license.

319 with phenotypic effect for a longer time than neutral mutations or perhaps that this mutations were
320 selected for in a new environment. All in all our results are compatible with natural positive selection
321 having already acted on root morphology variation that was generated by *de novo* mutations in this
322 colonizing lineage. To confirm such hypotheses of local adaptation by *de novo* mutations, it will be
323 necessary to grow collections of divergent HPG1 individuals in multiple contrasting locations over
324 several years, and ideally revive historical specimens to compare performance (49).

325 **Conclusions**

326 In summary, we have exploited whole-genome information from historic and contemporary collections
327 of a herbaceous plant to empirically characterize evolutionary forces during a recent colonization. With
328 this natural time series experiment we could directly estimate the nuclear substitution rate in wild *A.*
329 *thaliana* populations – a parameter difficult to characterize experimentally (9). This allowed us to date
330 the colonization time and spread of HPG1 in N. America. We provide evidence that purifying selection
331 has already changed the site frequency spectrum in the course of just a few centuries. Finally, we
332 discovered that a small number of *de novo* mutations that rose to intermediate frequency can together
333 explain quantitative variation in root traits across environments. This strengthens the hypothesis that
334 some *de novo* variation could have had an adaptive value during the colonization and expansion process,
335 a hypothesis that has been put forward as one of the possible solutions to the genetic paradox of
336 invasion in plants (17). This process might be more relevant in self-fertilizing plants, which typically have
337 less diversity than outcrossing ones (50), but have higher growth rates (43) and account for the majority
338 of successful plant colonizers (5). While *A. thaliana* HPG1 is not an invasive, i.e. harmful, species, it can
339 teach us about fundamental evolutionary processes behind successful colonizations and adaptation to
340 new environments. Our work should encourage others to search for similar natural experiments and to
341 unlock the potential of herbarium specimens to study "evolution in action".

bioRxiv preprint doi: https://doi.org/10.1101/050203; this version posted October 5, 2017. The copyright holder for this preprint (which was not certified by peer review) is the author/funder, who has granted bioRxiv a license to display the preprint in perpetuity. It is made available under aCC-BY-NC-ND 4.0 International license.

342 # METHODS

343 ## Sample collection and DNA sequencing

344 Modern *A. thaliana* accessions were from the collection described by Platt and colleagues (23), who
345 identified HPG1 candidates based on 149 genome-wide SNPs (Table S1, Supplementary Text 1).
346 Herbarium specimens were directly sampled by Max Planck colleagues Jane Devos and Gautam
347 Shirsekar, or sent to us by collection curators from various herbaria (Table S1, Supplementary Text 1).
348 Among the substantial number of specimens in the herbaria of the University of Connecticut, the
349 Chicago Field Museum and the New York Botanical Garden, we selected herbarium specimens spaced in
350 time so there was at least one sample per decade starting from the oldest record (1863). The
351 differences in geographic biases of herbarium and modern collections are difficult to know (2), thus we
352 did choose both historic and modern samples that were as regularly distributed in space as possible, and
353 sample overlapping locations wherever possible. DNA from herbarium specimens was extracted as
354 described (51) in a clean room facility at the University of Tübingen. Two sequencing libraries with
355 sample-specific barcodes were prepared following established protocols, with and without repair of
356 deaminated sites using uracil-DNA glycosylase and endonuclease VIII (refs. (52–54)) (Supplementary
357 Text 2). We also investigated patterns of DNA fragmentation and damage typical of ancient DNA (24)
358 (Supplementary Text 2). DNA from modern individuals was extracted from pools of eight siblings using
359 the DNeasy plant mini kit (Qiagen, Hilgendorf, Germany). Genomic DNA libraries were prepared using
360 the TruSeq DNA Sample or TruSeq Nano DNA sample prep kits (Illumina, San Diego, CA), and
361 sequenced on Illumina HiSeq 2000, HiSeq 2500 or MiSeq instruments. Paired-end reads from modern
362 samples were trimmed and quality filtered before mapping using the SHORE pipeline v0.9.0 (25,55).
363 Because ancient DNA fragments are short (Fig. S1) we merged forward and reverse reads for herbarium
364 samples after trimming, requiring a minimum of 11 bp overlap (51), and treated the resulting as

bioRxiv preprint doi: https://doi.org/10.1101/050203; this version posted October 5, 2017. The copyright holder for this preprint (which was not certified by peer review) is the author/funder, who has granted bioRxiv a license to display the preprint in perpetuity. It is made available under aCC-BY-NC-ND 4.0 International license.

365 single-end reads. Reads were mapped with GenomeMapper v0.4.5s (56) against an HPG1
366 pseudo-reference genome (25), and against the Col-0 reference genome, and SNPs were called with
367 SHORE for the HPG1 pseudo-reference genome mappings (25,57) using different thresholds
368 (Supplementary Text 3). Average coverage depth, number of covered genome positions, and number of
369 SNPs identified per accession relative to HPG1 are reported in Table S1. We also re-sequenced the
370 genomes of twelve Col-0 MA lines (57,58) (Table S2) (Supplementary text 4) to recalculate and update
371 the laboratory mutation rate from Ossowski et al. (38) with the newer sequencing technologies.

372 Phylogenetic methods and genome-wide statistics

373 We used the Pegas, Ape and Adegenet packages in R (59–61) to manipulate and visualize the genetic
374 distances of all samples as well as the HPG1 subset (Supplementary Text 7). We constructed parsimony
375 networks using SplitsTree v.4.12.3 (62), with confidence values calculated with 1,000 bootstrap
376 iterations. We built Maximum Clade Credibility Trees using the Bayesian phylogenetic tools
377 implemented in BEAST v.1.8 (63) (see below).

378 We estimated genetic diversity as Watterson´s θ (64) and nucleotide diversity π, and the
379 difference between these two statistics as Tajimas's *D (65)* using DnaSP v5 (66). We estimated pairwise
380 linkage disequilibrium (LD) between all possible combinations of informative sites, ignoring singletons, by
381 computing r^2, D and D' statistics using DnaSP v5 (66). For the modern individuals, we calculated the
382 recombination parameter rho ($4N_e r$) also using DnaSP v5 (66).

383 Substitution and mutation rate analyses

384 Similarly as in Fu et al. (67), we used genome-wide nuclear SNPs to calculate pairwise "net" genetic
385 distances using the equation $D'_{ij} = D_{ic} - D_{jc}$, where D'_{ij} is the net distance between a modern sample *i*
386 and a herbarium sample *j*; D_{ic} the distance between the modern sample *i* and the reference genome *c*;

bioRxiv preprint doi: https://doi.org/10.1101/050203; this version posted October 5, 2017. The copyright holder for this preprint (which was not certified by peer review) is the author/funder, who has granted bioRxiv a license to display the preprint in perpetuity. It is made available under aCC-BY-NC-ND 4.0 International license.

387 and D_{jc} is the distance between a modern sample (j) and the reference genome (c). We calculated a
388 pairwise time distance in years between the collection times, *T*'ij, and calculated the linear regression: D'
389 $= a+bT'$. The slope coefficient *b* describes the number of substitution changes per year. We used either
390 all SNPs or subsets of SNPs at different annotations (genic, intergenic etc.) appropriately scaled by
391 accessible genome length. Because the points used to calculate the regression are non-independent, a
392 bootstrap has been recommended to overcome to a certain extent the anti-conservative confidence
393 intervals (30) (Supplementary Text 7 and Fig. S3).

394 To fully account for the non-independence of points, we need to work with phylogenies. The
395 Bayesian phylogenetics approach we used is implemented in BEAST v1.8 (63) and is called tip-calibration,
396 and calculates a substitution rate along the phylogeny. Our analysis optimized simultaneously and in an
397 iterative fashion using a Monte Carlo Markov Chain (MCMC) a tree topology, branch length,
398 substitution rate, and a demographic Skygrid model (Supplementary Text 7). The demographic model is
399 a Bayesian nonparametric one that is optimized for multiple loci and that allows for complex
400 demographic trajectories by estimating population sizes in time bins across the tree based on the
401 number of coalescent - branching - events per bin (68). We also performed a second analysis run using a
402 fixed prior for substitution rate of 3×10^{-9} substitutions site^{-1} year^{-1} based on our previous net distance
403 estimate to confirm that the MCMC had the same parameter convergence, e.g. tree topology, as in the
404 first "estimate-all-parameters" run.

405 Having a substitution rate per year we can estimate the time to the most common recent
406 ancestor *L* solving $d = 2L \times \mu$ where *d* is the average pairwise genetic distance between our samples and
407 μ is the calculated substitution rate from the distance method. This yielded 363 years, which subtracted
408 to the average collection date of the samples, produced a point estimate of 1615. We compare this
409 estimate with the inferred phylogeny root from the BEAST analysis.

bioRxiv preprint doi: https://doi.org/10.1101/050203; this version posted October 5, 2017. The copyright holder for this preprint (which was not certified by peer review) is the author/funder, who has granted bioRxiv a license to display the preprint in perpetuity. It is made available under aCC-BY-NC-ND 4.0 International license.

410 **Inference of genome-wide selection**

411 We separately analyzed sequences at different annotations, since as they might be under different
412 selection regimes (i.e. evolutionary constraints). We computed one-tailed Fisher's exact test using the
413 base stats package in R (69) on tables of counts of the total number of positions in the genome
414 annotated as a coding or non-coding (intergenic, intronic, all other noncoding) and the number of SNPs
415 of each annotation present in the HPG1 dataset:

coding SNP	all coding base pairs
non-coding SNP	all non-coding base pairs

416 The test will return whether coding regions have a lower number of SNPs than other reference
417 annotation (intronic, interenic, all non-coding regions), as expected by the total number of positions in
418 the genome annotated as such. We also constructed contingency tables to test whether the SNPs are
419 more likely to be found at low (<5%) or intermediate (5≥%) frequency:

coding SNP low	coding SNP intermediate
non-coding SNP low	non-coding SNP intermediate

420 Finally, we calculated the unfolded Site Frequency Spectrum (SFS) based on the order of
421 appearance of genetic variants in the herbarium dataset. We then used the the Kolmogorov–Smirnov
422 two-samples test and 10,000 bootstrap resampling using the R package Matching v. 4.9-2 (ref. (70)) to
423 calculate whether the frequency spectrum was lower for coding SNPs than for other SNPs. Additionally,
424 we also repeated these analyses comparing nonsynonymous and synonymous mutations.

425 **Association analysis**

426 We collected flowering, seed and root morphology phenotypes for 63 accessions (Supplementary Text
427 8). For associations with climate parameters, we followed a similar rationale as previously described
428 (71). We extracted information from the bioclim database (http://www.worldclim.org/bioclim) at a 2.5

bioRxiv preprint doi: https://doi.org/10.1101/050203; this version posted October 5, 2017. The copyright holder for this preprint (which was not certified by peer review) is the author/funder, who has granted bioRxiv a license to display the preprint in perpetuity. It is made available under aCC-BY-NC-ND 4.0 International license.

429 degrees resolution raster and intersected it with geographic locations of HPG1 samples (n = 100). We
430 performed association analyses under several models and *p*-value corrections using the R package
431 GeneABEL (72) (Supplementary Text 8.2). To calculate the variance of the trait explained by all genetic
432 variants, we used a linear mixed model: $y = Xb + Zu + \varepsilon$; where y is the phenotype or climate variable,
433 X is the genotype states at a given SNP, b is the fixed phenotypic effect of such SNP, Z is the design
434 matrix of genome identities, u is the random genome background effect informed by the kinship matrix
435 and distributed as MVN (0, $\sigma_g A$), and ε is the random error term. The ratio of σ_g / σ_T is commonly
436 called narrow sense heritability, "chip" heritability, or proportion of variance explained by genotype (73).
437 Only SNPs with MAF>5% (n=391) were used to build a kinship or relationship matrix *A*. Note that the
438 differences between any two genotypes were of the order of one or few dozens of SNPs. While this
439 approach is appropriate to calculate a chip heritability, it would not be very useful to detect significant
440 SNP, as the random factor accumulates all the available variation (Table S4). We therefore run regular
441 GWA model without kinship matrix: $y = Xb + \varepsilon$; but generated a p-value empirical null distribution
442 based on running such model over 1,000 permuted datasets, which lead to conservative significance
443 calculation (Fig. S6, Data Appendix S1). The p-values from running the association in the real data that
444 were below the 5% tail in the empirical distribution could be considered significant. However, we also
445 established a conservative "double" Bonferroni correction, where the significant threshold was lowered
446 to 0.01% (= 5% / [number of SNPs + number of phenotypes tested]). All significant SNPs are shown in
447 Table S5, and a subset in Table 1. Although many phenotypic traits did not have significant SNPs, we
448 show all the QQ plots in the Data Appendix S1 file.

449 **Accession numbers.** Short reads have been deposited in the European Nucleotide Archive under the
450 accession number XXXXX.

bioRxiv preprint doi: https://doi.org/10.1101/050203; this version posted October 5, 2017. The copyright holder for this preprint (which was not certified by peer review) is the author/funder, who has granted bioRxiv a license to display the preprint in perpetuity. It is made available under aCC-BY-NC-ND 4.0 International license.

451 **Online Content** This article contains supplementary information including data sets, extended
452 methods and supplementary figures at xxx.

453 **Acknowledgments** For providing and retrieving herbarium specimens, we thank R. Capers, J. Devos,
454 G. Shirsekar, M. S. Dossmann, J. Freudenstein, C. M. Herring, C. Niezgoda, C. A. McCormick, J. Peter
455 and M. Thines. We thank X. Zhao and I. Henderson for recombination estimates, C. Lanz for sequencing
456 support, C. Goeschl, B. Zierfuss and B. Wohlrab for help with root analyses, and P. Lang, D. Seymour,
457 and D. Koenig for thorough proofreading and comments on the manuscript. We thank to Robert
458 Colautti for useful comments on the theoretical framing of the manuscript, M. Nordborg for discussions
459 and pointing us to the work of A.R. Templeton, K. Pruefer for input on data analysis, and the Weigel and
460 Burbano labs for comments. Supported by the President's Fund of the Max Planck Society (project
461 "Darwin"), ERC (AdG IMMUNEMESIS) and core funds of the Max Planck Society.

462 **Author Contributions** H.A.B. and D.W. conceived and supervised the project, and coordinated the
463 collaborative effort. J.B. coordinated the collection of modern seed samples. C.J., B.B. and J.B. performed
464 and analyzed flowering time and seed set greenhouse experiments. C.S. and R.S. performed and analyzed
465 root assays and seed size measurements under the supervision of W.B.; C.B. and J.H. sequenced and
466 curated modern samples, coordinated by D.W.; H.A.B. coordinated the collection and analysis of
467 herbarium samples. J.K. coordinated the extraction of DNA and library preparation of herbarium
468 samples. V.J.S. and E.R. prepared sequencing libraries from herbarium specimens. C.B. called variants in
469 HPG1. J.H. called variants in mutation accumulation lines. M.E.A. performed the population and
470 quantitative genomic analyses with supervision of R.N., C.B. and H.A.B. The first draft was written by
471 M.E.A. and the final manuscript was written by M.E.A., C.B., H.A.B. and D.W. with comments from all
472 coauthors.

473 Authors declare no conflict of interests.

bioRxiv preprint doi: https://doi.org/10.1101/050203; this version posted October 5, 2017. The copyright holder for this preprint (which was not certified by peer review) is the author/funder, who has granted bioRxiv a license to display the preprint in perpetuity. It is made available under aCC-BY-NC-ND 4.0 International license.

474 # REFERENCES

475
1. Green RE, Shapiro B. Human evolution: turning back the clock. Curr Biol. 2013 Apr 8;23(7):R286–8.
476 477
2. Crawford PHC, Hoagland BW. Can herbarium records be used to map alien species invasion and native species expansion over the past 100 years? J Biogeogr. 2009;36(4):651–61.
478 479
3. Colautti RI, Lau JA. Contemporary evolution during invasion: evidence for differentiation, natural selection, and local adaptation. Mol Ecol. 2015 May;24(9):1999–2017.
480 481
4. van Kleunen M, Dawson W, Essl F, Pergl J, Winter M, Weber E, et al. Global exchange and accumulation of non-native plants. Nature. 2015 Aug 19;525(7567):100–3.
482 483
5. Razanajatovo M, Maurel N, Dawson W, Essl F, Kreft H, Pergl J, et al. Plants capable of selfing are more likely to become naturalized. Nat Commun. 2016 Oct 31;7:13313.
484 485
6. Sax DF, Stachowicz JJ, Brown JH, Bruno JF, Dawson MN, Gaines SD, et al. Ecological and evolutionary insights from species invasions. Trends Ecol Evol. 2007 Sep;22(9):465–71.
486
7. Gauze GF. The struggle for existence. Baltimore: The Williams & Wilkins company; 1934. 192-192 p.
487 488
8. Hardouin EA, Tautz D. Increased mitochondrial mutation frequency after an island colonization: positive selection or accumulation of slightly deleterious mutations? Biol Lett. 2013 Apr 23;9(2):20121123.
489 490
9. Halligan DL, Keightley PD. Spontaneous mutation accumulation studies in evolutionary genetics. Annu Rev Ecol Evol Syst. 2009;40(1):151–72.
491 492
10. Roach JC, Glusman G, Smit AFA, Huff CD, Hubley R, Shannon PT, et al. Analysis of genetic inheritance in a family quartet by whole-genome sequencing. Science. 2010 Apr 30;328(5978):636–9.
493 494
11. Wolfe KH, Li WH, Sharp PM. Rates of nucleotide substitution vary greatly among plant mitochondrial, chloroplast, and nuclear DNAs. Proc Natl Acad Sci U S A. 1987 Dec;84(24):9054–8.
495 496
12. Leffler EM, Bullaughey K, Matute DR, Meyer WK, Ségurel L, Venkat A, et al. Revisiting an old riddle: what determines genetic diversity levels within species? PLoS Biol. 2012 Sep 11;10(9):e1001388.
497 498
13. Pennings PS, Hermisson J. Soft Sweeps II—Molecular Population Genetics of Adaptation from Recurrent Mutation or Migration. Mol Biol Evol. 2006 May 1;23(5):1076–84.
499 500
14. Karasov T, Messer PW, Petrov DA. Evidence that adaptation in Drosophila is not limited by mutation at single sites. PLoS Genet. 2010 Jun;6(6):e1000924.
501 502 503
15. Rouco M, López-Rodas V, Flores-Moya A, Costas E. Evolutionary changes in growth rate and toxin production in the cyanobacterium Microcystis aeruginosa under a scenario of eutrophication and temperature increase. Microb Ecol. 2011 Aug;62(2):265–73.
504 505
16. Scally A, Durbin R. Revising the human mutation rate: implications for understanding human evolution. Nat Rev Genet. 2012 Sep 11;13(10):745–53.
506 507
17. Estoup A, Ravigné V, Hufbauer R, Vitalis R, Gautier M, Facon B. Is There a Genetic Paradox of Biological Invasion? Annu Rev Ecol Evol Syst. 2016;47(1):51–72.
508
18. Barrett RDH, Schluter D. Adaptation from standing genetic variation. Trends Ecol Evol. 2008 Jan;23(1):38–44.

bioRxiv preprint doi: https://doi.org/10.1101/050203; this version posted October 5, 2017. The copyright holder for this preprint (which was not certified by peer review) is the author/funder, who has granted bioRxiv a license to display the preprint in perpetuity. It is made available under aCC-BY-NC-ND 4.0 International license.

509 19. Dlugosch KM, Parker IM. Founding events in species invasions: genetic variation, adaptive evolution, and the
510 role of multiple introductions. Mol Ecol. 2008 Jan;17(1):431–49.

511 20. Dlugosch KM, Anderson SR, Braasch J, Cang FA, Gillette HD. The devil is in the details: genetic variation in
512 introduced populations and its contributions to invasion. Mol Ecol. 2015 May;24(9):2095–111.

513 21. 1001 Genomes Consortium. 1,135 genomes reveal the global pattern of polymorphism in Arabidopsis
514 thaliana. Cell. 2016 Jun 9;166:481–91.

515 22. Durvasula A, Fulgione A, Gutaker RM, Alacakaptan SI, Flood PJ, Neto C, et al. African genomes illuminate the
516 early history and transition to selfing in Arabidopsis thaliana. Proceedings of the National Academy of Sciences
517 [Internet]. 2017 May 4; Available from: http://www.pnas.org/content/early/2017/05/03/1616736114.abstract

518 23. Platt A, Horton M, Huang YS, Li Y, Anastasio AE, Mulyati NW, et al. The scale of population structure in
519 Arabidopsis thaliana. PLoS Genet. 2010 Feb;6(2):e1000843.

520 24. Weiß CL, Schuenemann VJ, Devos J, Shirsekar G, Reiter E, Gould BA, et al. Temporal patterns of damage and
521 decay kinetics of DNA retrieved from plant herbarium specimens. Royal Society Open Science. 2016 Jun
522 1;3(6):160239.

523 25. Hagmann J, Becker C, Müller J, Stegle O, Meyer RC, Wang G, et al. Century-scale methylome stability in a
524 recently diverged Arabidopsis thaliana lineage. PLoS Genet. 2015;11(1):e1004920–e1004920.

525 26. Choi K, Zhao X, Kelly KA, Venn O, Higgins JD, Yelina NE, et al. Arabidopsis meiotic crossover hot spots
526 overlap with H2A.Z nucleosomes at gene promoters. Nat Genet. 2013 Nov;45(11):1327–36.

527 27. Bomblies K, Yant L, Laitinen R a., Kim S-T, Hollister JD, Warthmann N, et al. Local-scale patterns of genetic
528 variability, outcrossing, and spatial structure in natural stands of Arabidopsis thaliana. PLoS Genet. 2010
529 Mar;6(3):e1000890–e1000890.

530 28. Barrick JE, Lenski RE. Genome dynamics during experimental evolution. Nat Rev Genet. 2013
531 Dec;14(12):827–39.

532 29. Kimura M. On the evolutionary adjustment of spontaneous mutation rates. Genet Res. 1967 Apr;9(01):23–23.

533 30. Drummond A, Pybus OG, Rambaut A. Inference of viral evolutionary rates from molecular sequences. Adv
534 Parasitol. 2003;54:331–58.

535 31. Fu Q, Li H, Moorjani P, Jay F, Slepchenko SM, Bondarev AA, et al. Genome sequence of a 45,000-year-old
536 modern human from western Siberia. Nature. 2014 Oct 23;514(7523):445–9.

537 32. Ness RW, Morgan AD, Colegrave N, Keightley PD. Estimate of the spontaneous mutation rate in
538 Chlamydomonas reinhardtii. Genetics. 2012 Dec;192(4):1447–54.

539 33. Drummond AJ, Rambaut A. BEAST: Bayesian evolutionary analysis by sampling trees. BMC Evol Biol. 2007
540 Jan;7:214–214.

541 34. Millar CD, Dodd A, Anderson J, Gibb GC, Ritchie PA, Baroni C, et al. Mutation and evolutionary rates in
542 adélie penguins from the antarctic. PLoS Genet. 2008 Oct 3;4(10):e1000209.

543 35. Christin P-A, Spriggs E, Osborne CP, Strömberg CAE, Salamin N, Edwards EJ. Molecular dating, evolutionary
544 rates, and the age of the grasses. Syst Biol. 2014 Mar;63(2):153–65.

545 36. Klein Goldewijk K, Ramankutty N. Land cover change over the last three centuries due to human activities:
546 The availability of new global data sets. GeoJournal. 2004;61(4):335–44.

bioRxiv preprint doi: https://doi.org/10.1101/050203; this version posted October 5, 2017. The copyright holder for this preprint (which was not certified by peer review) is the author/funder, who has granted bioRxiv a license to display the preprint in perpetuity. It is made available under aCC-BY-NC-ND 4.0 International license.

547 37. Falahati-Anbaran M, Lundemo S, Stenøien HK. Seed dispersal in time can counteract the effect of gene flow
548 between natural populations of Arabidopsis thaliana. New Phytol. 2014 May;202(3):1043–54.

549 38. Ossowski S, Schneeberger K, Lucas-Lledó JI, Warthmann N, Clark RM, Shaw RG, et al. The rate and
550 molecular spectrum of spontaneous mutations in Arabidopsis thaliana. Science. 2010 Jan 1;327(5961):92–4.

551 39. Cao J, Schneeberger K, Ossowski S, Günther T, Bender S, Fitz J, et al. Whole-genome sequencing of multiple
552 Arabidopsis thaliana populations. Nat Genet. 2011 Oct;43(10):956–63.

553 40. Ho SYW, Lanfear R, Bromham L, Phillips MJ, Soubrier J, Rodrigo AG, et al. Time-dependent rates of
554 molecular evolution. Mol Ecol. 2011 Aug;20(15):3087–101.

555 41. Charlesworth B, Charlesworth D. Elements of Evolutionary Genetics. Roberts and Company Publishers; 2010.

556 42. Bush WS, Moore JH. Chapter 11: Genome-wide association studies. PLoS Comput Biol. 2012 Dec
557 27;8(12):e1002822.

558 43. van Kleunen M, Dawson W, Maurel N. Characteristics of successful alien plants. Mol Ecol. 2015
559 May;24(9):1954–68.

560 44. Templeton AR, Sing CF, Kessling A, Humphries S. A cladistic analysis of phenotype associations with
561 haplotypes inferred from restriction endonuclease mapping. II. The analysis of natural populations. Genetics.
562 1988 Dec;120(4):1145–54.

563 45. Grantham R. Amino acid difference formula to help explain protein evolution. Science. 1974 Sep
564 6;185(4154):862–4.

565 46. Kim S, Choi H-I, Ryu H-J, Park JH, Kim MD, Kim SY. ARIA, an Arabidopsis arm repeat protein interacting
566 with a transcriptional regulator of abscisic acid-responsive gene expression, is a novel abscisic acid signaling
567 component. Plant Physiol. 2004 Nov;136(3):3639–48.

568 47. Li G, Boudsocq M, Hem S, Vialaret J, Rossignol M, Maurel C, et al. The calcium-dependent protein kinase
569 CPK7 acts on root hydraulic conductivity. Plant Cell Environ. 2015 Jul;38(7):1312–20.

570 48. Choi H-I, Park H-J, Park JH, Kim S, Im M-Y, Seo H-H, et al. Arabidopsis calcium-dependent protein kinase
571 AtCPK32 interacts with ABF4, a transcriptional regulator of abscisic acid-responsive gene expression, and
572 modulates its activity. Plant Physiol. 2005 Dec;139(4):1750–61.

573 49. Franks SJ, Weis AE. A change in climate causes rapid evolution of multiple life-history traits and their
574 interactions in an annual plant. J Evol Biol. 2008 Sep;21(5):1321–34.

575 50. Arunkumar R, Ness RW, Wright SI, Barrett SCH. The evolution of selfing is accompanied by reduced efficacy
576 of selection and purging of deleterious mutations. Genetics. 2015 Mar;199(3):817–29.

577 51. Yoshida K, Schuenemann VJ, Cano LM, Pais M, Mishra B, Sharma R, et al. The rise and fall of the Phytophthora
578 infestans lineage that triggered the Irish potato famine. eLife. 2013 May 28;2:e00731.

579 52. Meyer M, Kircher M. Illumina sequencing library preparation for highly multiplexed target capture and
580 sequencing. Cold Spring Harb Protoc. 2010 Jun;2010(6):db.prot5448.

581 53. Briggs AW, Stenzel U, Meyer M, Krause J, Kircher M, Pääbo S. Removal of deaminated cytosines and
582 detection of in vivo methylation in ancient DNA. Nucleic Acids Res. 2010 Apr;38(6):e87.

583 54. Kircher M. Analysis of High-Throughput Ancient DNA Sequencing Data. In: Shapiro B, Hofreiter M, editors.
584 Ancient DNA. Humana Press; 2011. p. 197–228. (Methods in Molecular Biology).

bioRxiv preprint doi: https://doi.org/10.1101/050203; this version posted October 5, 2017. The copyright holder for this preprint (which was not certified by peer review) is the author/funder, who has granted bioRxiv a license to display the preprint in perpetuity. It is made available under aCC-BY-NC-ND 4.0 International license.

585 55. Ossowski S, Schneeberger K, Clark RM, Lanz C, Warthmann N, Weigel D. Sequencing of natural strains of
586 Arabidopsis thaliana with short reads. Genome Res. 2008 Dec;18(12):2024–33.

587 56. Schneeberger K, Hagmann J, Ossowski S, Warthmann N, Gesing S, Kohlbacher O, et al. Simultaneous
588 alignment of short reads against multiple genomes. Genome Biol. 2009 Sep 17;10(9):R98.

589 57. Becker C, Hagmann J, Müller J, Koenig D, Stegle O, Borgwardt K, et al. Spontaneous epigenetic variation in
590 the Arabidopsis thaliana methylome. Nature. 2011 Dec 8;480(7376):245–9.

591 58. Shaw RG, Byers DL, Darmo E. Spontaneous mutational effects on reproductive traits of arabidopsis thaliana.
592 Genetics. 2000 May;155(1):369–78.

593 59. Jombart T. adegenet: a R package for the multivariate analysis of genetic markers. Bioinformatics. 2008 Jun
594 1;24(11):1403–5.

595 60. Paradis E, Claude J, Strimmer K. APE: Analyses of Phylogenetics and Evolution in R language. Bioinformatics.
596 2004 Jan 22;20(2):289–90.

597 61. Paradis E. pegas: an R package for population genetics with an integrated–modular approach. Bioinformatics.
598 2010 Feb 1;26(3):419–20.

599 62. Huson DH, Bryant D. Application of phylogenetic networks in evolutionary studies. Mol Biol Evol. 2006
600 Feb;23(2):254–67.

601 63. Drummond AJ, Suchard MA, Xie D, Rambaut A. Bayesian phylogenetics with BEAUti and the BEAST 1.7. Mol
602 Biol Evol. 2012 Aug;29(8):1969–73.

603 64. Watterson GA. On the number of segregating sites in genetical models without recombination. Theor Popul
604 Biol. 1975 Apr;7(2):256–76.

605 65. Tajima F. Statistical method for testing the neutral mutation hypothesis by DNA polymorphism. Genetics.
606 1989 Nov 1;123(3):585–95.

607 66. Librado P, Rozas J. DnaSP v5: a software for comprehensive analysis of DNA polymorphism data.
608 Bioinformatics. 2009 Jun 1;25(11):1451–2.

609 67. Fu Q, Mittnik A, Johnson PLF, Bos K, Lari M, Bollongino R, et al. A revised timescale for human evolution
610 based on ancient mitochondrial genomes. Curr Biol. 2013 Apr;23(7):553–9.

611 68. Gill MS, Lemey P, Faria NR, Rambaut A, Shapiro B, Suchard M a. Improving Bayesian population dynamics
612 inference: a coalescent-based model for multiple loci. Mol Biol Evol. 2012 Mar;30(3):713–24.

613 69. R Core Team. R: A Language and Environment for Statistical Computing [Internet]. Vienna, Austria: R
614 Foundation for Statistical Computing; 2016. Available from: https://www.R-project.org/

615 70. Sekhon JS. Multivariate and Propensity Score Matching Software with Automated Balance Optimization: The
616 Matching Package for R [Internet]. Vol. 42, Journal of Statistical Software. 2011. p. 1–52. Available from:
617 http://www.jstatsoft.org/v42/i07/

618 71. Hancock AM, Brachi B, Faure N, Horton MW, Jarymowycz LB, Sperone FG, et al. Adaptation to climate
619 across the Arabidopsis thaliana genome. Science. 2011 Oct;334(6052):83–6.

620 72. Aulchenko YS, Ripke S, Isaacs A, van Duijn CM. GenABEL: an R library for genome-wide association analysis.
621 Bioinformatics. 2007 May 15;23(10):1294–6.

622 73. Yang J, Benyamin B, McEvoy BP, Gordon S, Henders AK, Nyholt DR, et al. Common SNPs explain a large

bioRxiv preprint doi: https://doi.org/10.1101/050203; this version posted October 5, 2017. The copyright holder for this preprint (which was not certified by peer review) is the author/funder, who has granted bioRxiv a license to display the preprint in perpetuity. It is made available under aCC-BY-NC-ND 4.0 International license.

623 proportion of the heritability for human height. Nat Genet. 2010 Jun 20;42(7):565–9.

bioRxiv preprint doi: https://doi.org/10.1101/050203; this version posted October 5, 2017. The copyright holder for this preprint (which was not certified by peer review) is the author/funder, who has granted bioRxiv a license to display the preprint in perpetuity. It is made available under aCC-BY-NC-ND 4.0 International license.

624 # TABLES

625 **Table 1. Genic SNPs associated with different traits.**

626 For nonsynonymous SNPs, the amino acid change and the Grantham score (ranging from 0 to 215),
627 which measures the physico-chemical properties of the amino acids, are reported. All SNPs in the table
628 were significant ($p < 0.05$) after raw p-values were corrected by an empirical p-value distribution from a
629 permutation procedure. * highlights those that also passed a double Bonferroni threshold, correcting by
630 number of SNPs and number of phenotypes ($p < 0.0001$). LD corresponds to how many other SNP hits
631 are in high linkage (r^2>0.5). Table S5 contains information on all significant SNPs and Table S4 for details
632 on phenotypes and climatic variables.

Trait †	Location (chr-bp)	Gene	Anno–tation	Protein	aa change	LD	Bonf.
G	1-958,948	AT1G03810	nonsyn	Oligonucleotide binding	A>P, 27	53	
D	1-13,994,958	AT1G36933	transposon	Copia		49	
S	1-20,324,050	AT1G54440	intronic	RRP6-LIKE 1		11	*
D	1-23,648,407	AT1G63740	nonsyn	TIR-NLR family	Y>S, 144	46	
G	2-358,395	AT2G01820	syn	RLK family		43	*
G	2-585,918	AT2G02220	syn	PSKR1		42	*
G	2-6,034,545	AT2G14247	syn	Expressed protein		38	*
G	2-7,047,529	AT2G16270	nonsyn	Unknown protein	P>A, 27	37	*
G	2-7,186,220	AT2G16580	intronic	SAUR8		36	*
G	2-10,495,275	AT2G24680	intronic	B3 family		34	*

bioRxiv preprint doi: https://doi.org/10.1101/050203; this version posted October 5, 2017. The copyright holder for this preprint (which was not certified by peer review) is the author/funder, who has granted bioRxiv a license to display the preprint in perpetuity. It is made available under aCC-BY-NC-ND 4.0 International license.

G	2-12,415,084	AT2G28900	intronic	OEP16		32	
S	2-16,039,488	AT2G38290	3' UTR	AMT2		8	*
S	2-16,247,290	AT2G38910	nonsyn	CPK20	A>G, 60	7	*
G	2-16,333,662	AT2G39160	nonsyn	Unknown protein	A>G, 60	29	
G	3-2,500,258	AT3G07830	syn	PGA3		28	*
G	3-3,629,794	AT3G11530	intronic	VPS55		26	*
G	3-4,269,626	AT3G13229	5' UTR	DUF868 domain		25	*
D	3-11,873,293	AT3G30219	transposon	Gypsy		0	
G & D	4-4,228,138	AT4G07440	transposon	Oligonucleotide binding		19	
G & D	4-9,046,942	AT4G15960	nonsyn	Alpha/beta-hydrolase	A>Q, 24	18	
G & D	4-15,646,341	AT4G32410	syn	ANY1		15	
G	4-15,845,001	AT4G32840	3' UTR	PFK6		14	
D	5-4,245,213	AT5G13260	syn	Unknown protein		12	
D	5-4,500,202	AT5G13950	nonsyn	Unknown protein	A>G, 60	11	
G	5-4,797,923	AT5G14830	transposon	Retrotransposon		10	
G	5-6,508,329	AT5G19330	nonsyn	ARIA	C>W, 215	0	
G	5-11,090,365	AT5G29037	transposon	Gypsy		4	
G	5-12,312,975	AT5G32630	pseudogene	–		3	
G	5-12,358,159	AT5G32825	transposon	CACTA		2	
S	5-16,024,197	AT5G40020	intronic	Thaumatin superfamily		2	*

bioRxiv preprint doi: https://doi.org/10.1101/050203; this version posted October 5, 2017. The copyright holder for this preprint (which was not certified by peer review) is the author/funder, who has granted bioRxiv a license to display the preprint in perpetuity. It is made available under aCC-BY-NC-ND 4.0 International license.

845 †Traits with significant associations were root gravitropism (G), size (S), or low summer precipitation.

bioRxiv preprint doi: https://doi.org/10.1101/050203; this version posted October 5, 2017. The copyright holder for this preprint (which was not certified by peer review) is the author/funder, who has granted bioRxiv a license to display the preprint in perpetuity. It is made available under aCC-BY-NC-ND 4.0 International license.

846 # FIGURES

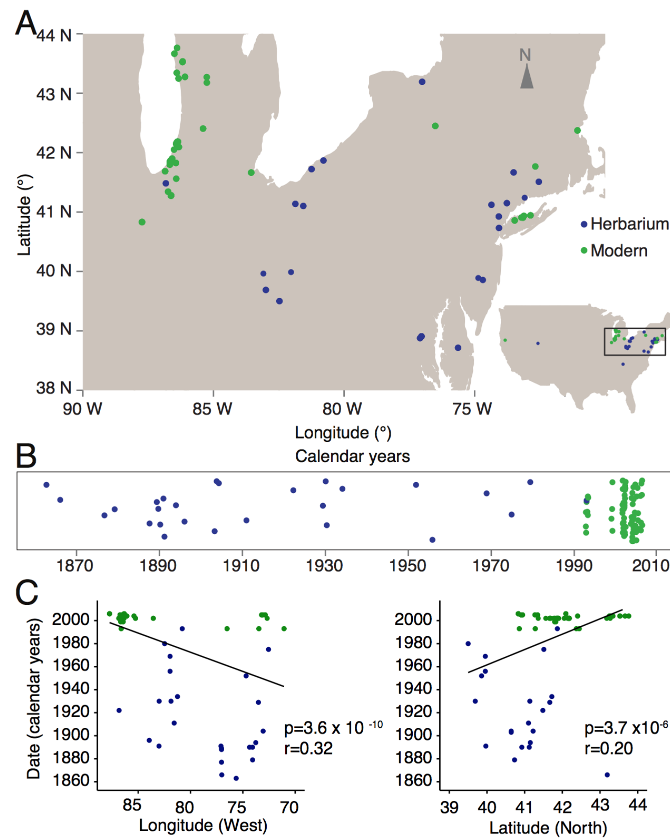

847

Figure 1. Geographic location and temporal distribution of HPG1 samples.

848 **(A)** Sampling locations of herbarium (blue) and modern individuals (green). **(B)** Temporal distribution of
849 samples (random vertical jitter for visualization purposes). **(C)** Linear regression of latitude and
850 longitude as a function of collection year (p-value of the slope and Pearson correlation coefficient are
851 indicated).

bioRxiv preprint doi: https://doi.org/10.1101/050203; this version posted October 5, 2017. The copyright holder for this preprint (which was not certified by peer review) is the author/funder, who has granted bioRxiv a license to display the preprint in perpetuity. It is made available under aCC-BY-NC-ND 4.0 International license.

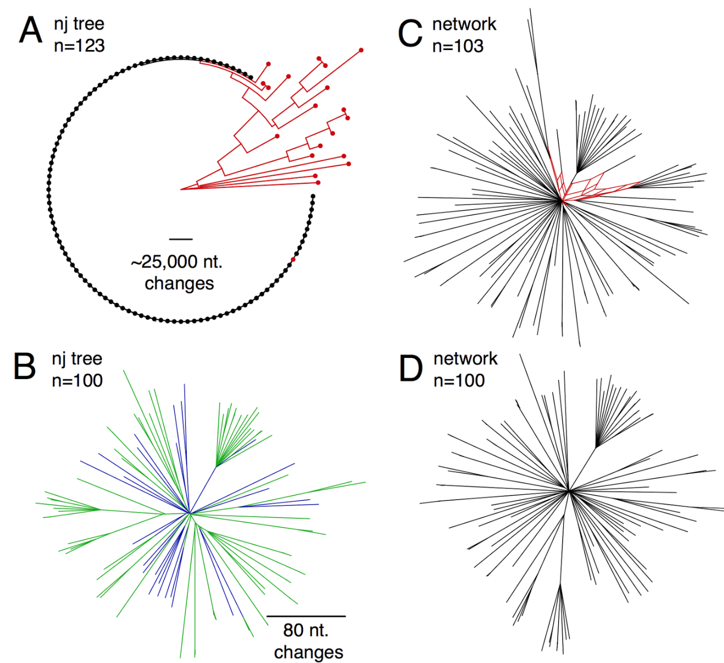

852 **Figure 2. Relationship among herbarium and modern samples.**

853 **(A)** Neighbor joining tree with all 123 samples (dots) and rooted with the most distant sample. The
854 black clade of almost-identical samples is the HPG1 lineage. Scale line shows the equivalent branch
855 length of over 25,000 nucleotide changes. **(B)** Neighbor joining tree only with the HPG1 black clade
856 from (A). Colors represent herbarium (blue) and modern individuals (green). Scale line shows the
857 equivalent branch length of 80 nucleotide changes. Note that no outgroup was included. **(C, D)**
858 Network of samples using the parsimony splits algorithm, before **(C)** and after **(D)** removing three
859 intra-HPG1 recombinants (in red). Note that the network algorithm returns in (D) a network devoid of
860 any reticulation, which indicates absence of intra-haplogroup recombination.

bioRxiv preprint doi: https://doi.org/10.1101/050203; this version posted October 5, 2017. The copyright holder for this preprint (which was not certified by peer review) is the author/funder, who has granted bioRxiv a license to display the preprint in perpetuity. It is made available under aCC-BY-NC-ND 4.0 International license.

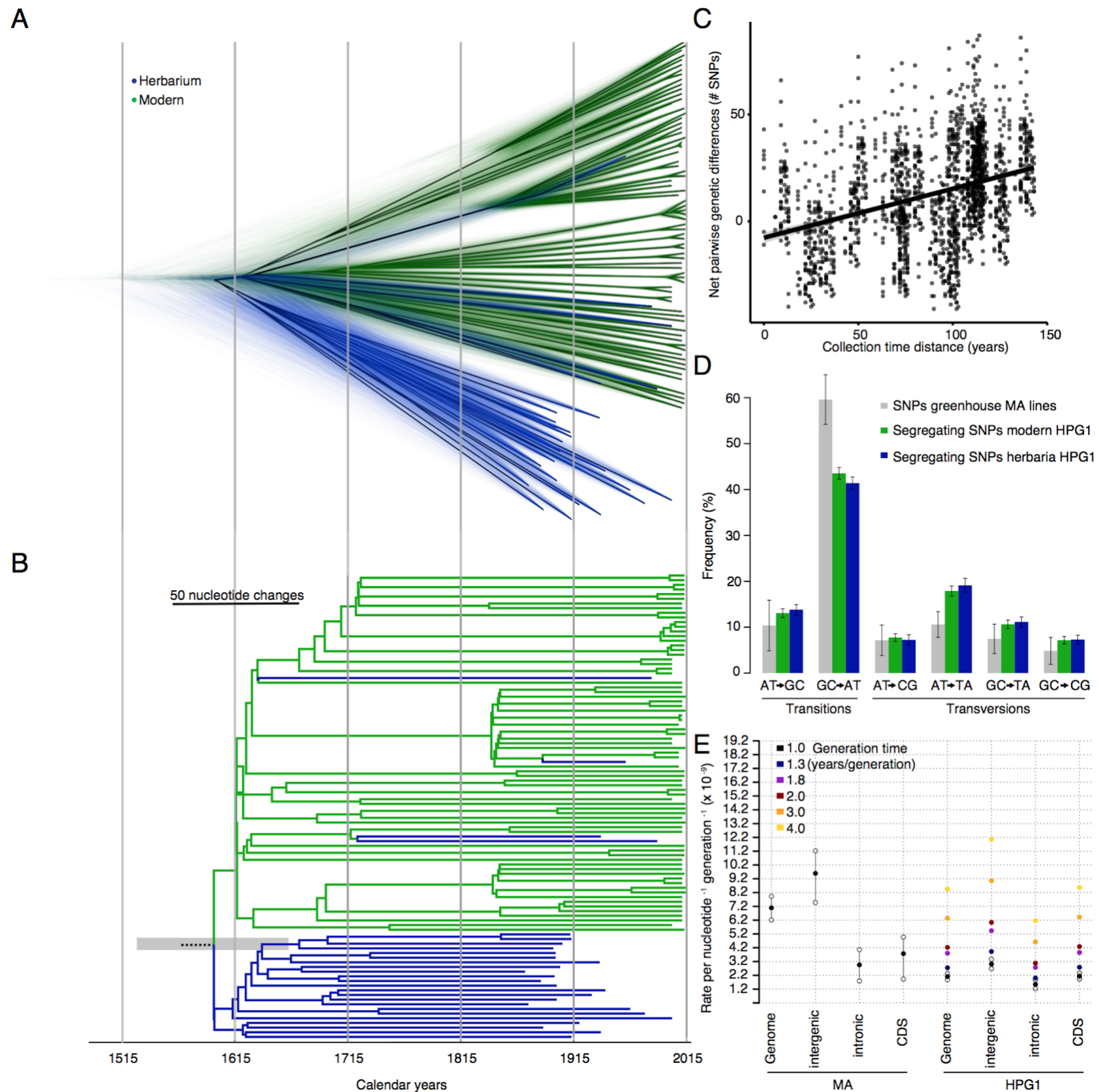

861 **Figure 3. Substitution rates.**

862 **(A)** Bayesian phylogenetic analyses employing tip-calibration. A total of 10,000 trees were superimposed
863 as transparent lines, and the most common topology was plotted solidly. Tree branches were calibrated
864 with their corresponding collection dates. **(B)** Maximum Clade Credibility (MCC) tree summarizing the

bioRxiv preprint doi: https://doi.org/10.1101/050203; this version posted October 5, 2017. The copyright holder for this preprint (which was not certified by peer review) is the author/funder, who has granted bioRxiv a license to display the preprint in perpetuity. It is made available under aCC-BY-NC-ND 4.0 International license.

865 trees in (A). Note the scale line shows the equivalent branch length of 50 nucleotide changes. The grey
866 transparent bar indicates the 95% Highest Posterior Probability of the root date. **(C)** Regression
867 between pairwise net genetic and time distances. The slope of the linear regression line corresponds to
868 the genome substitution rate per year. **(D)** Substitution spectra in HPG1 samples, compared to
869 greenhouse-grown mutation accumulation (MA) lines. **(E)** Comparison of genome-wide, intergenic,
870 intronic, and genic substitution rates in HPG1 and mutation rates in greenhouse-grown MA lines.
871 Substitution rates for HPG1 were re-scaled to a per generation basis assuming different generation
872 times. Confidence intervals in HPG1 substitution rates were obtained from 95% confidence intervals of
873 the slope from 1,000 bootstraps (Table S4 for actual values).

bioRxiv preprint doi: https://doi.org/10.1101/050203; this version posted October 5, 2017. The copyright holder for this preprint (which was not certified by peer review) is the author/funder, who has granted bioRxiv a license to display the preprint in perpetuity. It is made available under aCC-BY-NC-ND 4.0 International license.

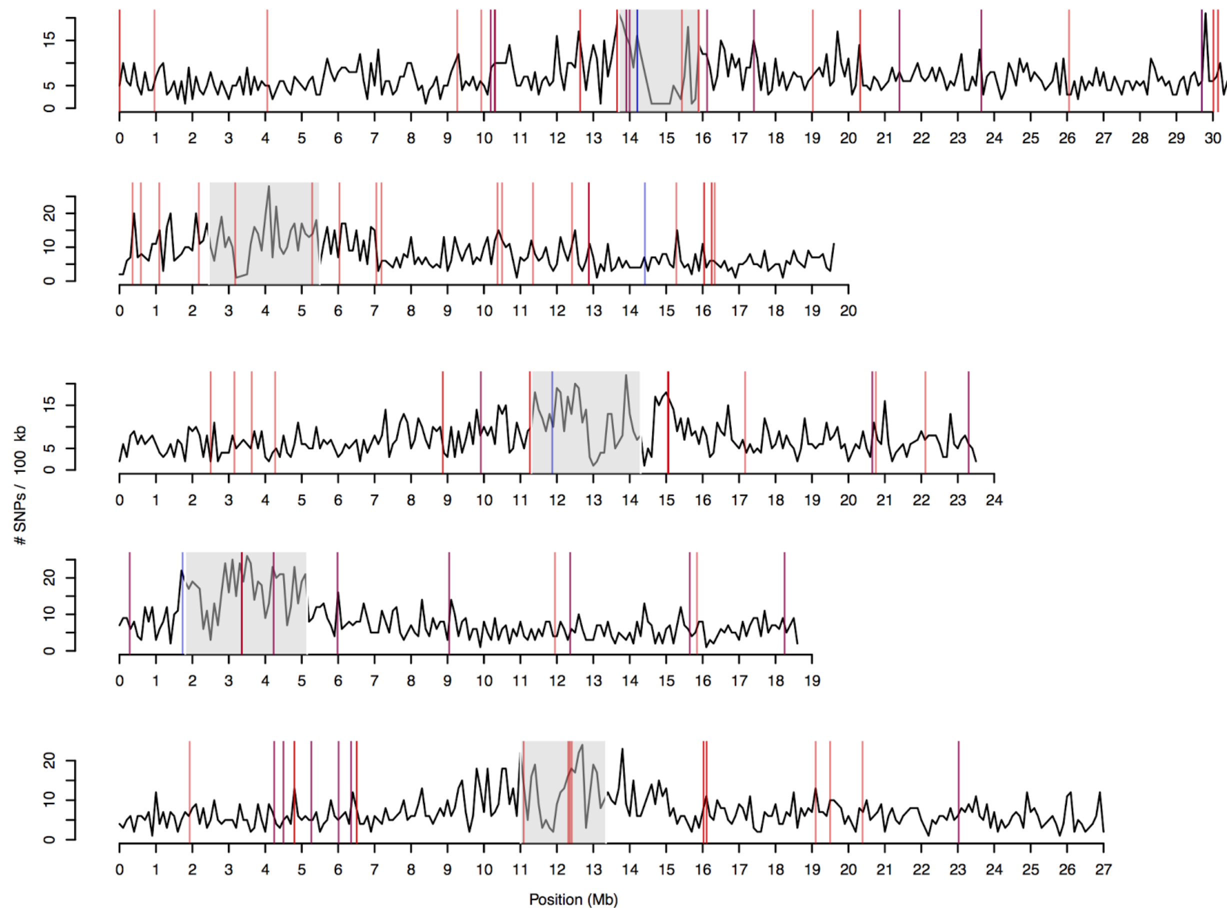

874 **Figure 4. Density of SNPs along all chromosomes and location of GWAS hits**

875 Black line shows number of SNPs per 100 kb window. Centromere locations are indicated by grey
876 shading. Vertical lines indicate SNPs associated with root phenotypes (red) and climatic variables (blue)
877 (Table 1 and Table S5).

bioRxiv preprint doi: https://doi.org/10.1101/050203; this version posted October 5, 2017. The copyright holder for this preprint (which was not certified by peer review) is the author/funder, who has granted bioRxiv a license to display the preprint in perpetuity. It is made available under aCC-BY-NC-ND 4.0 International license.

1 **Supplemental Information for Exposito-Alonso, Becker et al.:**

2
3 The rate and potential relevance of new mutations in a colonizing plant lineage

4 **SUPPLEMENTAL TEXT** 3
5 1. Sample collection and preparation 3
6 2. Authenticity of aDNA 3
7 3. SNP calling thresholds 3
8 4. Resequencing of Col-0 Mutation Accumulation lines 3
9 5. Identification of bona fide HPG1 accessions and mutations 4
10 5.1 HPG1 and other haplogroups in North America 4
11 5.2 North american private diversity 4
12 6. Extent of linkage disequilibrium and recombination 5
13 7. Substitution and mutation rate analyses 6
14 7.1 Greenhouse grown MA lines 6
15 7.2 Natural populations of HPG1 6
16 7.2.1 Net distances 6
17 7.2.2 Bayesian tip-calibration 7
18 7.2.3 Methylation status of mutated sites 7
19 8. Phenotypic association analyses and dating of newly arisen mutations 8
20 8.1. Phenotyping 8
21 8.1.1 Root 8
22 8.1.2 Seed size 8
23 8.1.3 Flowering in the growth chamber 9
24 8.1.4 Fecundity in the field 9
25 8.2 Quantitative genetic analyses 9
26 8.2.1 Heritability 10
27 8.2.2 Linear Models 10
28 8.2.3 Evaluation of significance 11
29 8.2.4 Context of de novo mutations associated with phenotypes 11
30 8.2.5 Functional information 11
31 8.2.6 Proof of concept examples 11
32
SUPPLEMENTAL REFERENCES 13
33
SUPPLEMENTAL TABLES 14
34
SUPPLEMENTAL FIGURES 15
35 Figure S1. Ancient-DNA characteristics of unrepaired herbarium libraries. 15
36 Figure S2. Separation between HPG1 and other North American lineages. 16
37 Figure S3. Substitution spectrum and rates. 17
38 Figure S4. Relationship between methylation and substitutions. 19
39 Figure S5. Comparison of Site Frequency Spectra across genomic annotations. 21

bioRxiv preprint doi: https://doi.org/10.1101/050203; this version posted October 5, 2017. The copyright holder for this preprint (which was not certified by peer review) is the author/funder, who has granted bioRxiv a license to display the preprint in perpetuity. It is made available under aCC-BY-NC-ND 4.0 International license.

40 Figure S5. Spatial and temporal emergence of root-associated mutations. 22
41 Figure S6. Linkage disequilibrium of significant SNPs. 23

bioRxiv preprint doi: https://doi.org/10.1101/050203; this version posted October 5, 2017. The copyright holder for this preprint (which was not certified by peer review) is the author/funder, who has granted bioRxiv a license to display the preprint in perpetuity. It is made available under aCC-BY-NC-ND 4.0 International license.

42 **SUPPLEMENTAL TEXT**

43 **1. Sample collection and preparation**

44 Seeds from modern accessions (Table S1) were bulked at the University of Chicago. Progeny for
45 DNA extraction was grown at the Max Planck Institute for Developmental Biology. We used 2 to 8
46 mm^2 of dried tissue for destructive sampling from the herbarium specimens (Table S1).

47 **2. Authenticity of aDNA**

48 First, unrepaired sequencing herbarium libraries were screened for authenticity by sequencing at low
49 coverage on Illumina HiSeq 2500 or MiSeq instruments. To verify the DNA retrieved from historical
50 samples of *A. thaliana* was authentic, we checked the percentage of endogenous DNA of the sample
51 (Fig. S1A) as well as typical postmortem DNA damages: high fragmentation of DNA (Fig. S1B),
52 enrichment of substitution from C to T at the first base pair (Fig. S1C) as well as purine enrichment
53 at breakpoints of DNA fragments (Fig. S1D) (for details see (1)). Sequencing to produce the final
54 genomes (101 bp paired end) was carried out on an Illumina HiSeq 2000 instrument after DNA
55 repair by uracil-DNA glycosylase (2–4). For a detailed analysis of authenticity in a fraction of our
56 samples, see Weiss et al. (1).

57 **3. SNP calling thresholds**

58 To assess the effect of SNP calling thresholds on the mutation rate, we employed three different
59 SHORE v0.9.0 quality thresholds following previous work (see Table S4 from (5)): allowing at most
60 one intermediate penalty in all strains (most stringent threshold; "32-32"); requesting that at least
61 one strain had at most one intermediate penalty, while all others were allowed up to two high and
62 one intermediate penalties (intermediate stringency, "32-15"); and finally allowing one high and one
63 intermediate penalty for all strains (most lenient stringency, "24-24"). On top of that, we would
64 either allow missing information per SNP in up to 50% of accessions, or request complete
65 information (0% missing rate). Thus, the most rigorous case would be 32-32 quality and 0% missing
66 rate, and the most relaxed 24-24 quality and 50% maximum missing rate. Substitution rate
67 calculations (section 7.2) were done for datasets from all combinations of these quality parameters
68 (Fig. S3), and we chose the regular 32_15 quality threshold and complete information for the final
69 estimate (Fig 3 C, E).

70 **4. Resequencing of Col-0 Mutation Accumulation lines**

71 We also sequenced the genomes of twelve greenhouse-grown mutation accumulation (MA) lines,
72 including ten that had been sequenced at lower coverage before (5,6) (Table S2). We called SNPs,
73 indels and structural variants (SVs), following the workflow and parameters described (7), but

bioRxiv preprint doi: https://doi.org/10.1101/050203; this version posted October 5, 2017. The copyright holder for this preprint (which was not certified by peer review) is the author/funder, who has granted bioRxiv a license to display the preprint in perpetuity. It is made available under aCC-BY-NC-ND 4.0 International license.

74 without iterations. This procedure resulted in 2,203 polymorphisms shared by all lines, indicating
75 errors in the reference sequence (12% of variants replaced N's in the TAIR9 genome) or genetic
76 differences in the founder plant of the MA population compared to the Col-0 reference genome. In
77 addition, we identified 388 segregating variants across the twelve lines (Table S2), of which 350 were
78 singletons. This analysis revealed on average 25.5 SNPs, 4.9 deletions and 3.2 insertions per MA line
79 at the 31st generation (Table S2), compared to 19.6 SNPs, 2.4 deletions and 1.0 insertions previously
80 detected in the 30th generation with shorter read length and lower read depth (8). The genome
81 length accessed in this sequencing effort, 115,954,227 bp, was used to scale the number of point
82 mutations to a rate of 7.1 x 10^{-9} mutations site^{-1} generation^{-1} (Table S3, Fig. 3E).

83 **5. Identification of *bona fide* HPG1 accessions and mutations**

84 **5.1 HPG1 and other haplogroups in North America**

85 The modern samples had been originally selected based on previous genotyping efforts of about
86 2,000 N. American accessions with for 149 nuclear, intermediate-frequency SNPs. This work had
87 pointed to there being a single haplogroup, HPG1, that was invariant at these 149 markers and that
88 accounted for about half of N. American individuals genotyped (9). We extracted from the 123
89 genomes we had completely sequenced the same 149 SNPs and built a neighbour joining tree (Fig.
90 S1A). We also built the same tree with the whole-genome sequences (Fig. S1B), which was mostly in
91 agreement with the 149 SNP tree.

92 The previous work had identified several other haplogroup in N. America (9). Not
93 surprisingly, HPG1 individuals outcross with other lineages, and this accounts for some of the
94 individuals which we later removed, because they did not agree completely in all 149 markers with
95 the HPG1 consensus.

96 **5.2 North american private diversity**

97 Having identified these *bona fide* HPG1 individuals, we wanted to confirm that the diversity has a
98 legitimate origin from *de novo* mutations. For that we used the 1001 Genomes resource
99 (www.1001genomes.org), which covers a sampling of populations from the native Eurasian and
100 African range. Subsetting the genomes from this resource to only European accessions, and limiting
101 the SNP set to those with ≥1% frequency of alternative alleles and a maximum of 50% missing data
102 (the same quality rate as our HPG1 SNP call), there were 300 variants out of all 5,181 HPG1 variants
103 that were also found in Europe or Asia (5.7%). Changing the maximum missing data to 10% we get a
104 more conservative estimate of 1.8% overlap, while increasing the maximum missing data to 90%, we
105 get the anti-conservative estimate of 6.5% overlap. Only one of the reported SNPs associated with
106 phenotypes (see Section 8) was among these shared variants.

bioRxiv preprint doi: https://doi.org/10.1101/050203; this version posted October 5, 2017. The copyright holder for this preprint (which was not certified by peer review) is the author/funder, who has granted bioRxiv a license to display the preprint in perpetuity. It is made available under aCC-BY-NC-ND 4.0 International license.

107 There are several scenarios that can explain these shared SNPs. One is simply that there was
108 not a single founding seed, but a few of closely related individuals coming from the native range.
109 Other explanations are that parallel mutations occurred in North America and Eurasia, that HPG1
110 individuals were reintroduced to Europe, or that reversion-mutation occurred in some HPG1
111 individuals. The latter is not implausible given the large population size of the species and the fact
112 that about 10% of all sites in the genome are SNPs in the 1001 Genomes collection. As explained in
113 the main text, SNP sharing due to admixture with other lineages is extremely unlikely, as such cases
114 should be evident as blocks of high SNP diversity along the genome (Fig. 4).
115 Finally, regarding chloroplast diversity, we did not find any SNP in the chloroplast of HPG1
116 individuals. This is probably because chloroplast mutation rates are much slower (10) and because
117 the founder colonizers actually came from a small batch of seeds from an identical mother
118 (chloroplast diversity in the native range is of 2,842 SNPs (11)).

119 **6. Extent of linkage disequilibrium and recombination**

120 We estimated pairwise linkage disequilibrium (LD) between all possible combinations of informative
121 sites, ignoring singletons, by computing r^2, *D* and *D'* statistics. LD decay was estimated using a linear
122 regression approach. Linkage disequilibrium parameter |*D'*| did not decay with physical distance
123 (intercept = 0.99, slope = 0.00) among all SNP pairs. Indeed 99.975% of pairwise SNP comparisons
124 had |*D'*|=1 meaning that 99.975% of those comparisons only three out of the four possible gametes
125 (ab, aB, Ab, AB) are found and thus mutation alone can explain their existence without the need of
126 invoking recombination. In other words, such three gametes can be represented in a tree structure.
127 LD and recombination related statistics were determined using DnaSP v5 (12).

128 **7. Substitution and mutation rate analyses**

129 <u>7.1 Greenhouse grown MA lines</u>

130 Mutation rates were estimated for each 31st generation greenhouse-grown MA line (5) as the
131 number of mutations divided by the total bp length of the genome (or a given annotation) and by 31
132 generations (the two MA lines with only three generations were excluded from this analysis). Mean
133 and confidence intervals across lines are reported (Table S3). The genome length was determined as
134 all base pairs with coverage higher or equal to 3, and a SHORE mapping quality score of at least 32 in
135 one sample (Table S2).

bioRxiv preprint doi: https://doi.org/10.1101/050203; this version posted October 5, 2017. The copyright holder for this preprint (which was not certified by peer review) is the author/funder, who has granted bioRxiv a license to display the preprint in perpetuity. It is made available under aCC-BY-NC-ND 4.0 International license.

136 ## 7.2 Natural populations of HPG1

137 ### *7.2.1 Net distances*

138 For the "net genetic distances" method, we computed confidence intervals of the *b* regression slope
139 coefficient ($D' = a+bT'$) using a bootstrap with replacement of 1,000 samples to avoid over-confident
140 confidence intervals due to lack of independence of points (13). We used either all SNPs or SNPs at
141 specific annotations to calculate different substitution rates and scaled the slope into a per-base rate
142 using all positions (of the given annotation) that passed alternative or reference call quality thresholds
143 rather than using a single value of genome length (Table S3). For all annotations we calculated
144 substitution rates with three quality thresholds and either full information per SNP or allowing a
145 maximum of 50% missing accessions per SNP (see Section 3 and Fig. S1C).

146 For some annotations substitution rates were not reliable. For instance, in 3' and 5' UTR
147 regions, we did not have enough mutations (on average ~1 SNP difference between any pair), and
148 thus do not report these regions' rates. We could also have less power to discover SNPs in
149 annotations with extensive structural variation such as active transposable elements (14).
150 Transposons, which comprise ~8% of the genome and ~19% of all the SNPs in greenhouse MA lines,
151 had fewer SNPs called than expected in HPG1. This would explain the atypically low transposon
152 substitution rate (Table S3). Therefore, transposon substitution rates in HPG1 cannot be trusted.

153 ### *7.2.2 Bayesian tip-calibration*

154 For the second approach to estimate a substitution rate, the Bayesian phylogenetics tip-calibration
155 approach, we performed systematic runs and chain convergence assessments of different
156 demographic and molecular clock models. We found the Skygrid demographic model (15) and the
157 lognormal relaxed molecular clock (16) the most appropriate models. Under a relaxed molecular
158 clock, the substitution rate is allowed to vary across branches with a lognormal distribution. The
159 prior used for molecular clock was a Continuous-Time Markov Chain (CTMC) (15,17). The analysis
160 was carried out remotely at CIPRES PORTAL (v3.1 www.phylo.org) using uninformative priors. The
161 run took about 1,344 CPU hours and performed 1,000 million steps in a Monte Carlo Markov Chain
162 (MCMC), sampling every 100,000 steps. Burn-in was adjusted to 10% of the steps. To visualize the
163 tree output we produced a Maximum Clade Credibility (MCC) tree with a minimum posterior
164 probability threshold of 0.8 and a 10% burn-in using TreeAnnotator (part of BEAST package), and
165 visualized the MCC tree using FigTree (tree.bio.ed.ac.uk/software/figtree/) (Fig. 3B). Additionally, we
166 used DensiTree (18) to simultaneously draw the 10,000 BEAST trees with the highest posterior
167 probability (Fig. 3A). Since all trees were drawn transparently, agreements in both topology and
168 branch lengths appear as densely colored regions, while areas with little agreement appear lighter.

bioRxiv preprint doi: https://doi.org/10.1101/050203; this version posted October 5, 2017. The copyright holder for this preprint (which was not certified by peer review) is the author/funder, who has granted bioRxiv a license to display the preprint in perpetuity. It is made available under aCC-BY-NC-ND 4.0 International license.

169 *7.2.3 Methylation status of mutated sites*

170 As in many other species, the spectrum of *de novo* mutations in the greenhouse-grown *A. thaliana*
171 MA lines is biased towards G:C→A:T transitions (8), leading to an inflated transition-to-transversion
172 ratio (Ts/Tv). This bias is less pronounced in recent mutations in a Eurasian collection of natural
173 accessions (Fig. 5A of (19) and in HPG1 accessions (Fig. 3D). A recent multigenerational salt stress
174 experiment in the greenhouse also showed a more balanced Ts/Tv (20). These findings indicate that
175 less benign conditions might promote a lower Ts/Tv, and one possible cause are methylation
176 patterns, known to change under different environments (21).

177 We interrogated the potential evolutionary role of cytosine methylation in the mutability of
178 cytosine bases in the HPG1 accessions. For reference DNA methylation data, we used previously
179 generated bisulfite-sequencing data of HPG1 strains (7) and of Col-0 MA lines (5), respectively. For
180 both datasets, methylation status was calculated as the fraction of reads with methylated cytosines by
181 the total number of reads at a certain cytosine position in the genome. Our rationale was that if
182 methylation affected mutability, the degree of methylation at positions were we find a new mutation
183 should be higher. To be sure that a given site in HPG1 was a new mutation, we only considered
184 positions for which we could determine that state by alignment to the *A. lyrata* genome (22). The
185 "tested sites" were positions in HPG1 that had a mutation both from *A. lyrata* and *A. thaliana* Col-0.
186 These positions can be of two kinds, "fixed" if all HPG1 individuals carry the alternative, or
187 "segregating" if both reference and alternative alleles exist in HPG1. As control, "control set", we
188 used cytosine positions that did not vary across HPG1, *A. lyrata* and *A. thaliana*. To produce the
189 methylation distribution of the control set we randomly chose 1,000 invariant cytosine positions. For
190 the test sets, we averaged the methylation degree and compared it with the control distribution.

191 Ancestral cytosines with higher methylation in both *A. thaliana* Col-0 reference and HPG1
192 pseudo-reference methylome datasets were more likely to mutate to thymines in HPG1 (Fig. S2
193 A-D). Additionally, the methylation degree at substitutions inside genes was higher in the HPG1
194 methylome (Fig. S2 B,D). While some C→T changes could be explained by higher spontaneous
195 deaminations known to happen more often at methylated cytosines, also C→A/G substitutions were
196 more likely to have been methylated. If this process is common enough, the Ts/Tv ratio should
197 decrease. We are far from understanding differences in Ts/Tv in natural and controlled conditions,
198 but definitely methylation status seems to have a strong statistical connection with mutability.

bioRxiv preprint doi: https://doi.org/10.1101/050203; this version posted October 5, 2017. The copyright holder for this preprint (which was not certified by peer review) is the author/funder, who has granted bioRxiv a license to display the preprint in perpetuity. It is made available under aCC-BY-NC-ND 4.0 International license.

199 **8. Phenotypic association analyses and dating of newly arisen mutations**

200 8.1. Phenotyping

201 *8.1.1 Root*

202 Fifteen root phenotypes were scored for ≥ 10 replicates per genotype over a time-series experiment
203 at the Gregor Mendel Institute in Vienna, using image analysis as described in detail elsewhere (23).
204 We used the means per genotypes and per time series for association analyses.

205 *8.1.2 Seed size*

206 We spread the seeds of given genotypes on separate plastic square 12 x 12 cm Petri dishes. For
207 faster image acquisition we used a cluster of eight Epson V600 scanners. The scanner cluster was
208 operated by the BRAT Multiscan image acquisition tool
209 (www.gmi.oeaw.ac.at/research-groups/wolfgang-busch/resources/brat/). The resulting 1600 dpi images
210 were analyzed in Fiji software. Scans were converted to 8-bit binary images, thresholded
211 (parameters: setAutoThreshold("Default dark"); setThreshold(20, 255)) and particles analyzed
212 (inclusion parameters: size=0.04-0.25 circularity=0.70-1.00). The 2D seed size was measured in
213 square millimeters (parameters: distance=1600 known=25.4 pixel=1 unit=mm) for 2 plants per
214 genotype, > 500 seeds per plant.

215 *8.1.3 Flowering in the growth chamber*

216 We estimated the flowering time in growth chambers under four vernalization treatments (0, 14, 28
217 and 63 days of vernalization). We grew 6 replicates per accession divided between two complete
218 randomized blocks for each treatment. Seeds were sown on a 1:1 mixture of Premier Pro-Mix and
219 MetroMix and cold stratified for 6 days (6°C, no light). We then let plants germinate and grow at
220 18°C, 14 hours of light, 65% humidity. After 3 weeks, we transferred the plants to vernalization
221 conditions (6°C, 8 hours of light, 65% humidity). After vernalization, plants were transferred back to
222 long day conditions. Trays were rotated around the growth chambers every other day throughout
223 the experiment, under both vernalization and ambient conditions. Germination, bolting and flowering
224 dates were recorded every other day until all plants had flowered. Days till flowering or bolting times
225 were calculated from the germination date until the first flower opened and until the first flower bud
226 was developed, respectively. The average flowering time and bolting time per genotype were used for
227 association analyses.

bioRxiv preprint doi: https://doi.org/10.1101/050203; this version posted October 5, 2017. The copyright holder for this preprint (which was not certified by peer review) is the author/funder, who has granted bioRxiv a license to display the preprint in perpetuity. It is made available under aCC-BY-NC-ND 4.0 International license.

228 *8.1.4 Fecundity in the field*

229 To investigate variation in fecundity in natural conditions, we grew three replicates of each accession
230 in a field experiment following a completely randomized block design. Seeds were sown from
231 09/20/2012 to 09/22/2012 in 66-well trays (well diameter = 4 cm) on soil from the field site where
232 plants were to be transplanted. The trays were cold stratified for seven days before being placed in a
233 cold frame at the University of Chicago (outdoors, no additional light or heat, but watered as needed
234 and protected from precipitation). Seedlings were transplanted directly into tilled ground at the
235 Warren Wood field station (41.84° N., 86.63° W.), Michigan, USA on 10/13/2012 and 10/14/2012.
236 Seedlings were watered-in and left to overwinter without further intervention. Upon maturation of
237 all fruits, stems were harvested and stored between sheets of newsprint paper. To estimate the
238 fecundity, stems were photographed on a black background and the size of each plant was estimated
239 as the number of pixels occupied by the plant on the image. This measure correlates well with the
240 total length of siliques produced, a classical estimator of fecundity in *A. thaliana* (Spearman's
241 rho=0.84, *p*-value<0.001, data not shown).

242 8.2 Quantitative genetic analyses

243 For 63 modern accessions, we measured time to bolting and flowering, seeds per plant, seed size,
244 and 15 root phenotypes in common chamber or common garden settings. For all 100 accessions,
245 climatic information from the bioclim database (www.worldclim.org/bioclim) was extracted using
246 their geographic coordinates. For historic samples, some locations were only known by county
247 name. In this case we assigned the geographic coordinate location of the centroid of the county.

248 *8.2.1 Heritability*

249 We performed association analyses using the R package GenABEL (24), with measured phenotypes
250 (p = 25) and climatic variables (c = 18) as response variables and SNPs as explanatory variables. A
251 Minimum Allele Frequency (MAF) cutoff of 5% was used. The number of assessed SNPs was 391 in a
252 dataset of only modern samples but with imputed genotypes for missing data using Beagle v4.0 (25),
253 and 456 SNPs with a dataset of modern and historic samples, without imputation. For all
254 associations, at least 63 individuals were genotyped for a specific SNP. We first investigated broad
255 sense heritability (H^2) of each trait using ANOVA partition of variance between and within lines using
256 replicates (Table S4). Significance was obtained by common F test in ANOVA. Secondly we used the
257 *polygenic_hglm* function to fit a genome wide kinship matrix to calculate a narrow sense heritability
258 estimate (h^2). This fits a model of the type $y = Zu + \varepsilon$ (see Main text Methods). Significance was
259 calculated employing a likelihood ratio test comparing with a null model. In principle, h^2 is a
260 component of H^2, then its values should theoretically be $h^2 < H^2$. That is not our case. Our result

bioRxiv preprint doi: https://doi.org/10.1101/050203; this version posted October 5, 2017. The copyright holder for this preprint (which was not certified by peer review) is the author/funder, who has granted bioRxiv a license to display the preprint in perpetuity. It is made available under aCC-BY-NC-ND 4.0 International license.

261 cannot be interpreted in this framework, since the calculation of both was not done with the same
262 samples: for the h^2 calculation we employed genotype means whereas for the H^2 we used multiple
263 replicated measurements per genotype. The averaging of replicates per genotype in h^2 reduced
264 environmental and developmental noise and thus we would expect $h^2>H^2$. We did this so the climatic
265 estimates of h^2, for which we only have one value per genotype, would be comparable with the
266 phenotypic h^2 ones (Table S4).

267 *8.2.2 Linear Models*

268 For association analyses we first employed a linear mixed model that fitted the kinship matrix using
269 the *mmscore* function. This model is of the type: $y = Xb + Zu + \varepsilon$ (see Main text Methods) (26).
270 Only three significant SNP hits were discovered using a 5% significance threshold after False
271 Discovery Rate correction (FDR). This was expected since we have few variants and these would
272 have originated in an approximated phylogeny structure. We concluded that fitting the kinship matrix
273 in our model was not appropriate since there would be no residual variation for association with
274 specific SNPs. With this rationale we employed a fixed effects linear model using the *qtscore* function
275 (27). This model is of the type: $y = Xb + \varepsilon$; where no random effect of genome background is fit. To
276 reduce the risk of having false-positives, we took a conservative permutation strategy by carrying out
277 association with over 1,000 randomized datasets (permuting phenotypes across individuals) and used
278 the resulting empirical p-value distribution to correct p-values estimated with the original dataset.
279 SNPs with p-values below 5% in the empirical p-value distribution should be considered significant
280 (but see next section). In climatic models, we included longitude and latitude as covariates to correct
281 for any spurious association between SNPs and climate gradients created by the migratory pattern of
282 isolation by distance.

283 *8.2.3 Evaluation of significance*

284 Significant SNPs were interspersed throughout the genome (Fig. 4) and their p-values and phenotypic
285 effects did not correlate with the minimum age of the SNPs nor with their allele frequency,
286 something that could have indicated that the significance was merely driven by the higher statistical
287 power of intermediate frequency variants. Using QQ plots to assess inflation or deflation of p-values,
288 we observed generally that permutation corrected p-values were deflated — another evidence of
289 our conservative strategy. Straight horizontal series of points in QQ plots indicate that multiple
290 SNPs have identical p-values, a pattern that we attributed to long range LD, i.e. lack of independence
291 (see Data Appendix S1 for trait distributions and QQ plots from each association analysis).

bioRxiv preprint doi: https://doi.org/10.1101/050203; this version posted October 5, 2017. The copyright holder for this preprint (which was not certified by peer review) is the author/funder, who has granted bioRxiv a license to display the preprint in perpetuity. It is made available under aCC-BY-NC-ND 4.0 International license.

292 To further ensure that we avoided false positive results, we also prioritized SNPs whose
293 empirical p-value was not below 5% only but also below 5% / (number of SNPs + number of traits) =
294 0.01%. This "double" Bonferroni correction was very conservative (Table 1, Table S5).

295 *8.2.4 Context of de novo mutations associated with phenotypes*

296 For each SNP in our dataset, we determined the ancestral and derived states, by identifying which
297 allele was found in the oldest herbarium samples. We compared the time of emergence and the
298 centroid of geographic distribution of the alternative alleles of SNP hits to random draws of SNPs
299 with the same MAF filtering (5%) (Fig. S1).

300 *8.2.5 Functional information*

301 On top of phenotypic and climatic associations of SNP hits, we also provide a likely functional effect
302 employing a commonly used amino acid matrix of biochemical effects (28). Functional information of
303 gene name and ontology categorization of SNP hits was obtained from
304 www.arabidopsis.org/portals/genAnnotation/gene_structural_annotation/annotation_data.jsp and
305 www.arabidopsis.org/tools/bulk/go/ (Table 1 and Table S5).

306 *8.2.6 Proof of concept examples*

307 We argue that the power of our association approach relies on the fact that HPG1 lines resemble
308 Near Isogenic Lines (NILs) produced by experimental crosses (29) (Fig. S2A). Similar to
309 genome-wide association studies (GWA), power depends on many factors, namely the noise of
310 phenotype under study, architecture of phenotypic trait, quality of genotyping, population structure,
311 sample diversity, sample size, allele frequency, and recombination. On one hand, association analyses
312 in NILs suffer from large linkage blocks, but confident results can be achieved due to accurate
313 measurement of phenotypes, limited genetic differences between any two lines, and high quality
314 genotypes. In common GWA studies such as in humans, there are multiple confounding effects.
315 Among the confounders are (1) that any two samples differ in hundreds of thousands of SNPs, and
316 (2) that historical and geographic stratification produce non-random correlations among those SNP
317 differences. This considerably complicates the identification of phenotypic effects at specific genes,
318 and power relies greatly on large sample sizes to achieve the sufficient number of recombination
319 between markers.

320 To provide support for the non-synonymous SNP on chromosome 5, at position 6,508,329
321 in AT5G19330, we looked for pairs of lines that carry the ancestral and the derived allele, but that
322 differ in few (or no other) SNPs in the genome. When considering all genic substitutions with a
323 minimum allele frequency of 5% (Fig. S2A), we identified 20 pairs of lines differing only in the

bioRxiv preprint doi: https://doi.org/10.1101/050203; this version posted October 5, 2017. The copyright holder for this preprint (which was not certified by peer review) is the author/funder, who has granted bioRxiv a license to display the preprint in perpetuity. It is made available under aCC-BY-NC-ND 4.0 International license.

324 AT5G19330 SNP and another linked SNP (located on a different chromosome, association p-value >
325 0.4). The phenotypic differences in mean gravitropic score of these almost-identical pairs were
326 significantly higher than phenotypic differences among all pairs of HPG1 lines, and genetically identical
327 pairs attending to substitutions inside genes (Fig. S2A). Furthermore, this SNP was not in complete
328 linkage with any other SNP hit ($r^2 < 0.5$) (Fig. S2D). The same approach was used to examine the
329 SNPs in AT1G54440 (Fig. S2E) and AT2G16580 (Fig. S2F), which represent an intermediate and a high
330 LD example.

bioRxiv preprint doi: https://doi.org/10.1101/050203; this version posted October 5, 2017. The copyright holder for this preprint (which was not certified by peer review) is the author/funder, who has granted bioRxiv a license to display the preprint in perpetuity. It is made available under aCC-BY-NC-ND 4.0 International license.

331 **SUPPLEMENTAL REFERENCES**

332 1. Weiß CL, Schuenemann VJ, Devos J, Shirsekar G, Reiter E, Gould BA, et al. Temporal patterns
333 of damage and decay kinetics of DNA retrieved from plant herbarium specimens. Royal Society
334 Open Science. 2016 Jun 1;3(6):160239.

335 2. Meyer M, Kircher M. Illumina sequencing library preparation for highly multiplexed target
336 capture and sequencing. Cold Spring Harb Protoc. 2010 Jun;2010(6):db.prot5448.

337 3. Briggs AW, Stenzel U, Meyer M, Krause J, Kircher M, Pääbo S. Removal of deaminated cytosines
338 and detection of in vivo methylation in ancient DNA. Nucleic Acids Res. 2010 Apr;38(6):e87.

339 4. Kircher M. Analysis of High-Throughput Ancient DNA Sequencing Data. In: Shapiro B, Hofreiter
340 M, editors. Ancient DNA. Humana Press; 2011. p. 197–228. (Methods in Molecular Biology).

341 5. Becker C, Hagmann J, Müller J, Koenig D, Stegle O, Borgwardt K, et al. Spontaneous epigenetic
342 variation in the Arabidopsis thaliana methylome. Nature. 2011 Dec 8;480(7376):245–9.

343 6. Shaw RG, Byers DL, Darmo E. Spontaneous mutational effects on reproductive traits of
344 arabidopsis thaliana. Genetics. 2000 May;155(1):369–78.

345 7. Hagmann J, Becker C, Müller J, Stegle O, Meyer RC, Wang G, et al. Century-scale methylome
346 stability in a recently diverged Arabidopsis thaliana lineage. PLoS Genet.
347 2015;11(1):e1004920–e1004920.

348 8. Ossowski S, Schneeberger K, Lucas-Lledó JI, Warthmann N, Clark RM, Shaw RG, et al. The rate
349 and molecular spectrum of spontaneous mutations in Arabidopsis thaliana. Science. 2010 Jan
350 1;327(5961):92–4.

351 9. Platt A, Horton M, Huang YS, Li Y, Anastasio AE, Mulyati NW, et al. The scale of population
352 structure in Arabidopsis thaliana. PLoS Genet. 2010 Feb;6(2):e1000843.

353 10. Wolfe KH, Sharp PM, Li W-H. Rates of synonymous substitution in plant nuclear genes. J Mol
354 Evol. 1989 Sep;29(3):208–11.

355 11. 1001 Genomes Consortium. 1,135 Genomes Reveal the Global Pattern of Polymorphism in
356 Arabidopsis thaliana. Cell. 2016 Jul 14;166(2):481–91.

357 12. Librado P, Rozas J. DnaSP v5: a software for comprehensive analysis of DNA polymorphism
358 data. Bioinformatics. 2009 Jun 1;25(11):1451–2.

359 13. Drummond A, Pybus OG, Rambaut A. Inference of viral evolutionary rates from molecular
360 sequences. Adv Parasitol. 2003;54:331–58.

361 14. Treangen TJ, Salzberg SL. Repetitive DNA and next-generation sequencing: computational
362 challenges and solutions. Nat Rev Genet. 2012 Jan;13(1):36–46.

363 15. Gill MS, Lemey P, Faria NR, Rambaut A, Shapiro B, Suchard M a. Improving Bayesian population
364 dynamics inference: a coalescent-based model for multiple loci. Mol Biol Evol. 2012
365 Mar;30(3):713–24.

366 16. Drummond AJ, Ho SYW, Phillips MJ, Rambaut A. Relaxed phylogenetics and dating with
367 confidence. PLoS Biol. 2006 May;4(5):e88–e88.

bioRxiv preprint doi: https://doi.org/10.1101/050203; this version posted October 5, 2017. The copyright holder for this preprint (which was not certified by peer review) is the author/funder, who has granted bioRxiv a license to display the preprint in perpetuity. It is made available under aCC-BY-NC-ND 4.0 International license.

368 17. Ferreira M a. R, Suchard M a. Bayesian analysis of elapsed times in continuous-time Markov
369 chains. Can J Stat. 2008 Sep;36(3):355–68.

370 18. Bouckaert RR. DensiTree: making sense of sets of phylogenetic trees. Bioinformatics. 2010 May
371 15;26(10):1372–3.

372 19. Cao J, Schneeberger K, Ossowski S, Günther T, Bender S, Fitz J, et al. Whole-genome
373 sequencing of multiple Arabidopsis thaliana populations. Nat Genet. 2011 Oct;43(10):956–63.

374 20. Jiang C, Mithani A, Belfield EJ, Mott R, Hurst LD, Harberd NP. Environmentally responsive
375 genome-wide accumulation of de novo Arabidopsis thaliana mutations and epimutations.
376 Genome Res. 2014 Nov;24(11):1821–9.

377 21. Wibowo A, Becker C, Marconi G, Durr J, Price J, Hagmann J, et al. Hyperosmotic stress
378 memory in Arabidopsis is mediated by distinct epigenetically labile sites in the genome and is
379 restricted in the male germline by DNA glycosylase activity. eLife. 2016 May 31;5:e13546.

380 22. Hu TT, Pattyn P, Bakker EG, Cao J, Cheng J-F, Clark RM, et al. The Arabidopsis lyrata genome
381 sequence and the basis of rapid genome size change. Nat Genet. 2011 May;43(5):476–81.

382 23. Slovak R, Göschl C, Su X, Shimotani K, Shiina T, Busch W. A scalable open-source pipeline for
383 large-scale root phenotyping of Arabidopsis. Plant Cell. 2014 Jun 10;26(6):2390–403.

384 24. Aulchenko YS, Ripke S, Isaacs A, van Duijn CM. GenABEL: an R library for genome-wide
385 association analysis. Bioinformatics. 2007 May 15;23(10):1294–6.

386 25. Browning BL, Browning SR. Genotype Imputation with Millions of Reference Samples. Am J
387 Hum Genet. 2016 Jan 7;98(1):116–26.

388 26. Wilson AJ, Réale D, Clements MN, Morrissey MM, Postma E, Walling CA, et al. An ecologist's
389 guide to the animal model. J Anim Ecol. 2010 Jan;79(1):13–26.

390 27. Aulchenko YS, de Koning D-J, Haley C. Genomewide rapid association using mixed model and
391 regression: a fast and simple method for genomewide pedigree-based quantitative trait loci
392 association analysis. Genetics. 2007 Sep;177(1):577–85.

393 28. Grantham R. Amino acid difference formula to help explain protein evolution. Science. 1974 Sep
394 6;185(4154):862–4.

395 29. Weigel D. Natural variation in Arabidopsis: from molecular genetics to ecological genomics.
396 Plant Physiol. 2012 Jan;158(1):2–22.

bioRxiv preprint doi: https://doi.org/10.1101/050203; this version posted October 5, 2017. The copyright holder for this preprint (which was not certified by peer review) is the author/funder, who has granted bioRxiv a license to display the preprint in perpetuity. It is made available under aCC-BY-NC-ND 4.0 International license.

397 **SUPPLEMENTAL TABLES**

398 **Table S1.** HPG1 sample information.

399 **Table S2.** Sample information for Col-0 mutation accumulation lines.

400 **Table S3.** Mutation rate estimates for different annotations in HPG1 and mutation accumulation
401 lines.

402 **Table S4.** Description of phenotypic and climatic variables for association mapping analyses.

403 **Table S5.** SNP hits from association analyses and several descriptors.

404 **Data Appendix S1**: For each trait employed in association analyses, we report the histogram
405 distribution and the QQ plot of p-values to ensure that no trait departs exaggeratedly from the
406 normal distribution, and that no inflation of p-values is observed (when lambda ≤ 1, there is no
407 inflation of false positives).

bioRxiv preprint doi: https://doi.org/10.1101/050203; this version posted October 5, 2017. The copyright holder for this preprint (which was not certified by peer review) is the author/funder, who has granted bioRxiv a license to display the preprint in perpetuity. It is made available under aCC-BY-NC-ND 4.0 International license.

408 **SUPPLEMENTAL FIGURES**

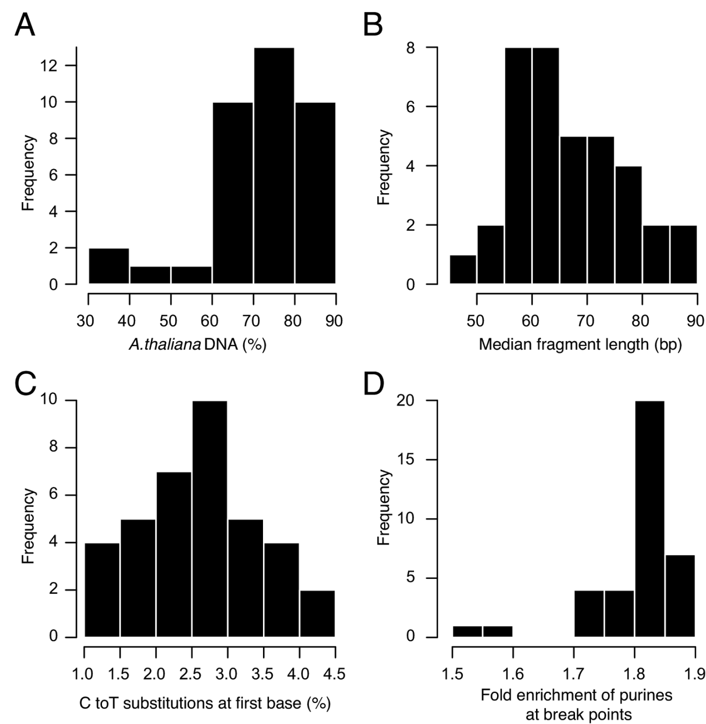

409 **Fig S1. Ancient-DNA characteristics of unrepaired herbarium libraries.**

410 **(A)** Fraction of *A. thaliana* DNA in sample. **(B)** Median length of merged reads. **(C)** Fraction of
411 cytosine to thymine (C-to-T) substitutions at first base (5' end). **(D)** Relative enrichment of purines
412 (adenine and guanine) at 5' end breaking points. Position -1 is compared with position -5 (negative
413 numbers indicate genomic context before upstream reads' 5' end).

bioRxiv preprint doi: https://doi.org/10.1101/050203; this version posted October 5, 2017. The copyright holder for this preprint (which was not certified by peer review) is the author/funder, who has granted bioRxiv a license to display the preprint in perpetuity. It is made available under aCC-BY-NC-ND 4.0 International license.

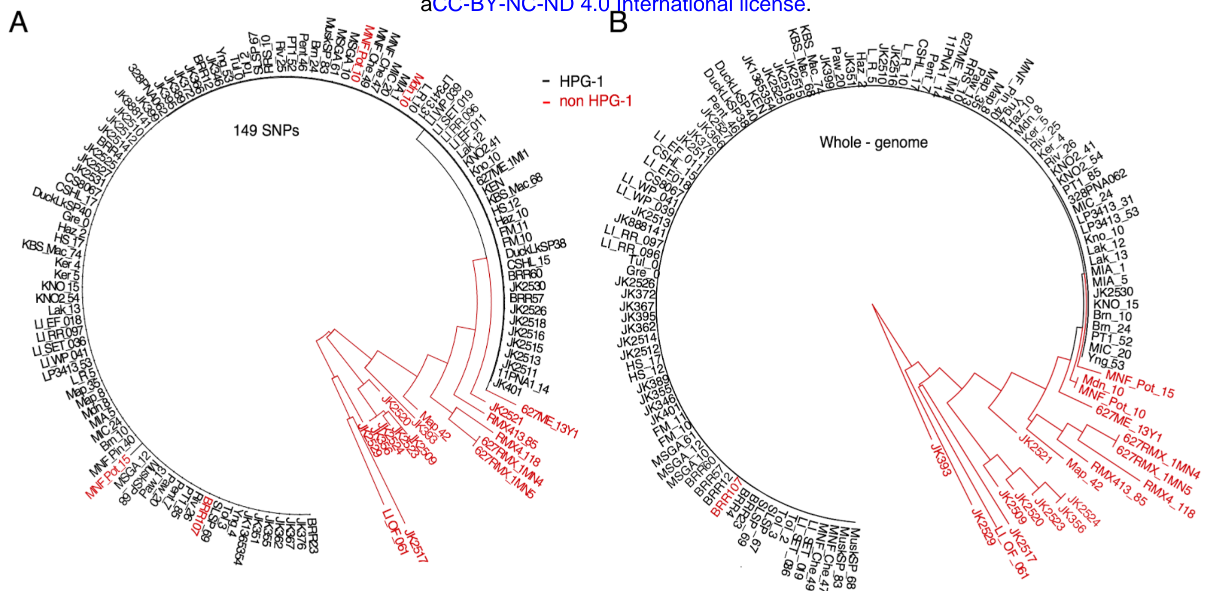

Fig S2. Separation between HPG1 and other North American lineages.

(A) Neighbor-joining tree built using Illumina-based SNP calls at the 149 genotyping markers originally used to identify HPG1 candidates. HPG1 accessions are shown in black, whereas other North American lineages are depicted in red (see explanation below for four HPG1-like accessions). **(B)** Neighbor-joining tree based on genome-wide SNPs. Accessions colored as in (A). Note that three accessions originally classified as HPG1 based on 149 SNPs (A) are placed outside this clade. A further accession (BRR7) within the HPG1 main branch was a recombinant removed from the analysis.

bioRxiv preprint doi: https://doi.org/10.1101/050203; this version posted October 5, 2017. The copyright holder for this preprint (which was not certified by peer review) is the author/funder, who has granted bioRxiv a license to display the preprint in perpetuity. It is made available under aCC-BY-NC-ND 4.0 International license.

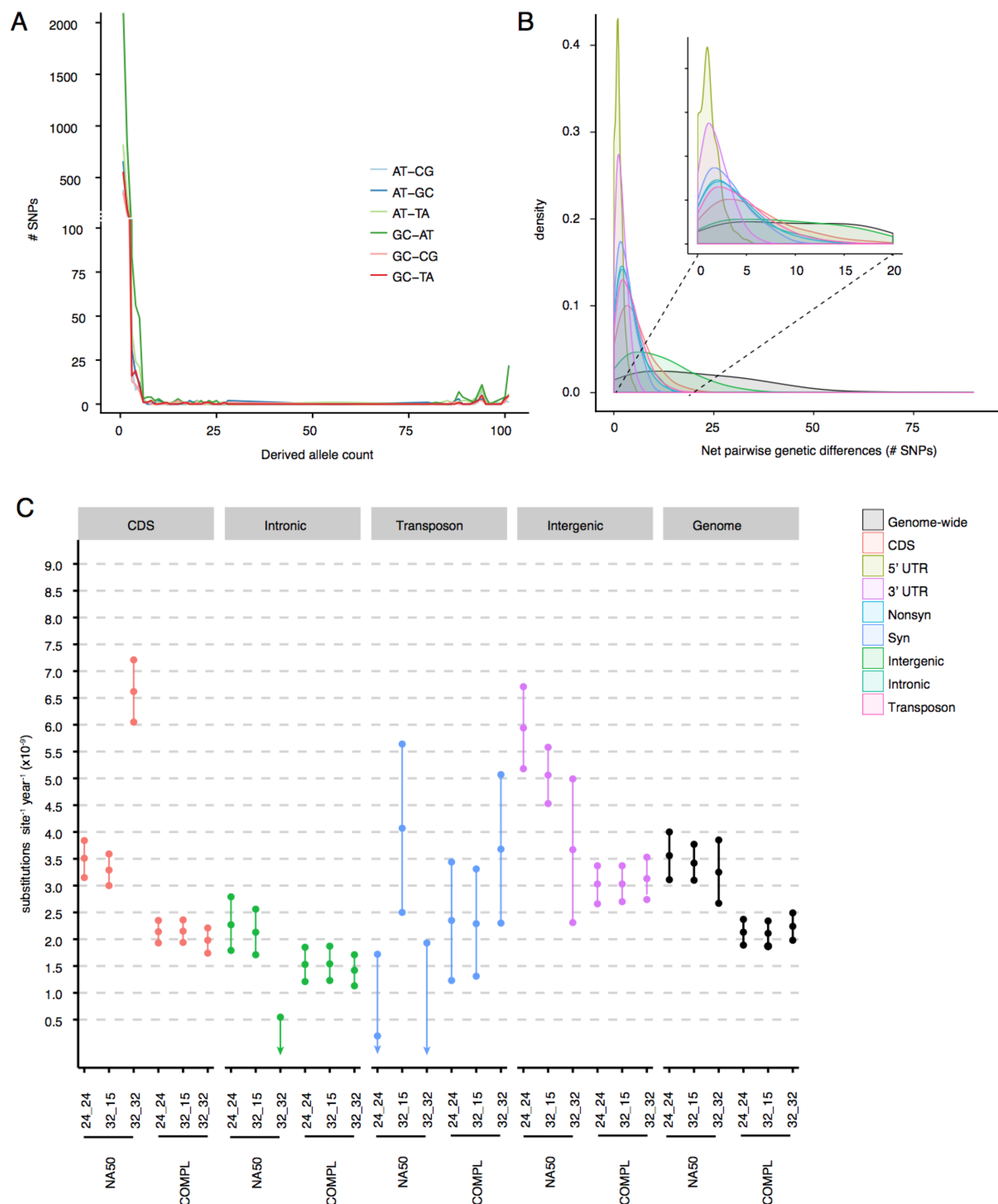

422 **Fig S3. Substitution spectrum and rates.**

423 **(A)** Site frequency spectrum for all transitions and transversions. **(B)** Distributions of "net" pairwise
424 genetic distances between historic and modern samples used to calculate mutation rates per
425 genomic annotation (from quality 32_15 and complete information per site). UTRs were excluded
426 because of the small number of SNPs. **(C)** Mutation rates calculated for different genomic
427 annotations and quality thresholds (32_32, 32_15, 24_24) and missing values (NA50: maximum 50%
428 missing data per SNP; COMPL: missing data 0%). Mean and 95% confidence intervals are shown.

bioRxiv preprint doi: https://doi.org/10.1101/050203; this version posted October 5, 2017. The copyright holder for this preprint (which was not certified by peer review) is the author/funder, who has granted bioRxiv a license to display the preprint in perpetuity. It is made available under aCC-BY-NC-ND 4.0 International license.

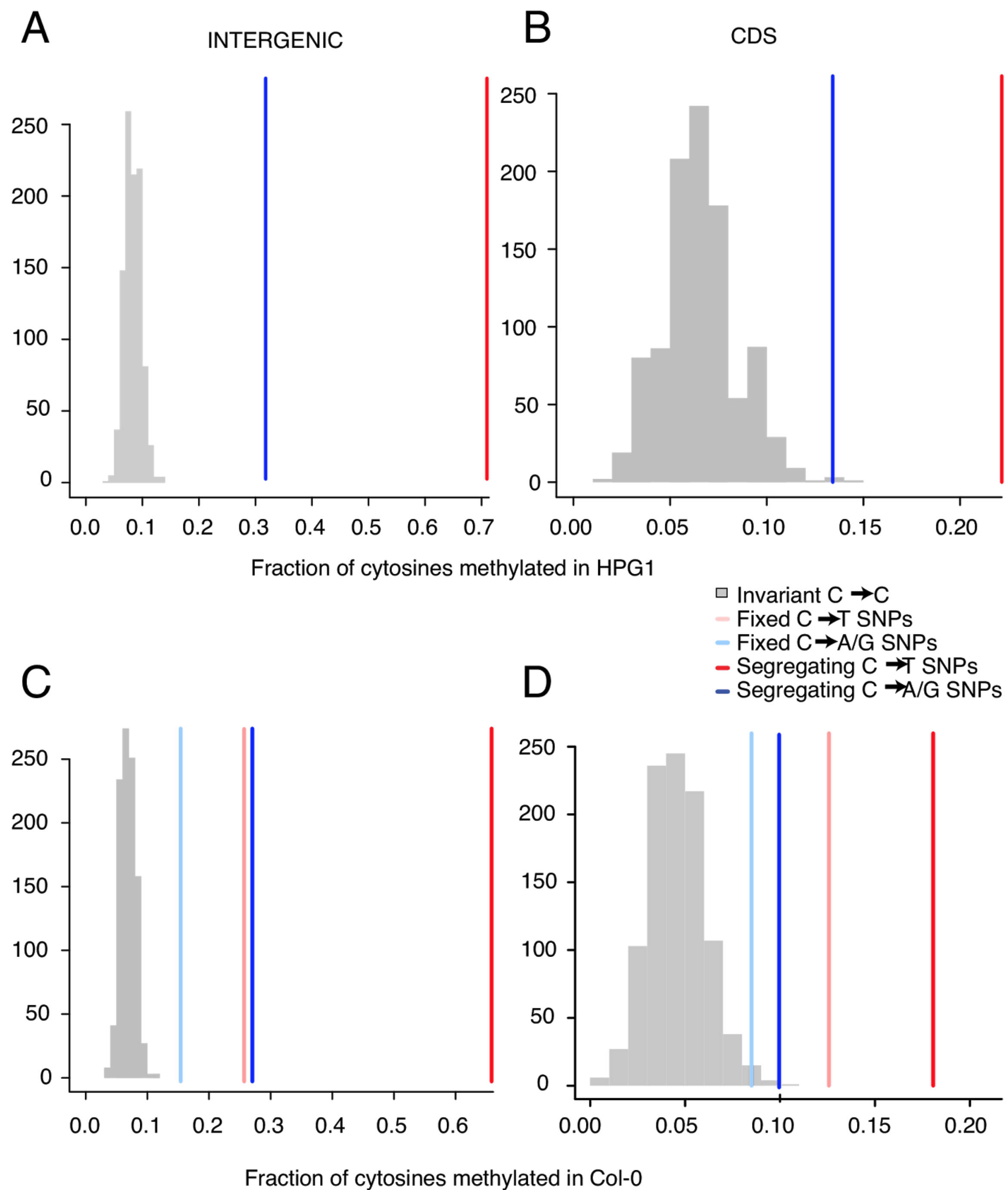

429 **Fig S4. Relationship between methylation and substitutions.**

430 **(A, B)** Fraction of methylation of cytosines in HPG1 pseudo-reference(7) at intergenic (A) or coding
431 regions (B). **(C, D)** Fraction of methylation of cytosines in Col-0 reference genome(5) at intergenic
432 (C) or coding regions (D). In each of the four comparisons, a grey histogram represents distribution
433 of methylation of 1,000 random sets of invariant cytosines. Lines represent average methylation
434 degree at those sites in HPG1 that changed from cytosine to thymine (red). We differentiate those

bioRxiv preprint doi: https://doi.org/10.1101/050203; this version posted October 5, 2017. The copyright holder for this preprint (which was not certified by peer review) is the author/funder, who has granted bioRxiv a license to display the preprint in perpetuity. It is made available under aCC-BY-NC-ND 4.0 International license.

435 substitutions that are shared - fixed - across all individuals (light red) or whose allele are present at
436 an intermediate - segregating - frequency (dark red). Likewise, average methylation is shown for sites
437 that changed from cytosine to adenine (blue) that that are fixed (light blue) or segregating (dark
438 blue). The fact that the average methylation is higher in new substitutions than in invariant positions
439 supports a connection between methylation and mutability of sites.

bioRxiv preprint doi: https://doi.org/10.1101/050203; this version posted October 5, 2017. The copyright holder for this preprint (which was not certified by peer review) is the author/funder, who has granted bioRxiv a license to display the preprint in perpetuity. It is made available under aCC-BY-NC-ND 4.0 International license.

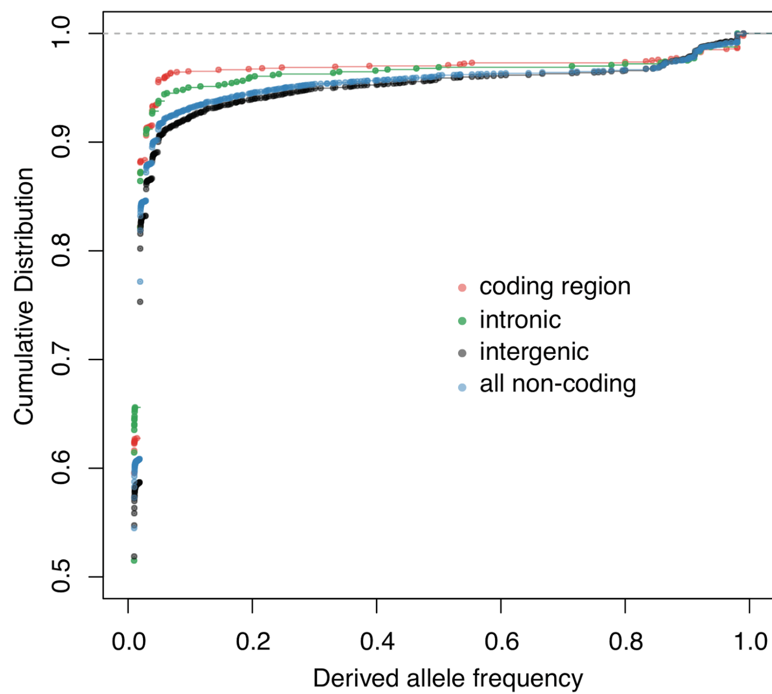

440 **Fig S5. Comparison of Site Frequency Spectra across genomic annotations.**

441 Cumulative empirical distribution, at different genomic annotations, of the unfolded Site Frequency

442 Spectrum of SNPs oriented based on the order of appearance of alleles in the herbarium genomes.

bioRxiv preprint doi: https://doi.org/10.1101/050203; this version posted October 5, 2017. The copyright holder for this preprint (which was not certified by peer review) is the author/funder, who has granted bioRxiv a license to display the preprint in perpetuity. It is made available under aCC-BY-NC-ND 4.0 International license.

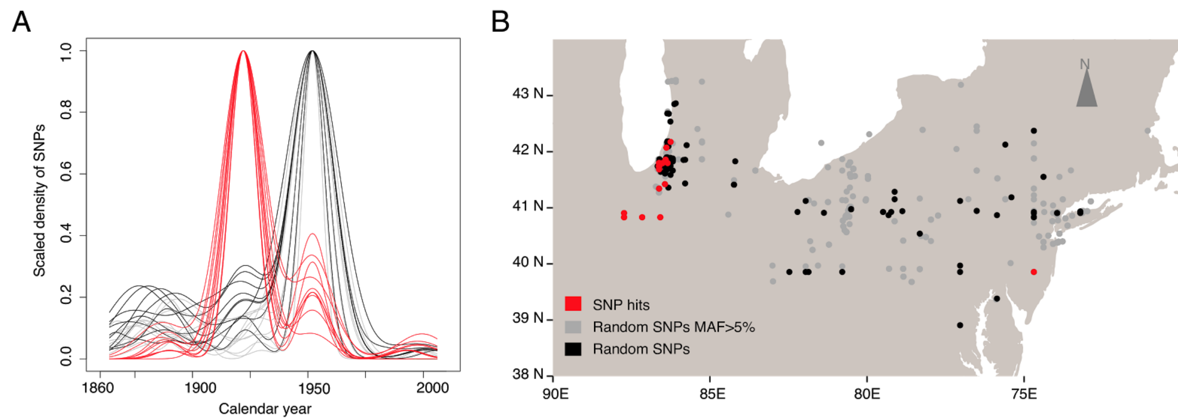

443 **Fig S5. Spatial and temporal emergence of root-associated mutations.**

444 **(A)** Age distribution of derived SNPs with a significant trait association (the herbarium sample in
445 which they were first recorded) (red), compared with genome-wide SNPs with at least 5% minor
446 allele frequency (grey), or without frequency cutoff (black). **(B)** Spatial centroid of all samples
447 carrying a derived allele. Since it is an average location, centroids can be in a body of water. Ten
448 random draws of 50 SNPs for each category were used to produce the density lines in (A) and
449 points in (B).

bioRxiv preprint doi: https://doi.org/10.1101/050203; this version posted October 5, 2017. The copyright holder for this preprint (which was not certified by peer review) is the author/funder, who has granted bioRxiv a license to display the preprint in perpetuity. It is made available under aCC-BY-NC-ND 4.0 International license.

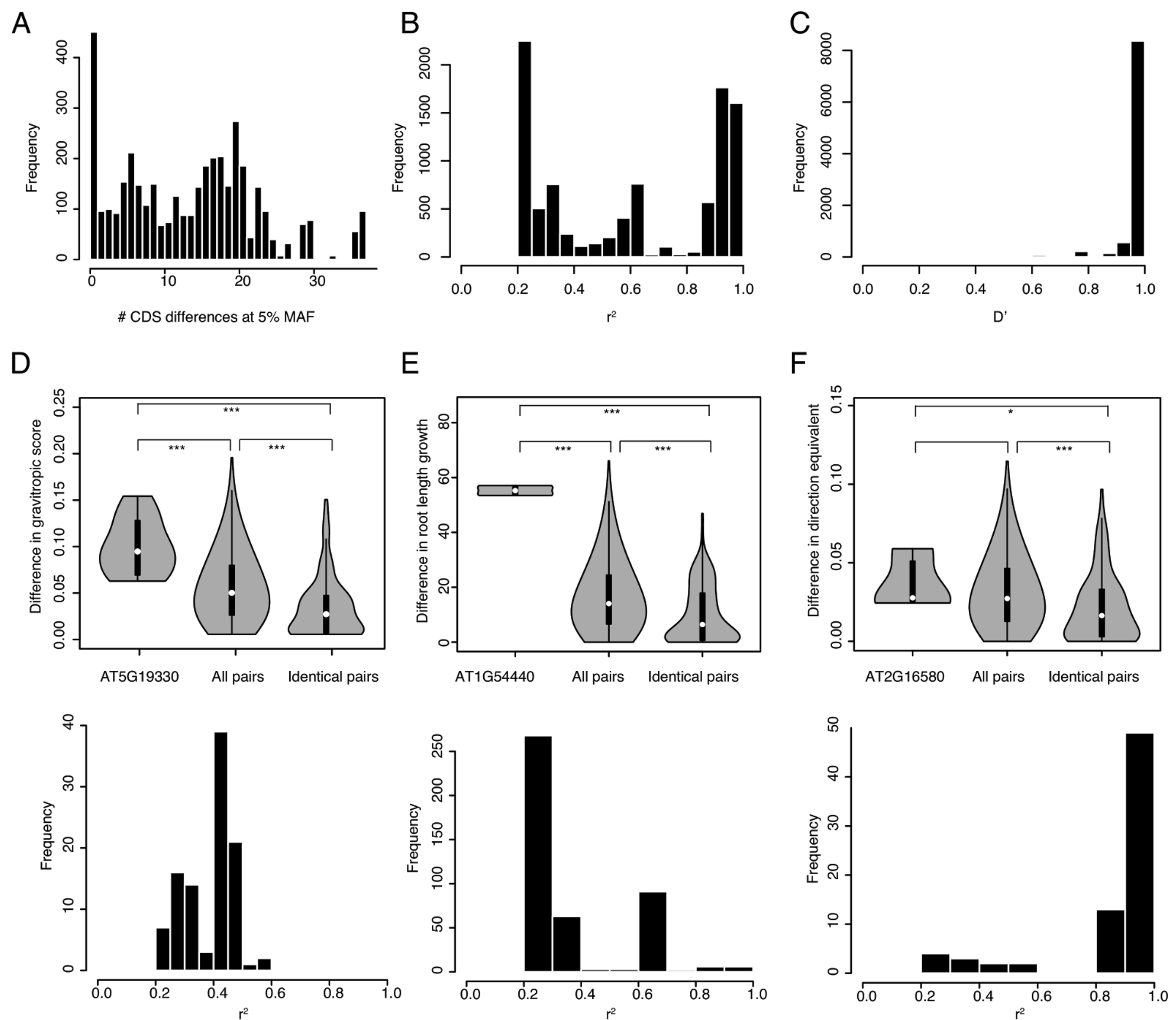

450 **Fig S6. Linkage disequilibrium of significant SNPs.**

451 **(A-F)** Linkage disequilibrium between SNPs with significant trait associations. Histogram of genetic
452 distances **(A)** between samples when evaluating only coding regions at 5% minimum allele frequency.
453 Linkage disequilibrium between SNP hits measured as r^2 **(B)** and D' **(C)**. Three significant SNPs were
454 further studied to exemplify the power of association analyses with HPG1. For each, phenotypic
455 differences between accessions that differ in the focal SNP and that are otherwise virtually genetically
456 identical are compared both with all pairs of accessions and with pairs of accessions completely
457 identical for coding regions. Below each violin plot is the histogram of linkage disequilibrium of the
458 focal SNP with all other SNP hits. The three focal SNPs evaluated are located in AT5G19330 **(D)**,
459 AT1G54440 **(E)** and AT2G16580 **(F)**.

Table S1. Sample information.

(Abbreviation H* indicates herbarium samples that cluster with the mo
dern HPG1 clade rather than the historic HPG1 clade in Fig. 3., highlighted as a star in the map from Fig. 1. Abbreviations of herbarium collections or seed sources: UCONN = University of Connecticut Herbarium; CFM = Chicago Field Museum; NY = New York Botanical Garden; ABRC = Arabidopsis Biological Resources Center; OSU = Ohio State University.)

Accession	Latitude (ºN)	Longitude (º E)	State	Date collected	Alternative name	Collector/ Herbarium	Average coverage (x)	Number of covered positions (≥3x) (mapped against HPG1 reference)	Number of covered positions (≥3x) (mapped against Col_0 reference)	SNPs vs HPG1 reference	Belongs to HPG1	Modern/ Herbarium	Column number in the available genome matrix
JK399	38.7155	-75.635591	DE	1863	888124	NY	9	105,053,631	99,889,683	142	yes	H	101
JK366	43.1921	-77.0102	NY	1866	888144	NY	6.8	100,379,839	95,118,236	123	yes	H	94
JK395	38.9068	-77.036667	DC	1877	888134	NY	10.3	103,620,791	98,888,406	167	yes	H	100
JK888141	40.732007	-74.068455	NJ	1879	888141	NY	42	107,211,409	102,634,255	161	yes	H	103
JK389	38.9068	-77.036667	DC	1888	1365363	NY	9.9	106,042,465	100,826,958	151	yes	H	98
JK362	38.9068	-77.036667	DC	1889	1365364	NY	8.8	103,997,716	98,876,320	153	yes	H	93
JK367	40.9249	-74.0755	NJ	1890	1365344	NY	16.7	107,236,732	102,176,782	181	yes	H	95
JK372	41.1222	-74.3569	NJ	1890	1365332	NY	14.8	106,285,178	101,480,369	163	yes	H	96
JK1365354	38.8782	-77.09048	VA	1891	1365354	NY	36.4	106,718,326	102,458,166	169	yes	H	88
JK376	39.97	-83.01	NY	1891	1365337	NY	12.3	105,962,154	100,840,125	145	yes	H	97
JK351	41.15	-73.766667	NY	1894	1365333	NY	16.1	106,531,302	101,841,156	153	yes	H	90
JK355	35.99	-83.94	TE	1896	1365374	NY	14.3	106,391,637	101,455,311	192	yes	H	91
JK356	n/a	n/a	GA	1897	1365375	NY	5.3	90,426,010	89,296,191	n/a	no	H	92
JK393	n/a	n/a	NC	1897	1365370	NY	30.4	102,894,430	101,298,068	n/a	no	H	99
JK346	40.643136	-111.95177	UT	1903	102365	NY	29.1	107,223,283	102,450,446	222	yes	H	89
JK2525	41.224343	-73.06021	CT	1904	79391	UNCONN	12.5	105,025,845	n/a	138	yes	H	118
JK2529	n/a	n/a	OH	1904	176849	CFM	11.4	100,620,441	n/a	n/a	no	H	121

JK401	40.643136	-111.95177	UT	1904	102364	NY	10.4	99,572,736	94,661,828	216	yes	H	102
JK2513	41.102121	-81.560547	OH	1911	25	OSU	18.2	106,309,854	n/a	176	yes	H	108
JK2509	n/a	n/a	CT	1917	11	OSU	15.1	102,169,546	n/a	n/a	no	H	104
JK2530	41.482862	-86.822602	IN	1922	531679	CFM	22.2	107,043,540	n/a	161	yes	H	122
JK2526	41.666667	-73.508455	CT	1929	79409	UNCONN	16.3	107,026,827	n/a	161	yes	H	119
JK2515	41.137296	-81.863779	OH	1930	30	OSU	21.3	106,893,416	n/a	193	yes	H	110
JK2511	41.721618	-81.243317	OH	1934	14	OSU	5.6	95,822,372	n/a	109	yes	H	106
JK2523	n/a	n/a	OH	1940	25707	UNC	13.1	101,421,749	n/a	n/a	no	H	116
JK2520	n/a	n/a	OH	1945	54051	UNC	20.3	102,831,697	n/a	n/a	no	H	114
JK2524	39.856783	-74.686954	NJ	1952	63978	UNC	13.8	100,778,282	n/a	n/a	no	H	117
JK2512	39.95607	-81.953309	OH	1956	21	OSU	16.7	106,801,844	n/a	189	yes	H	107
JK2514	39.95607	-81.953309	OH	1969	27	OSU	28.4	107,044,415	n/a	219	yes	H	109
JK2517	n/a	n/a	OH	1981	34	OSU	21.7	102,643,436	n/a	n/a	no	H	112
JK2521	n/a	n/a	OH	1992	565960	UNC	2.9	62,673,938	n/a	n/a	no	H	115
JK2518	41.867643	-80.789021	OH	1993	40	OSU	14.8	106,578,197	n/a	177	yes	H	113
JK2531	39.856783	-74.686954	NJ	1952	1507461	CFM	15.1	106,158,181	n/a	177	yes	H*	123
JK2510	39.688861	-82.993218	OH	1930	13	OSU	21	106,305,970	n/a	178	yes	H*	105
JK2527	41.509059	-72.543694	CT	1975	79389	UNCONN	8.3	104,089,205	n/a	200	yes	H*	120
JK2516	39.500862	-82.472413	OH	1980	32	OSU	18.1	106,464,569	n/a	198	yes	H*	111
CSHL_15	40.8585	-73.4675	NY	1993	CSHL-15	ABRC	39.3	108,189,771	105,955,885	243	yes	M	16
CSHL_17	40.8585	-73.4675	NY	1993	CSHL-17	ABRC	41.5	108,194,960	105,982,511	240	yes	M	17
FM_10	42.4489	-76.5072	NY	1993	FM-10	ABRC	44.6	108,203,215	106,052,866	269	yes	M	20
FM_11	42.4489	-76.5072	NY	1993	FM-11	ABRC	44.4	108,214,008	106,040,276	288	yes	M	21
HS_12	42.373	-71.0627	MA	1993	HS-12	ABRC	48.8	108,230,030	106,124,249	251	yes	M	25
HS_17	42.373	-71.0627	MA	1993	HS-17	ABRC	55.3	108,242,062	106,155,362	254	yes	M	26
Kno_10	41.2816	-86.621	IN	1993	Kno-10	ABRC	39.4	108,198,601	105,985,288	226	yes	M	32
KNO_15	41.2816	-86.621	IN	1993	KNO-15	ABRC	43.6	108,219,683	106,069,077	231	yes	M	33
Gre_0	43.178	-85.2532	MI	1995	Gre-0	ABRC	44.6	108,209,345	106,032,827	207	yes	M	22
Tul_0	43.2708	-85.2563	MI	1995	CS6877	ABRC	31.2	108,140,393	105,806,418	221	yes	M	85
CS8067	41.3599	-122.755	CA	1996	Buckhorn Pas	ABRC	66.4	108,260,489	106,243,277	294	yes	M	15
Tol_2	41.6639	-83.5553	OH	1996	CS8022	ABRC	61	108,241,333	106,194,209	238	yes	M	83
Tol_3	41.6639	-83.5553	OH	1996	CS8023	ABRC	40.2	108,184,749	105,953,559	232	yes	M	84
MIA_1	41.7976	-86.6691	MI	1999	MIA-1	ABRC	73.1	108,279,881	106,291,612	234	yes	M	56

MIA_5	41.7976	-86.6691	MI	1999	MIA-5	ABRC	62.9	108,263,557	106,250,560	235	yes	M	57
MIC_20	41.8266	-86.4366	MI	1999	MIC-20	ABRC	39.9	108,200,416	106,010,135	237	yes	M	58
MIC_24	41.8266	-86.4366	MI	1999	MIC-24	ABRC	33.8	108,176,527	105,728,326	237	yes	M	59
Brn_10	41.9	-86.583	MI	2002	Brn-10	ABRC	33.3	108,177,381	105,905,097	243	yes	M	7
Brn_24	41.9	-86.583	MI	2002	Brn-24	ABRC	38.4	108,208,482	105,951,803	228	yes	M	8
Haz_10	41.879	-86.607	MI	2002	Haz-10	ABRC	33.8	108,154,100	105,903,700	230	yes	M	23
Haz_2	41.879	-86.607	MI	2002	Haz-2	ABRC	39.7	108,201,103	106,004,251	288	yes	M	24
Ker_4	42.184	-86.358	MI	2002	Ker-4	ABRC	32.1	108,132,127	105,806,486	261	yes	M	30
Ker_5	42.184	-86.358	MI	2002	Ker-5	ABRC	62.9	108,259,905	106,246,278	259	yes	M	31
L_R_10	41.847	-86.67	MI	2002	L-R-10	ABRC	22.4	108,062,944	105,496,224	186	yes	M	49
L_R_5	41.847	-86.67	MI	2002	L-R-5	ABRC	60.6	108,255,795	106,209,826	299	yes	M	50
Lak_12	41.8	-86.67	MI	2002	Lak-12	ABRC	37.8	108,176,901	105,775,999	237	yes	M	36
Lak_13	41.8	-86.67	MI	2002	Lak-13	ABRC	28.5	107,955,559	105,553,559	226	yes	M	37
Map_35	42.166	-86.412	MI	2002	Map-35	ABRC	64.7	108,265,863	106,224,216	290	yes	M	51
Map_42	42.166	-86.412	MI	2002	Map-42	ABRC	46	107,303,032	106,093,945	n/a	no	M	52
Map_8	42.166	-86.412	MI	2002	Map-8	ABRC	33.4	108,155,999	105,921,907	287	yes	M	53
Mdn_10	42.051	-86.509	MI	2002	Mdn-10	ABRC	34.9	108,106,772	105,906,924	n/a	no	M	54
Mdn_8	42.051	-86.509	MI	2002	Mdn-8	ABRC	37.4	108,199,679	105,940,666	266	yes	M	55
Paw_13	42.148	-86.431	MI	2002	Paw-13	ABRC	43	108,159,739	105,980,721	267	yes	M	70
Paw_20	42.148	-86.431	MI	2002	Paw-20	ABRC	41.3	108,218,762	106,059,867	241	yes	M	71
Riv_25	42.184	-86.382	MI	2002	Riv-25	ABRC	36.8	108,186,632	105,779,717	273	yes	M	76
Riv_26	42.184	-86.382	MI	2002	Riv-26	ABRC	35.7	108,194,281	105,958,738	260	yes	M	77
Yng_4	41.865	-86.646	MI	2002	Yng-4	ABRC	41.3	108,182,789	106,000,003	289	yes	M	86
Yng_53	41.865	-86.646	MI	2002	Yng-53	ABRC	46	108,230,553	106,125,861	191	yes	M	87
RRS_10	41.5609	-86.4251	IN	2003	RRS-10	ABRC	41.8	108,208,144	106,033,465	274	yes	M	80
DuckLkSP38	43.3431	-86.4045	MI	2004	DuckLkSP38	ABRC	37.1	108,171,751	105,932,415	253	yes	M	18
DuckLkSP40	43.3431	-86.4045	MI	2004	DuckLkSP40	ABRC	39.6	108,204,654	105,969,244	257	yes	M	19
KBS_Mac_68	42.405	-85.398	MI	2004	KBS-Mac-68	ABRC	41.3	108,181,390	105,870,424	259	yes	M	27
KBS_Mac_74	42.405	-85.398	MI	2004	KBS-Mac-74	ABRC	37.7	108,160,645	105,801,702	265	yes	M	28
MNF_Che_47	43.5251	-86.1843	MI	2004	MNF-Che-47	ABRC	27.6	108,093,393	105,596,885	281	yes	M	60
MNF_Che_49	43.5251	-86.1843	MI	2004	MNF-Che-49	ABRC	28.5	108,082,202	105,661,610	274	yes	M	61
MNF_Pin_40	43.5356	-86.1788	MI	2004	MNF-Pin-40	ABRC	47.9	108,238,775	106,099,919	287	yes	M	62
MNF_Pot_10	43.595	-86.2657	MI	2004	MNF-Pot-10	ABRC	61.4	108,189,553	106,228,588	n/a	no	M	63

MNF_Pot_15	43.595	-86.2657	MI	2004	MNF-Pot-15	ABRC	25.2	108,543,185	107,022,924	n/a	no	M	64
MSGA_10	43.2749	-86.0891	MI	2004	MSGA-10	ABRC	41.9	108,191,659	106,019,404	233	yes	M	65
MSGA_12	43.2749	-86.0891	MI	2004	MSGA-12	ABRC	42.8	108,227,214	106,032,928	240	yes	M	66
MSGA_61	43.2749	-86.0891	MI	2004	MSGA-61	ABRC	45.5	108,210,152	106,077,183	247	yes	M	67
MuskSP_68	43.2483	-86.3368	MI	2004	MuskSP-68	ABRC	25.8	108,063,297	105,588,467	215	yes	M	68
MuskSP_83	43.2483	-86.3368	MI	2004	MuskSP-83	ABRC	29.9	108,099,368	105,721,042	222	yes	M	69
Pent_46	43.7623	-86.3929	MI	2004	Pent-46	ABRC	48.3	108,227,763	106,099,890	238	yes	M	72
Pent_7	43.7623	-86.3929	MI	2004	Pent-7	ABRC	55.7	108,220,625	106,144,167	240	yes	M	73
SLSP_67	43.665	-86.496	MI	2004	SLSP-67	ABRC	53.5	108,238,880	106,143,530	245	yes	M	81
SLSP_69	43.665	-86.496	MI	2004	SLSP-69	ABRC	35.5	108,160,835	105,899,252	249	yes	M	82
KNO2_41	41.273	-86.625	IN	2005	KNO2.41	ABRC	44.7	108,209,694	106,063,235	219	yes	M	34
KNO2_54	41.273	-86.625	IN	2005	KNO2.54	ABRC	44	108,212,430	105,903,373	218	yes	M	35
LI_EF_011	40.9064	-73.1493	NY	2005	LI-EF-011	ABRC	68.6	108,267,109	106,250,331	259	yes	M	38
LI_EF_018	40.9064	-73.1493	NY	2005	LI-EF-018	ABRC	39	108,244,306	105,898,497	230	yes	M	39
LI_OF_061	40.7777	-72.9069	NY	2005	LI-OF-061	ABRC	58	104,897,841	105,729,196	n/a	no	M	40
LI_RR_096	40.9447	-72.8615	NY	2005	LI-RR-096	ABRC	63.5	108,264,679	106,251,487	261	yes	M	41
LI_RR_097	40.9447	-72.8615	NY	2005	LI-RR-097	ABRC	40.8	108,211,310	105,992,095	249	yes	M	42
LI_SET_019	40.9352	-73.114	NY	2005	LI-SET-019	ABRC	29.9	108,085,297	105,737,781	259	yes	M	43
LI_SET_036	40.9352	-73.114	NY	2005	LI-SET-036	ABRC	41.5	108,216,592	106,006,605	238	yes	M	44
LI_WP_039	40.9076	-73.2089	NY	2005	LI-WP-039	ABRC	104.8	108,301,282	106,273,259	239	yes	M	45
LI_WP_041	40.9076	-73.2089	NY	2005	LI-WP-041	ABRC	76.5	108,287,248	106,322,146	235	yes	M	46
PT1_52	41.3423	-86.7368	IN	2005	PT1.52	ABRC	50.6	108,240,431	106,154,252	219	yes	M	74
PT1_85	41.3423	-86.7368	IN	2005	PT1.85	ABRC	46.1	108,220,150	106,097,633	233	yes	M	75
RMX4_118	42.036	-86.511	MI	2005	RMX4.118	ABRC	41.8	106,178,554	105,685,651	n/a	no	M	78
11PNA1_14	42.0945	-86.3253	MI	2006	11PNA1.14	ABRC	47.5	108,227,783	106,133,372	276	yes	M	1
328PNA062	42.0945	-86.3253	MI	2006	328PNA062	ABRC	47.3	108,221,709	106,127,272	223	yes	M	2
627ME_13Y1	42.093	-86.359	MI	2006	n/a	ABRC	53.4	107,908,679	106,148,671	n/a	no	M	3
627ME_1MI1	42.093	-86.359	MI	2006	627ME-1MI1	ABRC	57.8	108,252,617	106,173,403	281	yes	M	4
627RMX_1MN4	42.0333	-86.5128	MI	2006	n/a	ABRC	43.6	106,799,549	105,789,469	n/a	no	M	5
627RMX_1MN5	42.0333	-86.5128	MI	2006	n/a	ABRC	50.6	106,885,430	105,897,441	n/a	no	M	6
BRR107	40.8313	-87.735	IL	2006	BRR107	ABRC	28.5	108,896,513	107,320,745	n/a	no	M	9
BRR12	40.8313	-87.735	IL	2006	BRR12	ABRC	43.9	108,190,572	106,031,493	232	yes	M	10
BRR23	40.8313	-87.735	IL	2006	BRR23	ABRC	30.7	108,095,072	105,726,913	236	yes	M	11

BRR4	40.8313	-87.735	IL	2006	BRR4	ABRC	44.7	108,180,840	106,033,507	219	yes	M		12
BRR57	40.8313	-87.735	IL	2006	BRR57	ABRC	28.4	108,093,033	105,630,963	225	yes	M		13
BRR60	40.8313	-87.735	IL	2006	BRR60	ABRC	42.9	108,281,285	106,199,572	229	yes	M		14
KEN	41.767	-72.677	CT	n/a	KEN	ABRC	55.2	108,233,232	106,158,223	249	yes	M		29
LP3413_31	41.6862	-86.8513	IN	n/a	LP3413.31	ABRC	55.9	108,244,332	106,190,596	227	yes	M		47
LP3413_53	41.6862	-86.8513	IN	n/a	LP3413.53	ABRC	51.2	108,157,453	105,994,665	245	yes	M		48
RMX413_85	42.036	-86.511	MI	n/a	RMX413.85	ABRC	38	106,816,221	105,483,632	n/a	no	M		79

Table S2. Sample information for Col-0 mutation accumulation lines.

Information about each Mutation Accumulation (MA) line and their number of SNPs at different annotations. Also the total number of SNPs, average number of mutations and total bp covered in the genome per annotation are reported.

MA line	Read depth	Generation	Total	SNPs	Deletions	insertions	CDS	Nonsyn	Syn	Intron	5' UTR	3' UTR	TE	Intergenic
0-4-26	57	3	7	6	1	0	0	0	0	0	0	0	1	5
0-8-87	49	3	7	5	0	2	1	1	0	1	0	0	0	3
30-109	45	31	31	23	7	1	3	3	0	3	0	0	2	15
30-119	45	31	33	26	2	5	1	1	0	1	2	0	4	18
30-29	51	31	39	26	10	3	2	1	1	3	0	1	5	15
30-39	48	31	28	18	7	3	1	1	0	1	0	1	4	11
30-49	50	31	30	23	3	4	4	4	0	0	0	0	6	13
30-59	40	31	46	31	8	7	5	2	3	2	0	0	6	18
30-69	50	31	26	21	3	2	4	3	1	1	1	1	6	8
30-79	50	31	31	25	3	3	6	4	2	2	0	0	8	9
30-89	39	31	35	27	5	3	4	3	1	1	1	0	2	19
30-99	44	31	37	35	1	1	6	5	1	2	0	2	8	17
Total SNPs				274			38	28	10	17	4	5	52	158
average (31st)			33.6	25.5	4.9	3.2	3.6	2.7	0.9	1.6	0.4	0.5	5.1	14.3
stdev (31st)			5.9	4.9	3.0	1.8	1.8	1.4	1.0	1.0	0.7	0.7	2.1	3.9
Total bp			115,954,227				30,753,966			17,446,837	4,289,789	2,508,199	9,267,413	48,090,487

Table S3. Mutation rate estimates for different annotations in HPG1 and mutation accumulation lines.

Mutation rates from MA lines are compared to HPG1 substitution rates from the dataset of 32_15 quality filter and complete information (see SOM) (Abbreviations: stat, descriptive statistic; bp, base pairs; lower and upper, lower and upper 95% CI; Nonsyn. and Syn., nonsynonymous and synonymous sites; UTR, untranslated region sites; HPG1 adj., substitution rate of HPG1 adjusted by a mean generation time of 1.3 years)

Dataset	stat	CDS	Syn.	Nonsyn.	Intronic	5' UTR	3' UTR	Transposon	Intergenic	Genome
MA	mean	3.776	n/a	n/a	2.958	3.008	6.431	17.752	9.592	7.094
MA	sem	1.928	n/a	n/a	1.786	5.258	9.094	7.420	2.628	1.352
MA	lower	2.581	n/a	n/a	1.851	-0.251	0.794	13.153	7.964	6.256
MA	upper	4.971	n/a	n/a	4.065	6.267	12.067	22.351	11.221	7.932
HPG1	mean	2.149	n/a	n/a	1.540	n/a	n/a	2.290	3.029	2.114
HPG1	sem	0.108	n/a	n/a	0.165	n/a	n/a	0.536	0.173	0.119
HPG1	lower	1.943	n/a	n/a	1.231	n/a	n/a	1.314	2.698	1.871
HPG1	upper	2.364	n/a	n/a	1.874	n/a	n/a	3.309	3.368	2.344
HPG1 adj.	mean	2.794	n/a	n/a	2.002	n/a	n/a	2.977	3.938	2.748
HPG1 adj.	sem	0.140	n/a	n/a	0.214	n/a	n/a	0.697	0.225	0.154
HPG1 adj.	lower	2.526	n/a	n/a	1.600	n/a	n/a	1.708	3.508	2.432
HPG1 adj.	upper	3.073	n/a	n/a	2.436	n/a	n/a	4.302	4.378	3.047
Distribution of pairwise SNP differences	min	0	0	0	0	0	0	0	0	0
	1st qu.	2	1	1	1	0	1	2	5	9
	median	5	3	3	3	1	2	4	10	18
	mean	5.6	3	3.1	3.8	1.2	1.9	4.3	11.3	21.1
	3rd qu.	8	5	4	5	2	3	6	16	31
	max.	27	17	11	15	5	7	22	43	87
Total number of SNPs		971	531	448	629	74	158	656	2498	5013
Total bp		32119233	n/a	n/a	18132262	2632130	4480510	6209512	43601507	108434034

Table S4. Description of phenotypic and climatic variables for association mapping analyses.

Mean and standard deviation (s.d.) across accessions for each phenotypic and climatic variables. Broad sense heritabilities (H2) were calculated from between line and within line (between replicate) variance in ANOVA. P-value corresponds to F test. Narrow sense heritabilities (h2) were calculated employing linear mixed models and kinship matrix from mean accession values. P-values correspond to Likelihood Ratio test.

Variable	Description	mean	s.d.	H2	p-value	h2	p-value
FT_V0	Time from germination until the first flower opens (days) under 0 days of vernalization	101	4.53	0.009	7.28E-03	0.017	1.97E-25
FT_V1	Time from germination until the first flower opens (days) under 14 days of vernalization	107	4.12	0.013	6.87E-04	0.395	1.83E-25
FT_V2	Time from germination until the first flower opens (days) under 28 days of vernalization	102	3.22	0.012	1.04E-03	0.429	3.37E-27
FT_V3	Time from germination until the first flower opens (days) under 63 days of vernalization	110	1.32	0.010	5.11E-03	0.226	9.52E-25
B_V0	Time from germination until the first developed bud (days) under 0 days of vernalization	88.8	4	0.013	8.99E-04	0.018	2.26E-25
B_V1	Time from germination until the first developed bud (days) under 14 days of vernalization	93.9	3.84	0.009	7.45E-03	0.340	3.98E-25
B_V2	Time from germination until the first developed bud (days) under 28 days of vernalization	89.2	2.13	0.005	6.92E-02	0.252	2.22E-25
B_V3	Time from germination until the first developed bud (days) under 63 days of vernalization	101	0.45	0.006	5.79E-02	0.177	1.99E-24
Fecundity	Pixel area of inflorescence (correlation with number of fruits, rho=0.84)	0.02	0.0042	0.001	3.56E-01	0.240	1.02E-22
seed_size	Average seed size (mm2)	0.134	0.0053	0.016	4.73E-03	0.149	3.58E-24
GR_rootLength	Average root growth rate	181	14.9	0.131	4.76E-77	0.640	3.13E-29
GR_shootArea	Average of shoot area growth rate	2279	253	0.053	2.33E-24	0.812	1.77E-31
rootLength	Average root length	467	35.8	0.048	2.01E-21	0.409	2.57E-28

dirEquivalent	Average root direction index. Score for average pixel-by-pixel deviations from growth relative to vector of gravity	0.393	0.0277	0.059	2.62E-28	0.544	1.14E-26
stdDevXY	Average root linearity coefficient of linear determination; R2 of linear regression line fitted to pixels of primary root skeleton	0.725	0.0429	0.018	4.54E-06	0.303	1.41E-25
meanRootWidth	Average root width	5.27	0.177	0.038	5.30E-16	0.359	1.52E-25
rootWidth20	Average width over first interval of the primary root length (0 to 20%) at hypocotyl/root junction	5.75	0.124	0.018	5.11E-06	0.166	3.37E-25
rootWidth40	Average width over first interval of the primary root length (20 to 40%) at hypocotyl/root junction	5.35	0.19	0.033	3.87E-13	0.291	1.76E-25
rootWidth60	Average width over first interval of the primary root length (40 to 60%) at hypocotyl/root junction	5.2	0.212	0.039	1.49E-16	0.405	6.51E-26
rootWidth80	Average width over first interval of the primary root length (60 to 80%) at hypocotyl/root junction	5.11	0.241	0.045	4.67E-20	0.381	5.47E-26
rootWidth100	Average width over first interval of the primary root length (80 to 100%) at hypocotyl/root junction	4.9	0.222	0.038	4.06E-16	0.351	8.81E-26
gravitropicDir	Average root angle between root vector and the vertical axis of the picture (assumed vector of gravity) (°)	-7.22	2.56	0.024	7.69E-09	0.210	4.68E-27
gravitropicScore	Average score for root angle intervals	0.1	0.0457	0.044	2.83E-19	0.642	7.56E-27
TotLen.EucLen	Average root tortuosity: Total root length divided by Euclidian length	1.1	0.0097	0.009	6.83E-03	0.422	2.53E-25
GR.TL	Average relative root growth rate: Root growth rate divided by total length at the earlier time point	0.673	0.0796	0.011	1.20E-03	0.393	2.69E-24
BIO1	Annual Mean Temperature (ºC x 10)	98.1	12.8	n/a	n/a	0.066	3.22E-40
BIO2	Mean Diurnal Range (Mean of monthly (max temp - min temp))	107	7.65	n/a	n/a	0.073	1.02E-40
BIO3	Isothermality (BIO2/BIO7) (x 100)	28.9	1.8	n/a	n/a	0.361	4.91E-39
BIO4	Temperature Seasonality (standard deviation x 100)	9169	483	n/a	n/a	0.383	4.68E-47
BIO5	Max Temperature of Warmest Month (ºC x 10)	283	10.1	n/a	n/a	0.152	3.78E-40
BIO6	Min Temperature of Coldest Month (ºC x 10)	-80.9	18	n/a	n/a	0.275	4.79E-42
BIO7	Temperature Annual Range (BIO5-BIO6) (ºC x 10)	364	17.5	n/a	n/a	0.239	6.31E-42
BIO8	Mean Temperature of Wettest Quarter (ºC x 10)	176	55.1	n/a	n/a	0.016	3.58E-43

BIO9	Mean Temperature of Driest Quarter (ºC x 10)	-7.11	48.7	n/a	n/a	0.000	3.58E-43
BIO10	Mean Temperature of Warmest Quarter (ºC x 10)	213	10.8	n/a	n/a	0.205	3.33E-40
BIO11	Mean Temperature of Coldest Quarter (ºC x 10)	-24.1	18.2	n/a	n/a	0.270	1.71E-41
BIO12	Annual Precipitation (mm)	990	109	n/a	n/a	0.219	3.94E-44
BIO13	Precipitation of Wettest Month (mm)	103	6.72	n/a	n/a	0.206	1.53E-40
BIO14	Precipitation of Driest Month (mm)	54.1	16.7	n/a	n/a	0.104	1.51E-40
BIO15	Precipitation Seasonality (Coefficient of Variation)	17.8	5.51	n/a	n/a	0.157	8.93E-40
BIO16	Precipitation of Wettest Quarter (mm)	291	19.7	n/a	n/a	0.269	1.55E-42
BIO17	Precipitation of Driest Quarter (mm)	191	44.8	n/a	n/a	0.084	3.67E-42
BIO18	Precipitation of Warmest Quarter (mm)	277	25.2	n/a	n/a	0.342	7.42E-44
BIO19	Precipitation of Coldest Quarter (mm)	197	47	n/a	n/a	0.022	2.68E-42

Table S5. SNP hits from association analyses and several descriptors.

SNP hits significant at the 5% level after permutation correction are shown. Additionally, if raw p-values pass a double Bonferroni threshold of 0.01% are marked with a "tick". (Abbreviations: nonsyn. and syn., nonsynonymous and synonymous changes; regular one-letter abbreviation was used for amino acid changes)

Trait	Chromosome	Position	Ancestral	Derived	Effect	Effect standard error	Sample size	p - value raw	p- value false discovery rate	p- value permutation corrected	Allele frequency	Allele frequency in modern set	Oldest herbarium individual	Longitude	Latitude	Substitution type	AA change	Gene	Biochemical effect (Grantham score)	Significant permutation	Significant double Bonferroni	LD
dirEquivalent	1	958948	G	T	-0.014	0.004	63	5.30E-04	0.0052	0.018	0.186	0.227	1922	41.7	-85.3	nonsyn	A->P	AT1G03810	27	✓		53
gravitropicScore	1	9925177	C	T	0.033	0.010	63	7.10E-04	0.0651	0.016	0.078	0.092	1952	40.9	-82.3	interg.				✓		1
bio18	1	10187610	T	C	6.830	1.987	99	5.83E-04	0.0124	0.047	0.196	0.24	1922	41.7	-85.3	interg.				✓		52
GR_rootLength	1	12638692	C	T	-12.100	3.164	63	1.33E-04	0.0037	0.003	0.087	0.105	1952	40.9	-81.3	interg.				✓	✓	13
GR_shootArea	1	12638692	C	T	-231.000	53.774	63	1.75E-05	0.0005	0.001	0.087	0.105	1952	40.9	-81.3	interg.				✓	✓	13
GR_rootLength	1	13652509	C	A	-12.100	3.164	63	1.33E-04	0.0037	0.003	0.093	0.107	1952	40.9	-82.9	interg.				✓	✓	12
GR_shootArea	1	13652509	C	A	-231.000	53.774	63	1.75E-05	0.0005	0.001	0.093	0.107	1952	40.9	-82.9	interg.				✓	✓	12
bio18	1	13904611	C	T	6.570	1.756	90	1.83E-04	0.0124	0.016	0.217	0.237	1922	41.7	-85.3	interg.				✓		49
bio18	1	13994958	G	A	6.830	1.987	99	5.83E-04	0.0124	0.047	0.196	0.24	1922	41.7	-85.3	tranposon		AT1G36933		✓		49
bio18	1	17408807	C	T	6.830	1.987	99	5.83E-04	0.0124	0.047	0.196	0.24	1922	41.7	-85.3	interg.				✓		48
dirEquivalent	1	19024876	C	T	-0.014	0.004	63	5.30E-04	0.0052	0.018	0.19	0.23	1922	41.7	-85.3	interg.				✓		47
GR_shootArea	1	20324050	G	A	-231.000	53.774	63	1.75E-05	0.0005	0.001	0.087	0.105	1952	40.9	-82.9	interg.		AT1G54440		✓	✓	11
GR_rootLength	1	20324050	G	A	-12.100	3.164	63	1.33E-04	0.0037	0.003	0.087	0.105	1952	40.9	-82.9	interg.		AT1G54440		✓	✓	11
bio18	1	23648407	A	C	6.830	1.987	99	5.83E-04	0.0124	0.047	0.196	0.24	1922	41.7	-85.3	nonsyn	Y->S	AT1G63740	144	✓		46
dirEquivalent	1	26052913	A	T	-0.014	0.004	63	5.30E-04	0.0052	0.018	0.185	0.224	1922	41.7	-85.3	interg.				✓		45
GR_shootArea	1	29696198	G	A	-121.000	33.911	63	3.68E-04	0.0096	0.016	0.278	0.329	1922	41.5	-84.9	interg.				✓		42

bio16	1	29696198	G	A	5.250	1.377	94	1.39E-04	0.0632	0.016	0.278	0.329	1922	41.5	-84.9	interg.				✓		42
bio18	1	29696198	G	A	6.340	1.569	94	5.36E-05	0.0124	0.004	0.278	0.329	1922	41.5	-84.9	interg.				✓		42
GR_rootLength	1	30015381	T	A	-12.100	3.164	63	1.33E-04	0.0037	0.003	0.087	0.105	1952	40.9	-82.9	interg.				✓	✓	10
GR_shootArea	1	30015381	T	A	-231.000	53.774	63	1.75E-05	0.0005	0.001	0.087	0.105	1952	40.9	-82.9	interg.				✓	✓	10
GR_rootLength	1	30143319	G	A	-12.100	3.164	63	1.33E-04	0.0037	0.003	0.088	0.105	1952	40.9	-82.9	interg.				✓	✓	9
GR_shootArea	1	30143319	G	A	-231.000	53.774	63	1.75E-05	0.0005	0.001	0.088	0.105	1952	40.9	-82.9	interg.				✓	✓	9
dirEquivalent	2	358395	C	T	-0.016	0.004	63	1.15E-04	0.0032	0.006	0.194	0.237	1922	41.7	-85.3	syn.	V->V	AT2G01820		✓	✓	43
dirEquivalent	2	585918	C	T	-0.016	0.004	63	1.15E-04	0.0032	0.006	0.194	0.237	1922	41.7	-85.3	syn.	G->G	AT2G02220		✓	✓	42
dirEquivalent	2	1093203	C	T	-0.016	0.004	63	1.15E-04	0.0032	0.006	0.194	0.237	1922	41.7	-85.3	interg.				✓	✓	41
dirEquivalent	2	2176891	T	C	-0.016	0.004	63	1.15E-04	0.0032	0.006	0.194	0.237	1922	41.7	-85.3	interg.				✓	✓	40
GR_rootLength	2	3174832	T	A	6.340	1.869	63	6.97E-04	0.017	0.017	0.529	0.566	1879	41.3	-84.3	interg.				✓		0
TotLen.EucLen	2	5285907	C	A	-0.006	0.002	63	3.05E-04	0.0241	0.037	0.162	0.194	1922	41.5	-85	interg.				✓	✓	39
dirEquivalent	2	5285907	C	A	-0.019	0.005	63	2.64E-05	0.0032	0.001	0.162	0.194	1922	41.5	-85	interg.				✓	✓	39
dirEquivalent	2	6034545	C	T	-0.016	0.004	63	1.15E-04	0.0032	0.006	0.194	0.237	1922	41.7	-85.3	syn.	S->S	AT2G14247		✓	✓	38
dirEquivalent	2	7047529	G	T	-0.016	0.004	63	1.15E-04	0.0032	0.006	0.194	0.237	1922	41.7	-85.3	nonsyn	P->A	AT2G16270	27	✓	✓	37
dirEquivalent	2	7186220	C	T	-0.016	0.004	63	1.15E-04	0.0032	0.006	0.194	0.237	1922	41.7	-85.3	intron		AT2G16580		✓	✓	36
dirEquivalent	2	10369545	T	C	-0.016	0.004	63	1.15E-04	0.0032	0.006	0.194	0.237	1922	41.7	-85.3	interg.				✓	✓	35
dirEquivalent	2	10495275	A	C	-0.016	0.004	63	1.15E-04	0.0032	0.006	0.196	0.237	1922	41.7	-85.3	intron		AT2G24680		✓	✓	34
dirEquivalent	2	11346211	C	A	-0.014	0.004	63	5.30E-04	0.0052	0.018	0.186	0.227	1922	41.7	-85.3	interg.				✓		33
dirEquivalent	2	12415084	T	A	-0.014	0.004	63	5.30E-04	0.0052	0.018	0.186	0.227	1922	41.7	-85.3	intron		AT2G28900		✓		32
dirEquivalent	2	12876361	A	C	-0.015	0.004	63	1.56E-04	0.0041	0.006	0.262	0.29	1922	41.7	-84.6	interg.				✓		31
gravitropicScore	2	12876361	A	C	-0.021	0.006	63	1.08E-03	0.0651	0.027	0.262	0.29	1922	41.7	-84.6	interg.				✓		31
bio13	2	14417366	A	G	3.990	0.959	64	3.22E-05	0.0147	0.004	0.077	0	1890	39.5	-77.9	interg.				✓		1
dirEquivalent	2	15278350	A	G	-0.014	0.004	63	5.30E-04	0.0052	0.018	0.186	0.227	1922	41.7	-85.3	interg.				✓		30
GR_shootArea	2	16039488	T	G	-231.000	53.774	63	1.75E-05	0.0005	0.001	0.087	0.105	1952	40.9	-82.9	3' UTR		AT2G38290		✓	✓	8
GR_rootLength	2	16039488	T	G	-12.100	3.164	63	1.33E-04	0.0037	0.003	0.087	0.105	1952	40.9	-82.9	3' UTR		AT2G38290		✓	✓	8
GR_rootLength	2	16247290	G	T	-12.100	3.164	63	1.33E-04	0.0037	0.003	0.088	0.105	1952	40.9	-82.9	nonsyn	A->G	AT2G38910	60	✓	✓	7
GR_shootArea	2	16247290	G	T	-231.000	53.774	63	1.75E-05	0.0005	0.001	0.088	0.105	1952	40.9	-82.9	nonsyn	A->G	AT2G38910	60	✓	✓	7
dirEquivalent	2	16333662	G	A	-0.014	0.004	63	5.30E-04	0.0052	0.018	0.186	0.227	1922	41.7	-85.3	nonsyn	A->G	AT2G39160	60	✓		29
dirEquivalent	3	2500258	C	A	-0.016	0.004	63	1.15E-04	0.0032	0.006	0.194	0.237	1922	41.7	-85.3	syn.	K->K	AT3G07830		✓	✓	28
dirEquivalent	3	3154804	C	T	-0.016	0.004	63	1.15E-04	0.0032	0.006	0.194	0.237	1922	41.7	-85.3	interg.				✓	✓	27
dirEquivalent	3	3629794	C	T	-0.016	0.004	63	1.15E-04	0.0032	0.006	0.194	0.237	1922	41.7	-85.3	intron		AT3G11530		✓	✓	26
dirEquivalent	3	4269626	G	T	-0.016	0.004	63	1.15E-04	0.0032	0.006	0.194	0.237	1922	41.7	-85.3	5' UTR		AT3G13229		✓	✓	25
GR_shootArea	3	8873116	C	T	-231.000	53.774	63	1.75E-05	0.0005	0.001	0.097	0.118	1952	40.9	-81.9	interg.				✓	✓	6
GR_rootLength	3	8873116	C	T	-12.100	3.164	63	1.33E-04	0.0037	0.003	0.097	0.118	1952	40.9	-81.9	interg.				✓	✓	6

GR_rootLength	3	11259214	A	T	-12.100	3.164	63	1.33E-04	0.0037	0.003	0.088	0.105	1952	40.9	-82.9	interg.				✓	✓	5
GR_shootArea	3	11259214	A	T	-231.000	53.774	63	1.75E-05	0.0005	0.001	0.088	0.105	1952	40.9	-82.9	interg.				✓	✓	5
bio8	3	11873293	A	G	37.800	8.736	65	1.52E-05	0.0069	0.006	0.939	1	1890	41.8	-83.7	tranposon		AT3G30219		✓		0
GR_rootLength	3	15050751	G	A	-12.100	3.164	63	1.33E-04	0.0037	0.003	0.108	0.105	1888	40.2	-82.5	interg.				✓	✓	4
GR_shootArea	3	15050751	G	A	-231.000	53.774	63	1.75E-05	0.0005	0.001	0.108	0.105	1888	40.2	-82.5	interg.				✓	✓	4
dirEquivalent	3	17164638	C	A	-0.014	0.004	63	5.30E-04	0.0052	0.018	0.19	0.227	1922	41.7	-85.3	interg.				✓		24
bio18	4	279210	T	G	6.830	1.987	99	5.83E-04	0.0124	0.047	0.196	0.24	1922	41.7	-85.3	interg.				✓		22
bio11	4	1732480	T	A	-5.550	1.564	79	3.89E-04	0.0195	0.045	0.063	0.068	2002	41	-87.5	interg.				✓		2
bio4	4	1732480	T	A	224.000	63.967	79	4.67E-04	0.0128	0.044	0.063	0.068	2002	41	-87.5	interg.				✓		2
dirEquivalent	4	3355152	C	G	-0.014	0.004	63	4.45E-04	0.0052	0.016	0.204	0.25	1922	41.7	-85.4	interg.				✓		21
bio18	4	3355152	C	G	6.850	1.944	##	4.25E-04	0.0124	0.035	0.204	0.25	1922	41.7	-85.4	interg.				✓		21
dirEquivalent	4	3355946	G	C	-0.014	0.004	63	4.45E-04	0.0052	0.016	0.204	0.25	1922	41.7	-85.4	interg.				✓		20
bio18	4	3355946	G	C	6.850	1.944	##	4.25E-04	0.0124	0.035	0.204	0.25	1922	41.7	-85.4	interg.				✓		20
dirEquivalent	4	4228138	A	G	-0.014	0.004	63	4.45E-04	0.0052	0.016	0.196	0.24	1922	41.7	-85.3	tranposon		AT4G07440		✓		19
bio18	4	4228138	A	G	6.830	1.987	99	5.83E-04	0.0124	0.047	0.196	0.24	1922	41.7	-85.3	tranposon		AT4G07440		✓		19
dirEquivalent	4	9046942	G	C	-0.014	0.004	63	4.45E-04	0.0052	0.016	0.204	0.25	1922	41.7	-85.4	nonsyr	H->Q	AT4G15960	24	✓		18
bio18	4	9046942	G	C	6.850	1.944	##	4.25E-04	0.0124	0.035	0.204	0.25	1922	41.7	-85.4	nonsyr	H->Q	AT4G15960	24	✓		18
dirEquivalent	4	11948961	T	A	-0.014	0.004	63	4.45E-04	0.0052	0.016	0.198	0.25	1952	41.7	-85.3	interg.				✓		17
dirEquivalent	4	12365323	C	T	-0.014	0.004	63	4.45E-04	0.0052	0.016	0.204	0.25	1922	41.7	-85.4	interg.				✓		16
bio18	4	12365323	C	T	6.850	1.944	##	4.25E-04	0.0124	0.035	0.204	0.25	1922	41.7	-85.4	interg.				✓		16
dirEquivalent	4	15646341	C	A	-0.014	0.004	63	4.45E-04	0.0052	0.016	0.206	0.25	1922	41.7	-85.4	syn.	E->E	AT4G32410		✓		15
bio18	4	15646341	C	A	6.720	1.936	99	5.14E-04	0.0124	0.042	0.206	0.25	1922	41.7	-85.4	syn.	E->E	AT4G32410		✓		15
dirEquivalent	4	15845001	A	T	-0.014	0.004	63	4.45E-04	0.0052	0.016	0.194	0.25	1922	41.8	-85.9	3' UTR		AT4G32840		✓		14
dirEquivalent	4	18249171	T	A	-0.014	0.004	63	4.45E-04	0.0052	0.016	0.274	0.328	1922	41.8	-85.9	interg.				✓		13
bio18	4	18249171	T	A	6.910	2.005	71	5.62E-04	0.0124	0.047	0.274	0.328	1922	41.8	-85.9	interg.				✓		13
bio18	5	4245213	A	T	6.830	1.987	99	5.83E-04	0.0124	0.047	0.196	0.24	1922	41.7	-85.3	syn.	I->I	AT5G13260		✓		12
bio18	5	4500202	G	A	6.830	1.987	99	5.83E-04	0.0124	0.047	0.196	0.24	1922	41.7	-85.3	nonsyr	A->G	AT5G13950	60	✓		11
dirEquivalent	5	4797923	A	T	-0.014	0.004	63	5.30E-04	0.0052	0.018	0.188	0.227	1922	41.7	-85.3	tranposon		AT5G14830		✓		10
dirEquivalent	5	4797976	G	A	-0.014	0.004	63	5.30E-04	0.0052	0.018	0.257	0.293	1922	41.7	-85.3	tranposon		AT5G14830		✓		10
dirEquivalent	5	4798526	A	G	-0.014	0.004	63	5.30E-04	0.0052	0.018	0.339	0.362	1922	41.7	-85.3	interg.				✓		9
gravitropicScore	5	6508329	A	G	-0.020	0.006	63	5.20E-04	0.0651	0.008	0.35	0.447	1922	42	-85	nonsyr	C->W	AT5G19330	215	✓		0
dirEquivalent	5	11090365	T	A	-0.014	0.004	63	5.30E-04	0.0052	0.018	0.186	0.224	1922	41.7	-85.3	TE		AT5G29037		✓		4
dirEquivalent	5	12312975	C	G	-0.014	0.004	63	5.30E-04	0.0052	0.018	0.185	0.224	1922	41.7	-85.3	TE		AT5G32630		✓		3
dirEquivalent	5	12358159	C	T	-0.014	0.004	63	5.30E-04	0.0052	0.018	0.186	0.224	1922	41.7	-85.3	tranposon		AT5G32825		✓		2
dirEquivalent	5	12409027	G	A	-0.014	0.004	63	5.30E-04	0.0052	0.018	0.185	0.224	1922	41.7	-85.3	interg.				✓		1

GR_rootLength	5	16024197	A	T	-12.100	3.164	63	1.33E-04	0.0037	0.003	0.098	0.118	1952	40.9	-81.9	intron	AT5G40020	✓	✓	2
GR_shootArea	5	16024197	A	T	-231.000	53.774	63	1.75E-05	0.0005	0.001	0.098	0.118	1952	40.9	-81.9	intron	AT5G40020	✓	✓	2
GR_shootArea	5	16109431	G	A	-231.000	53.774	63	1.75E-05	0.0005	0.001	0.865	0.877	1993	42.2	-84.4	interg.		✓	✓	1
GR_rootLength	5	16109431	G	A	-12.100	3.164	63	1.33E-04	0.0037	0.003	0.865	0.877	1993	42.2	-84.4	interg.		✓	✓	1
dirEquivalent	5	19099082	G	C	-0.014	0.004	63	5.30E-04	0.0052	0.018	0.186	0.227	1922	41.7	-85.3	interg.		✓		0
GR_rootLength	5	20388107	A	T	-10.700	3.164	63	6.94E-04	0.017	0.017	0.099	0.12	2002	41	-86.6	interg.		✓		0

Data Appendix S1

bioRxiv preprint doi: https://doi.org/10.1101/050203; this version posted October 5, 2017. The copyright holder for this preprint (which was not certified by peer review) is the author/funder, who has granted bioRxiv a license to display the preprint in perpetuity. It is made available under aCC-BY-NC-ND 4.0 International license.

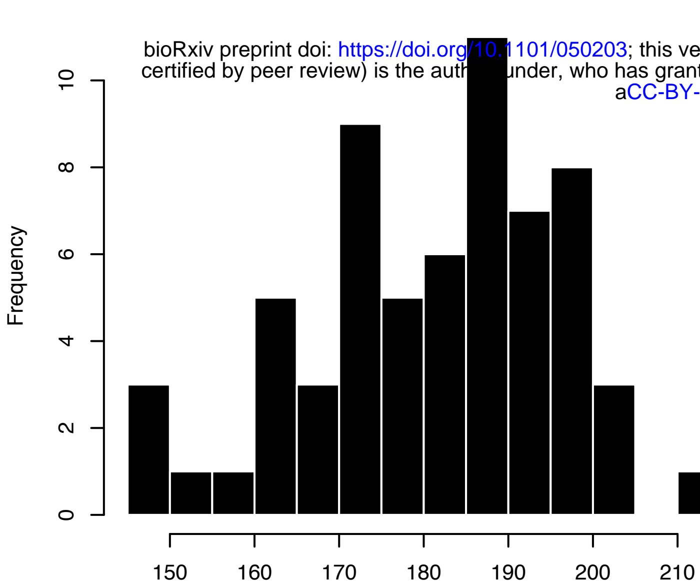

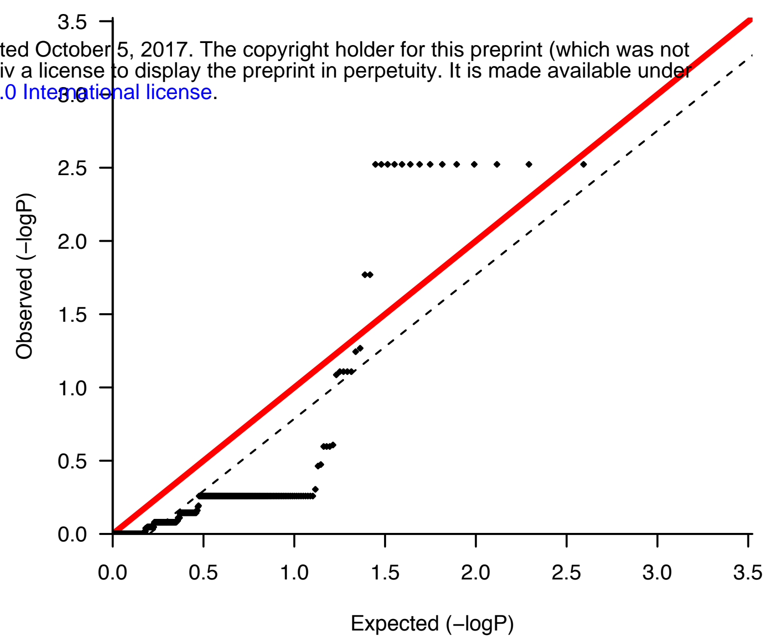

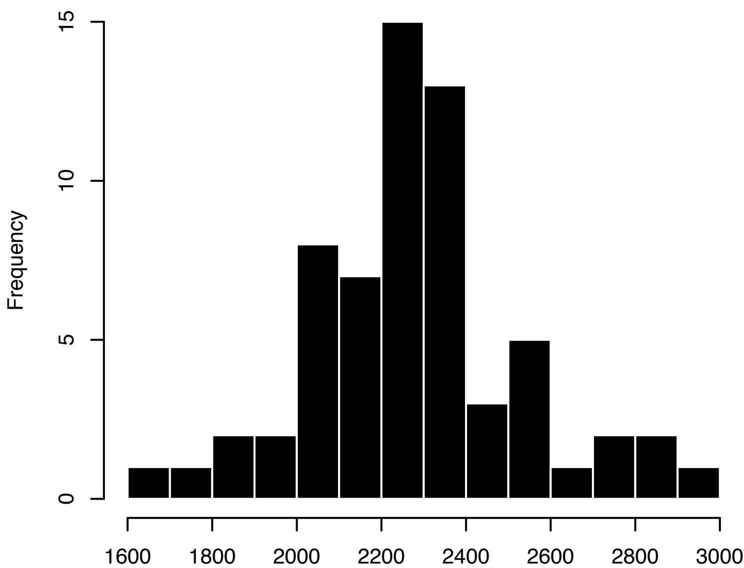

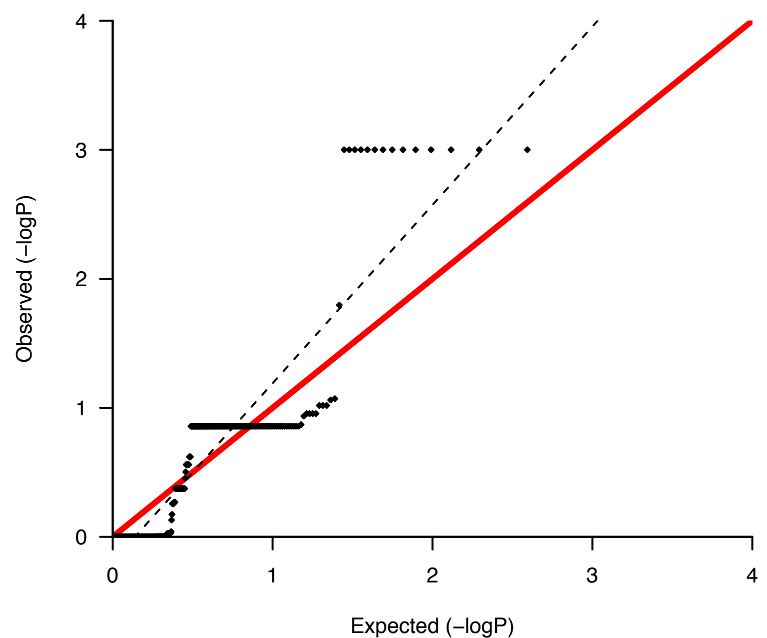

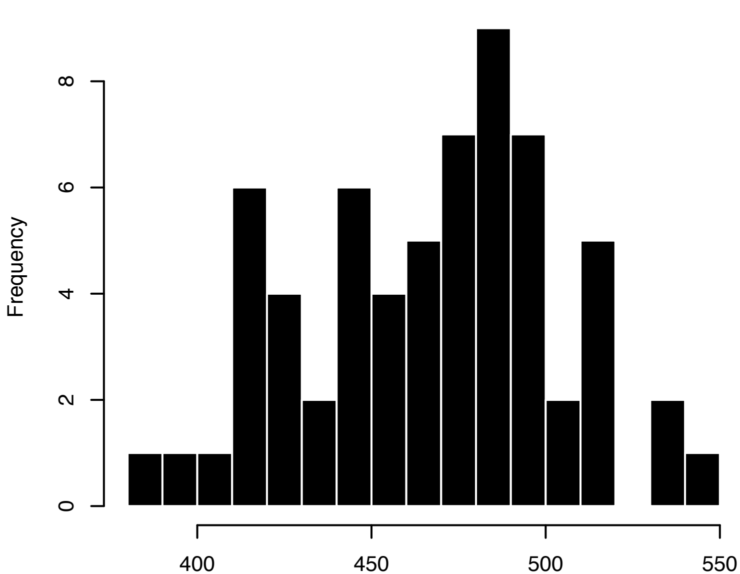

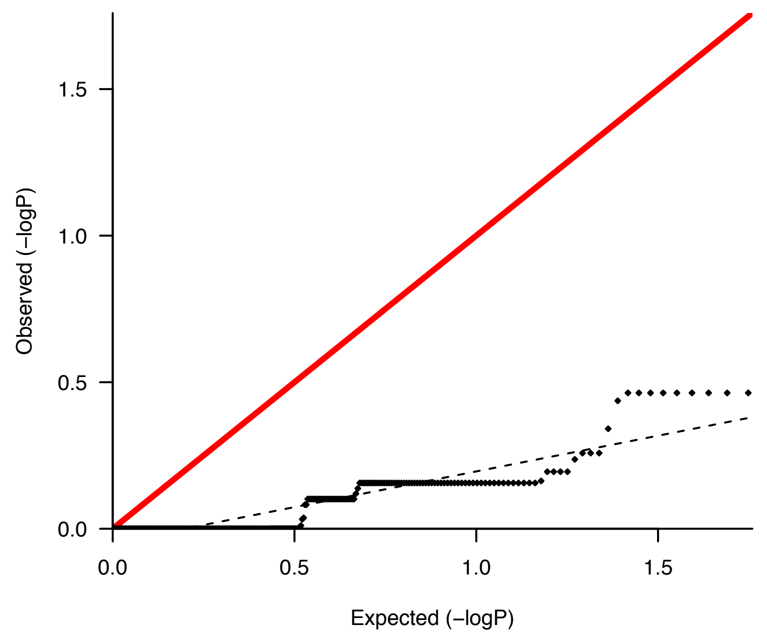

bioRxiv preprint doi: https://doi.org/10.1101/050203; this version posted October 5, 2017. The copyright holder for this preprint (which was not certified by peer review) is the author/funder, who has granted bioRxiv a license to display the preprint in perpetuity. It is made available under aCC-BY-NC-ND 4.0 International license.

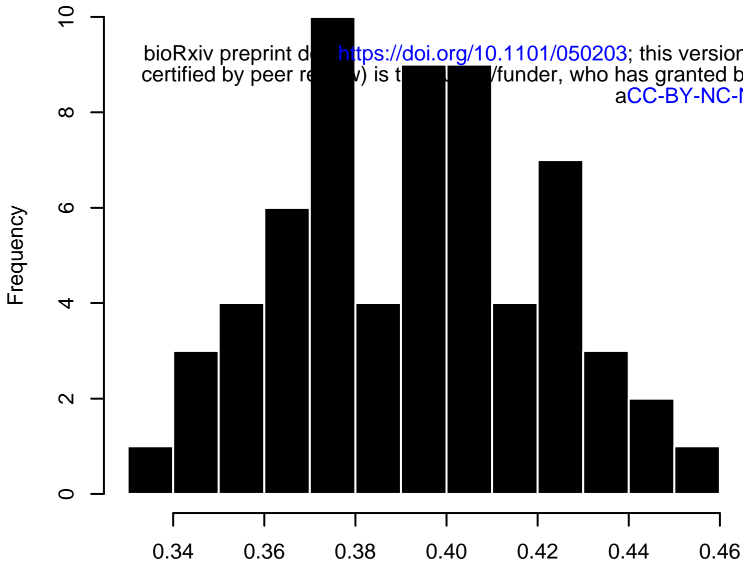

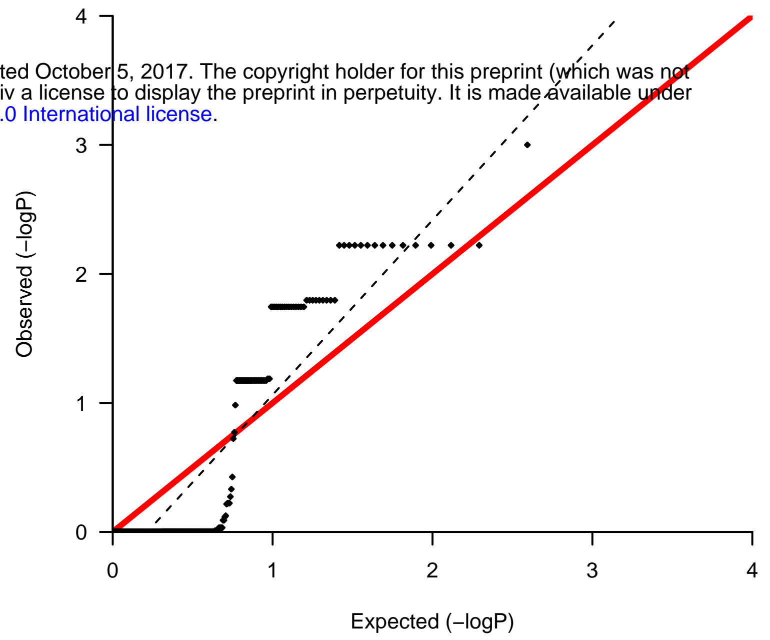

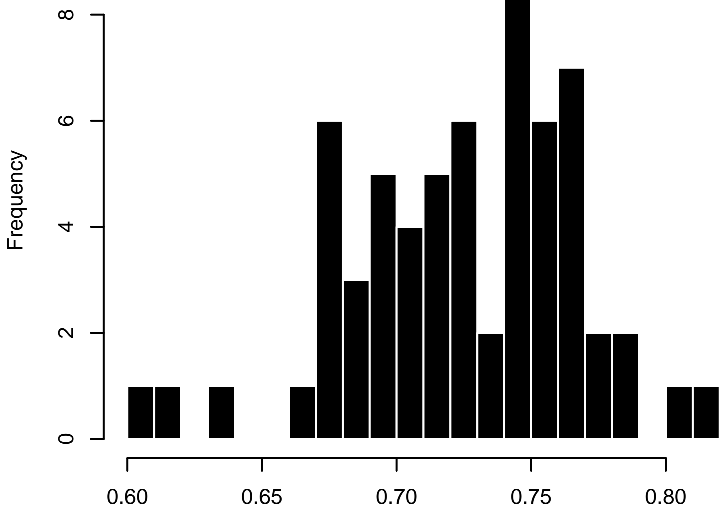

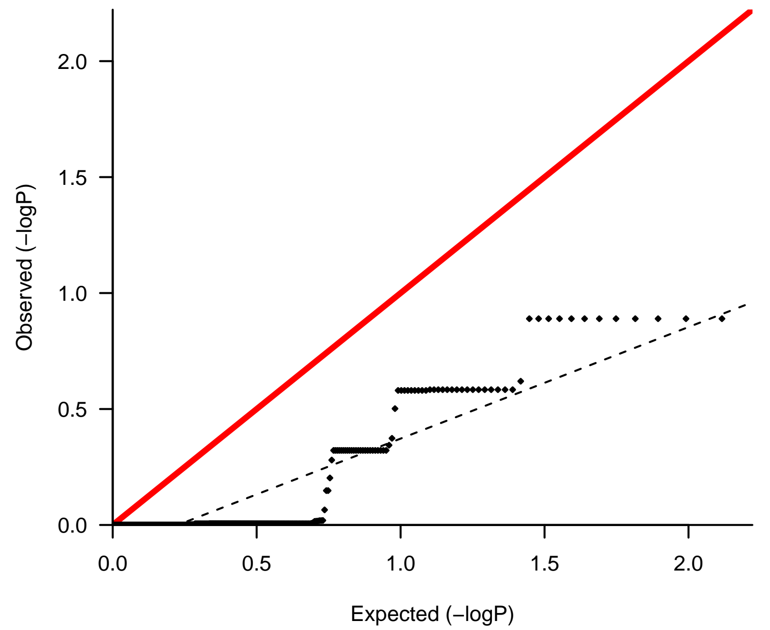

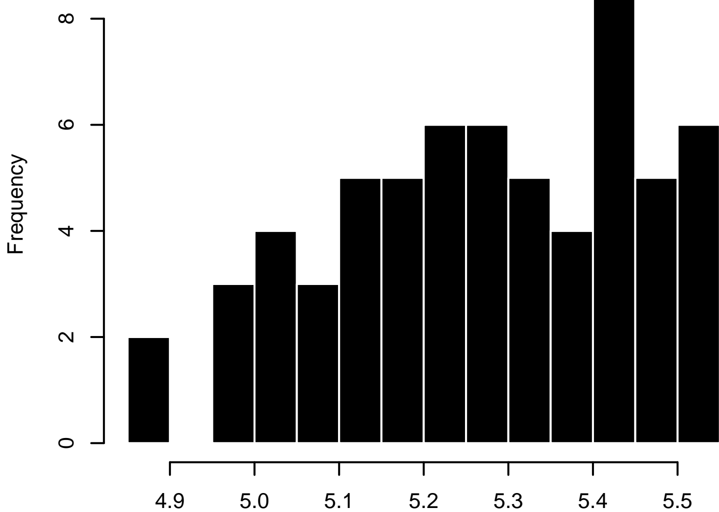

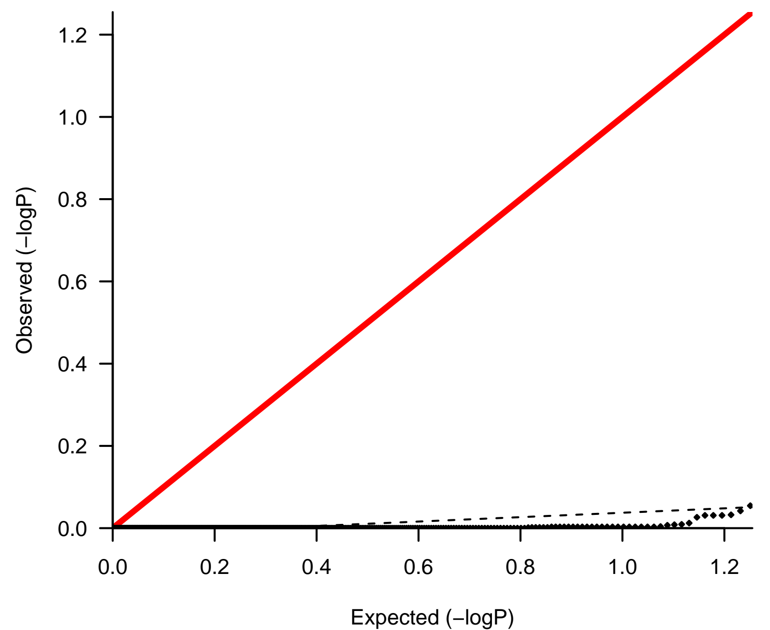

bioRxiv preprint doi: https://doi.org/10.1101/050203; this version posted October 5, 2017. The copyright holder for this preprint (which was not certified by peer review) is the author/funder, who has granted bioRxiv a license to display the preprint in perpetuity. It is made available under aCC-BY-NC-ND 4.0 International license.

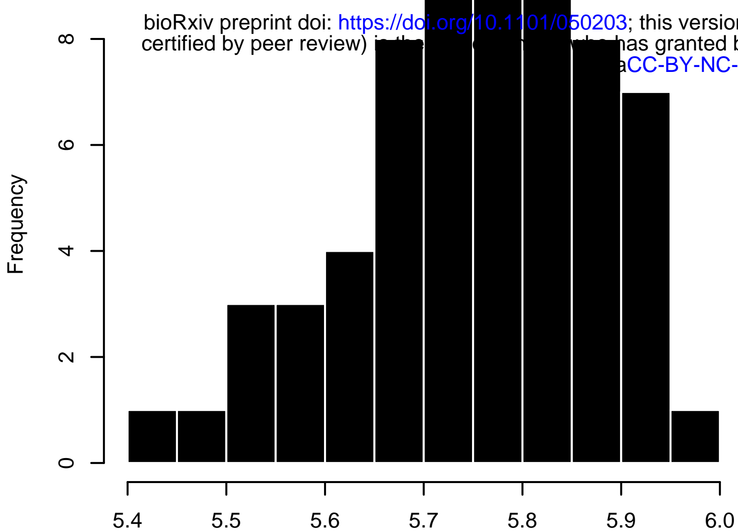

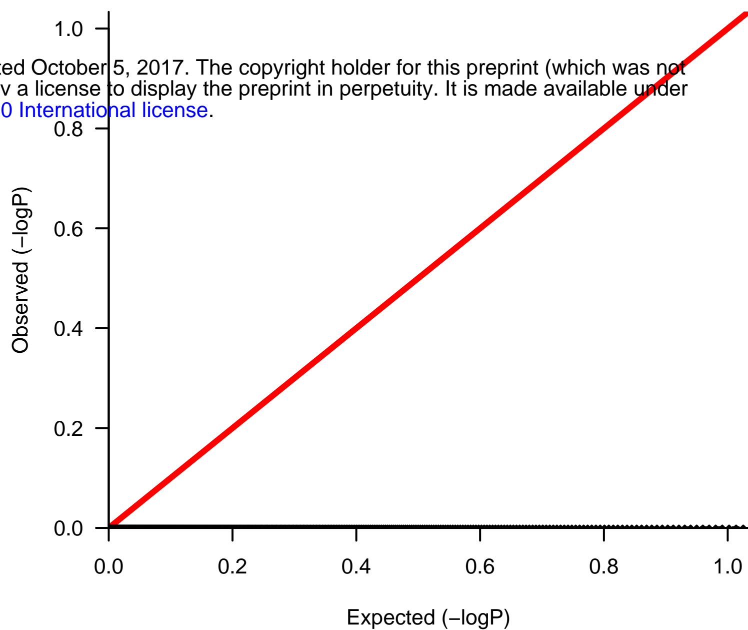

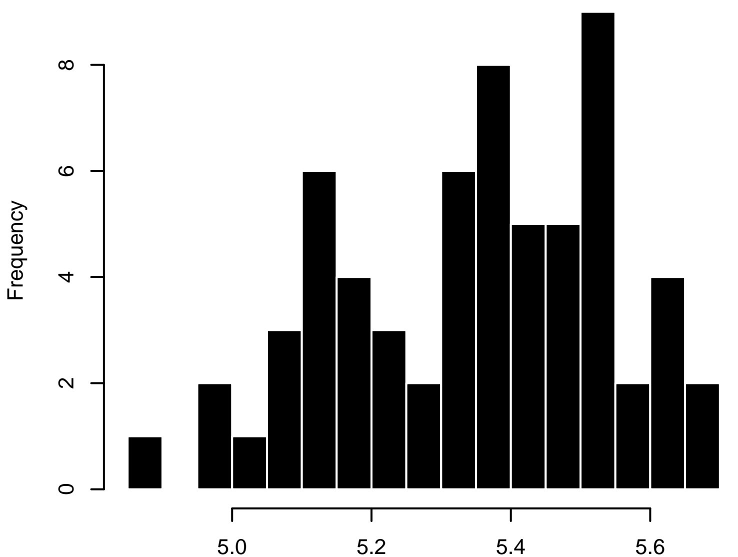

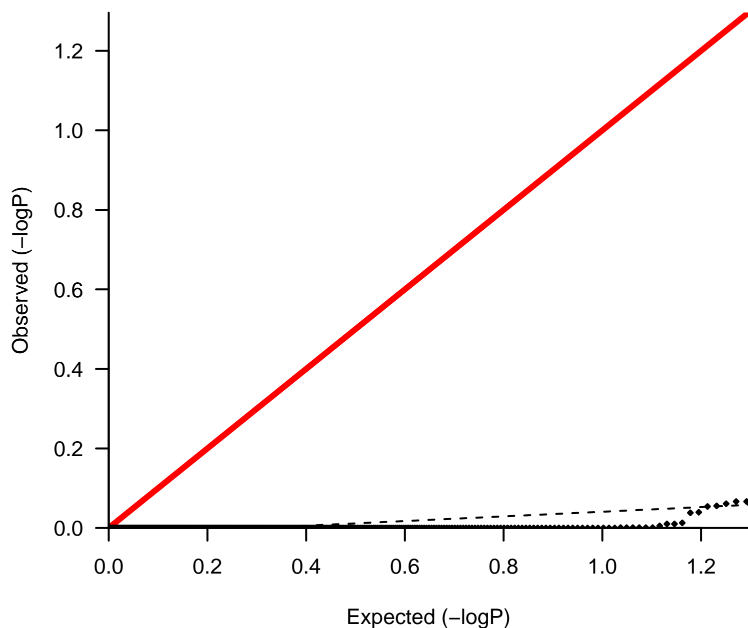

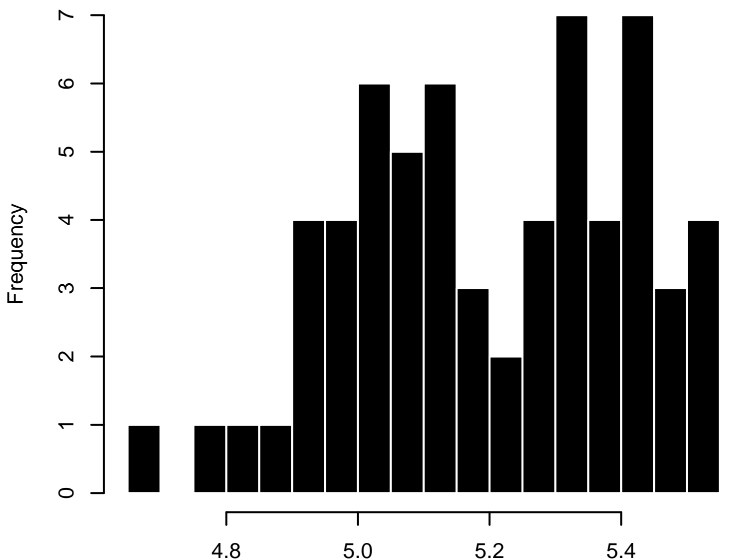

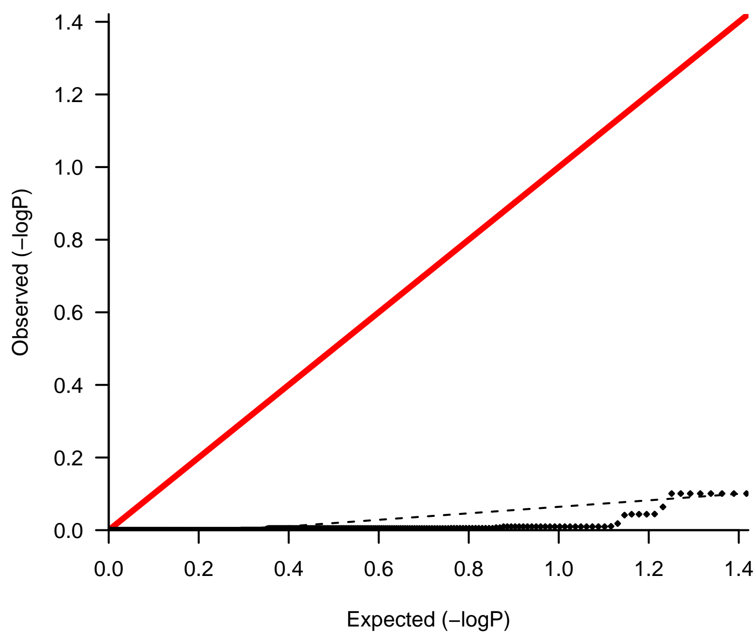

bioRxiv preprint doi: https://doi.org/10.1101/050203; this version posted October 5, 2017. The copyright holder for this preprint (which was not certified by peer review) is the author/funder, who has granted bioRxiv a license to display the preprint in perpetuity. It is made available under aCC-BY-NC-ND 4.0 International license.

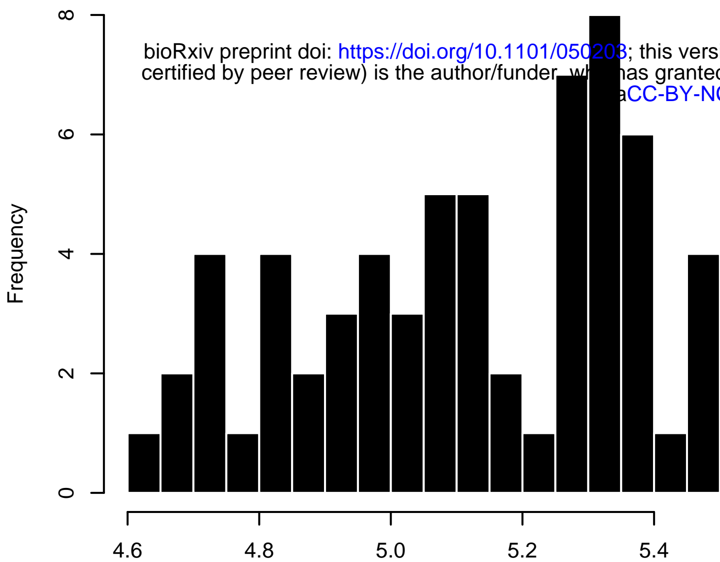

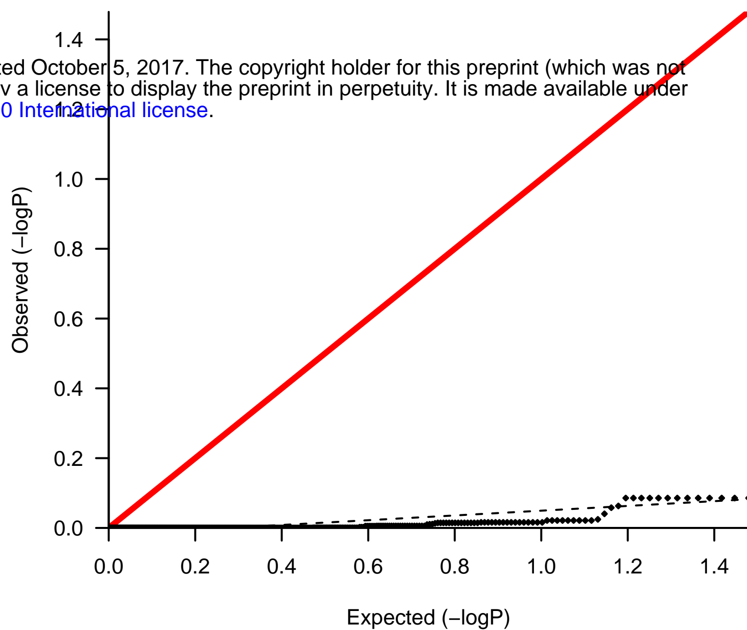

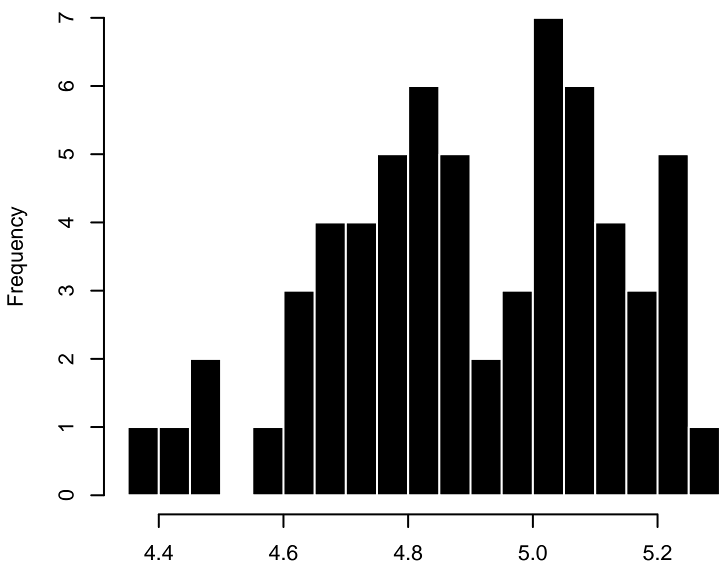

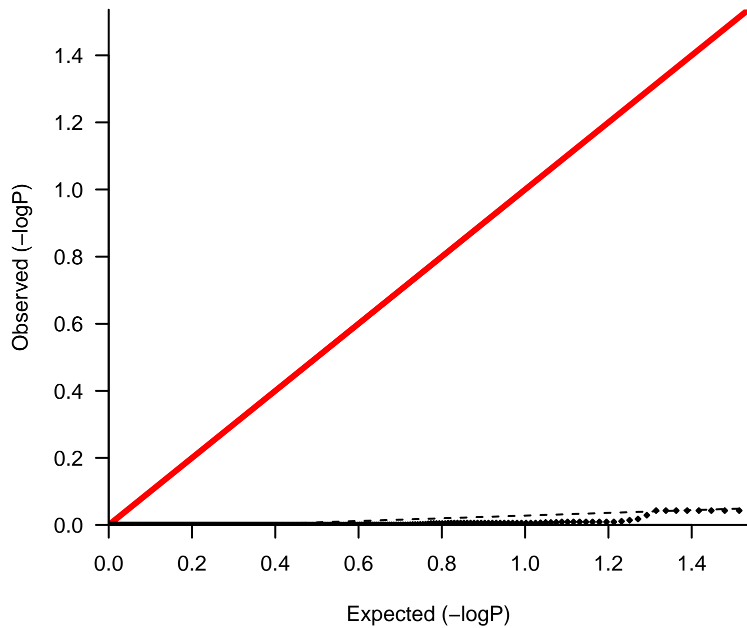

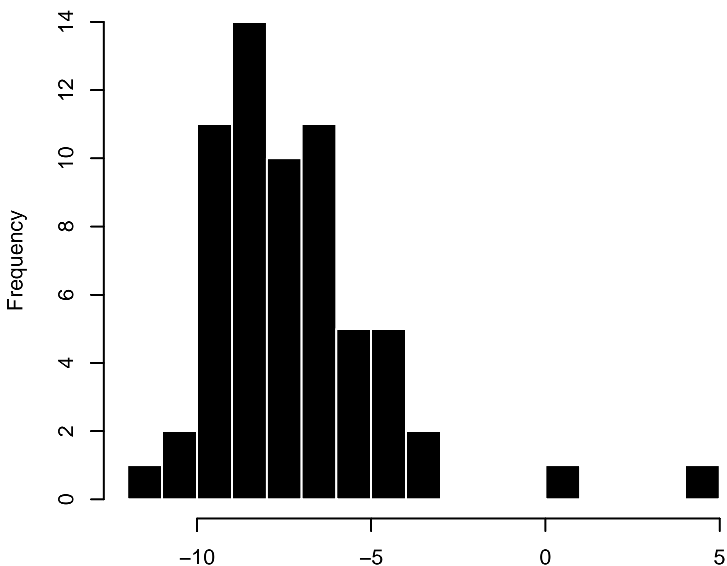

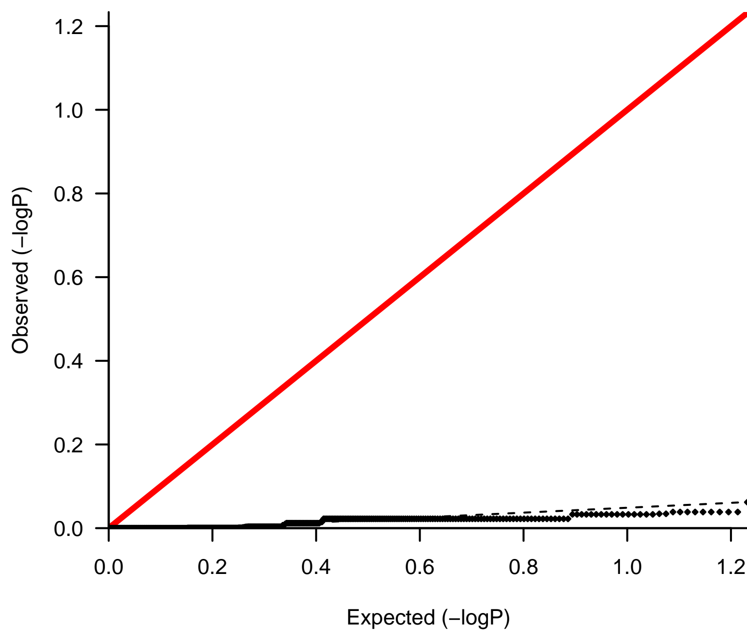

bioRxiv preprint doi: https://doi.org/10.1101/050203; this version posted October 5, 2017. The copyright holder for this preprint (which was not certified by peer review) is the author/funder, who has granted bioRxiv a license to display the preprint in perpetuity. It is made available under aCC-BY-NC-ND 4.0 International license.

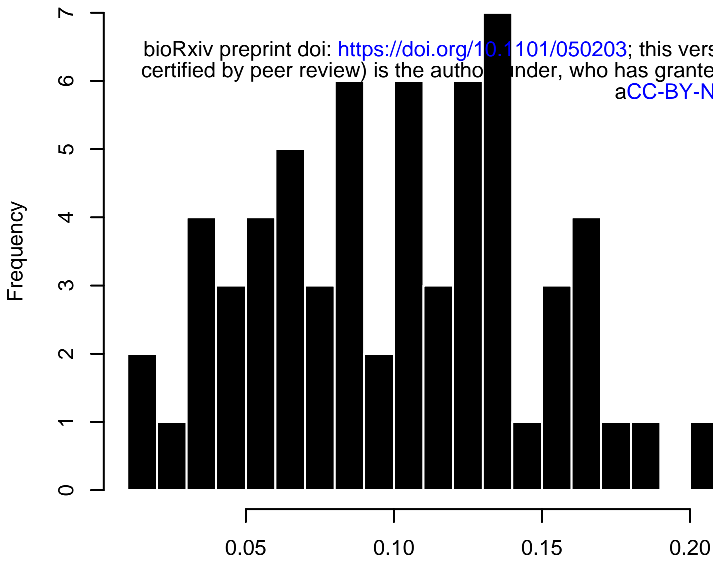

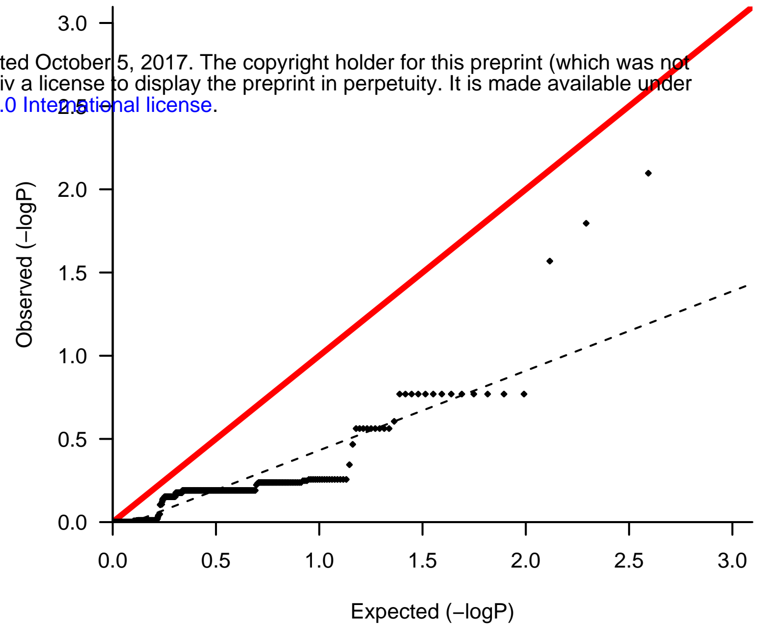

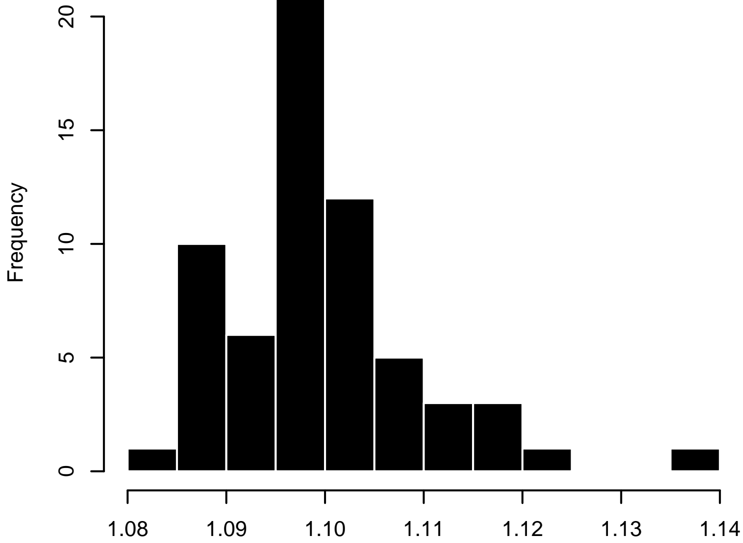

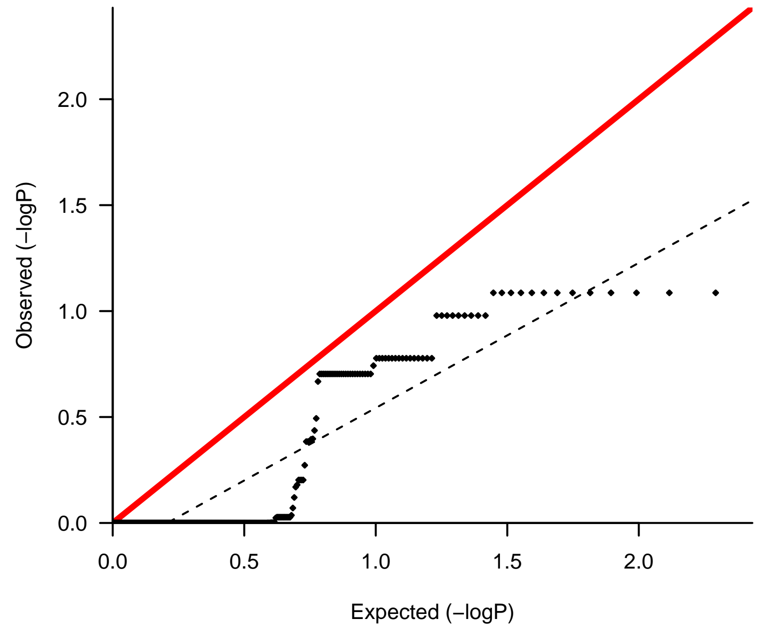

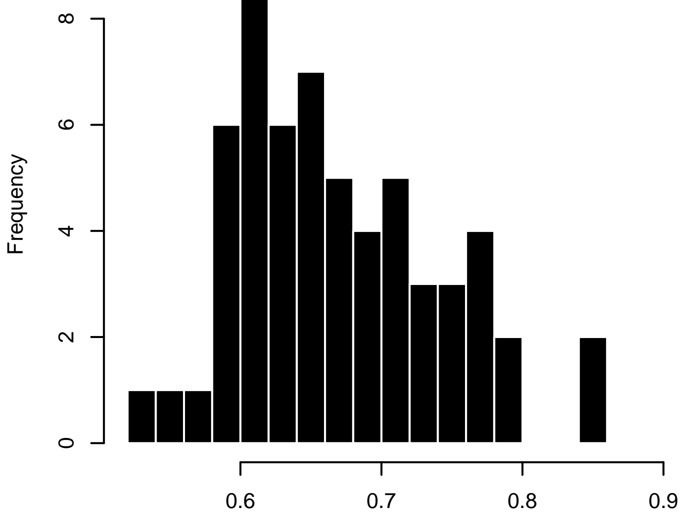

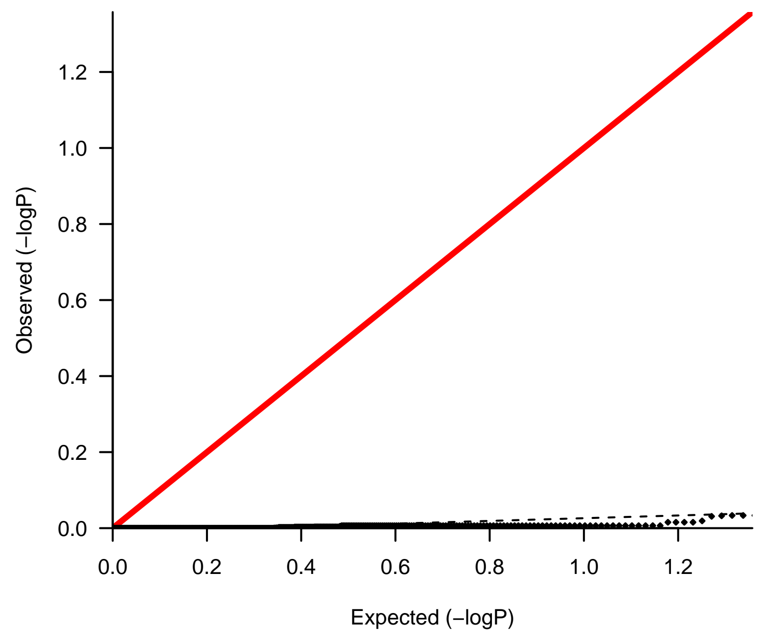

bioRxiv preprint doi: https://doi.org/10.1101/050203; this version posted October 5, 2017. The copyright holder for this preprint (which was not certified by peer review) is the author/funder, who has granted bioRxiv a license to display the preprint in perpetuity. It is made available under aCC-BY-NC-ND 4.0 International license.

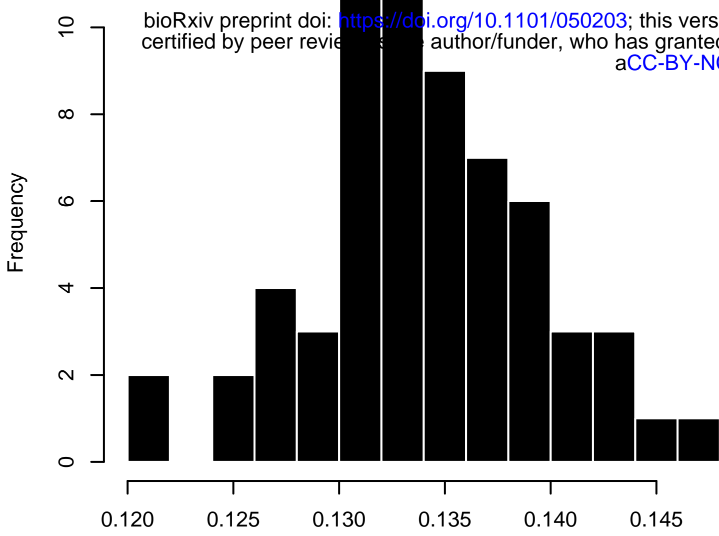

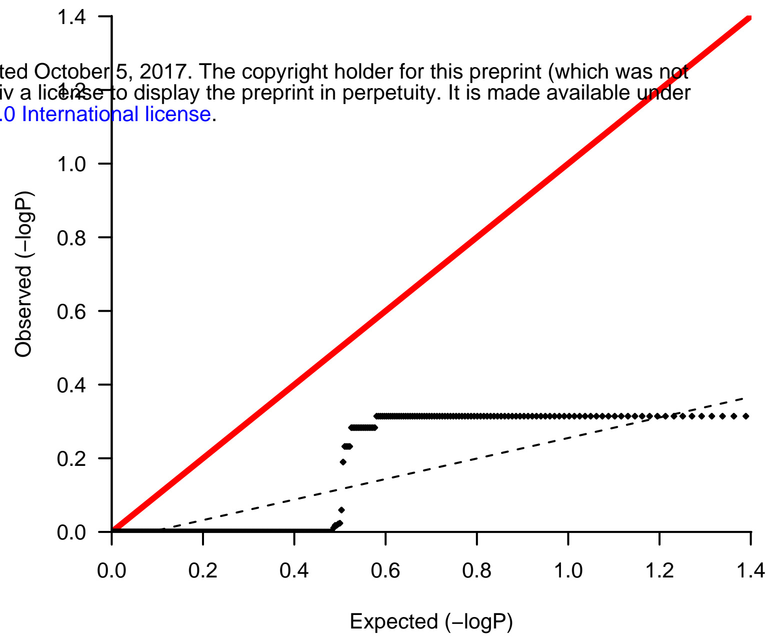

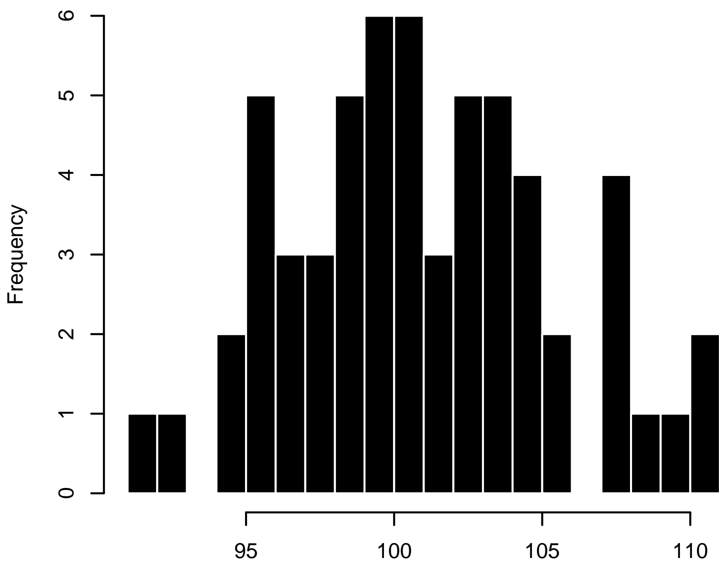

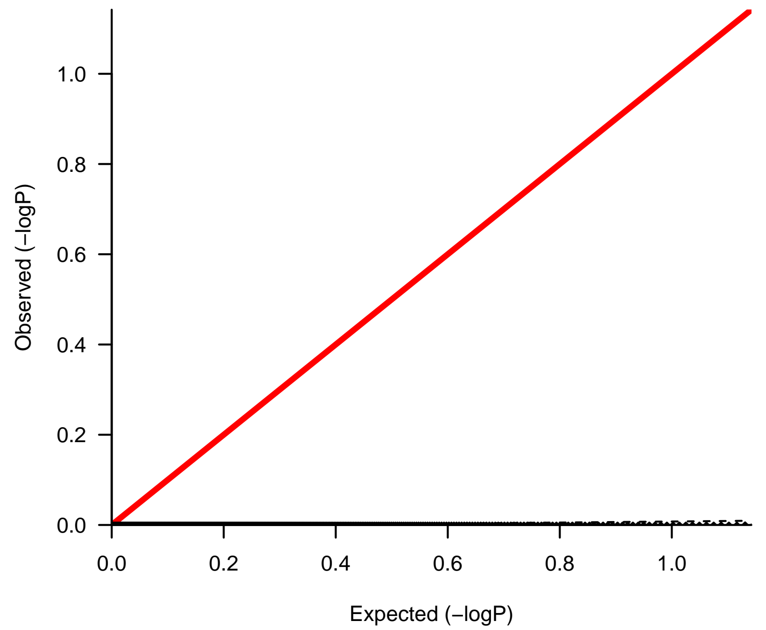

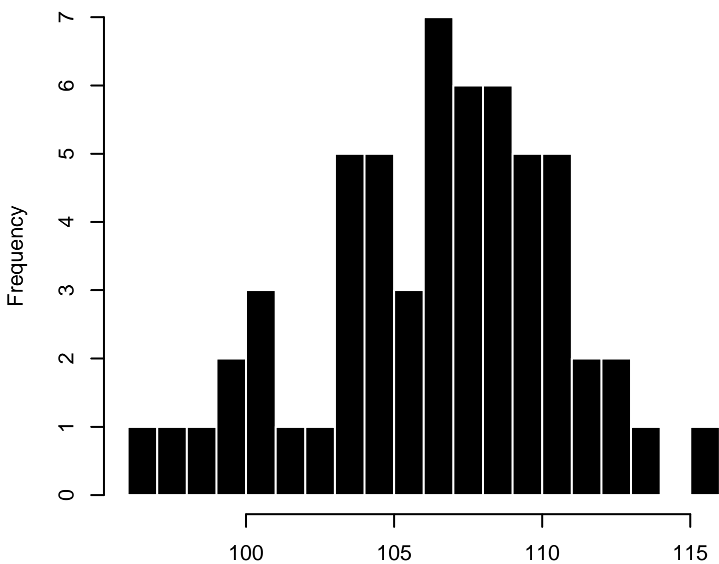

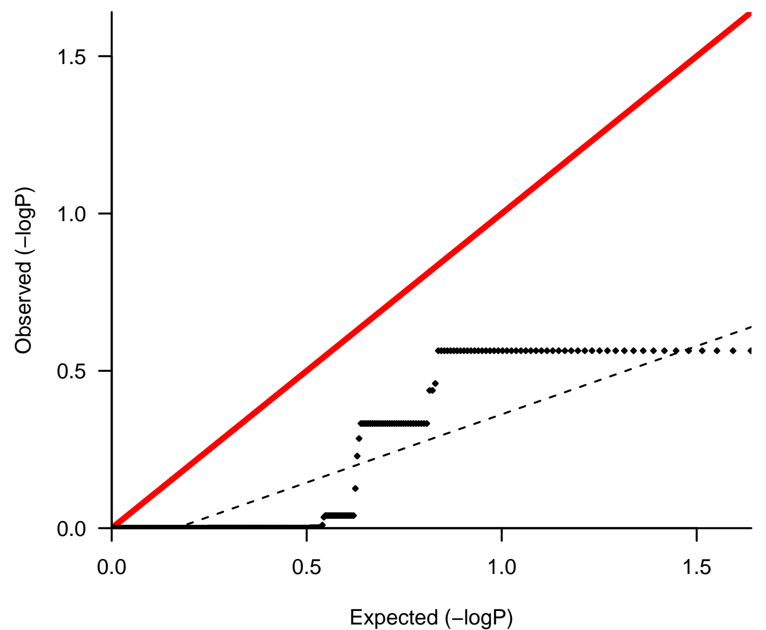

bioRxiv preprint doi: https://doi.org/10.1101/050203; this version posted October 5, 2017. The copyright holder for this preprint (which was not certified by peer review) is the author/funder, who has granted bioRxiv a license to display the preprint in perpetuity. It is made available under aCC-BY-NC-ND 4.0 International license.

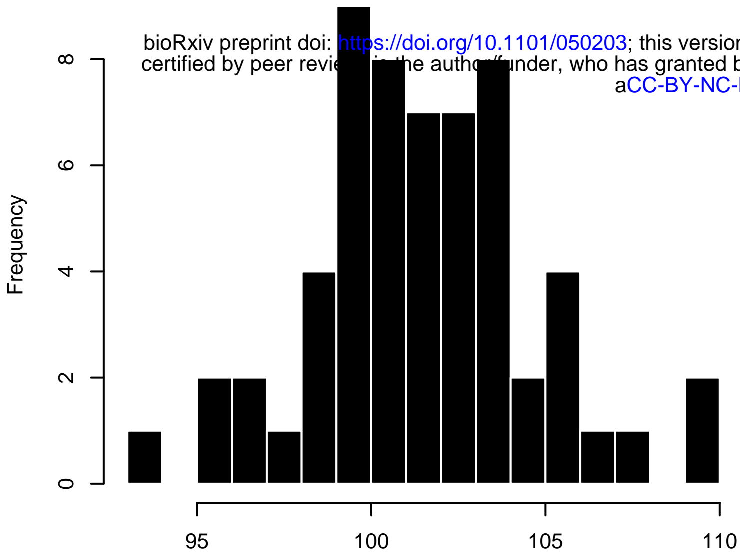

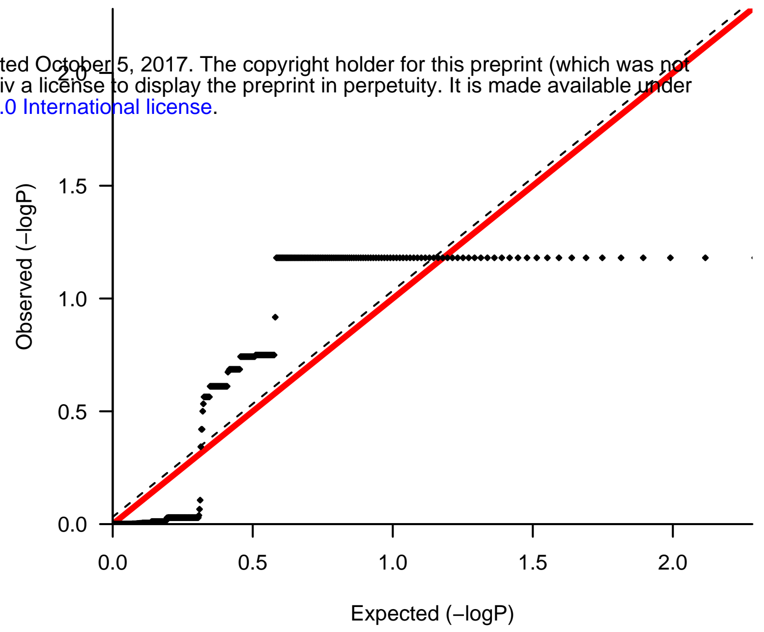

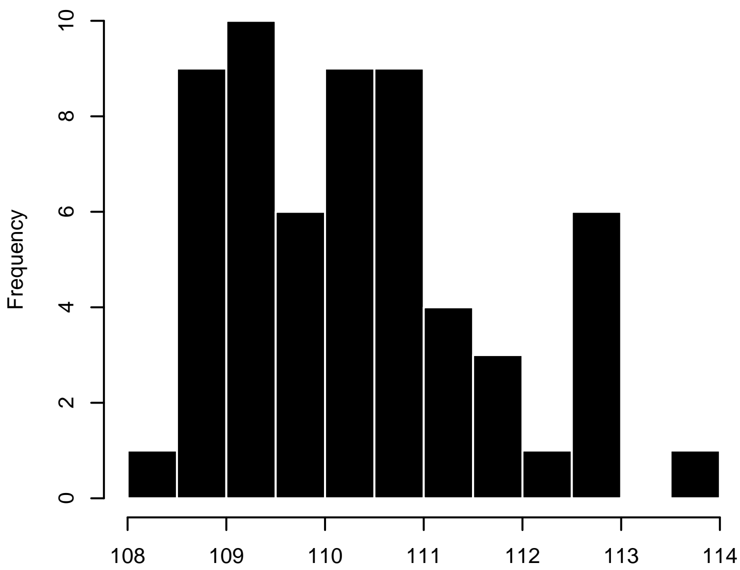

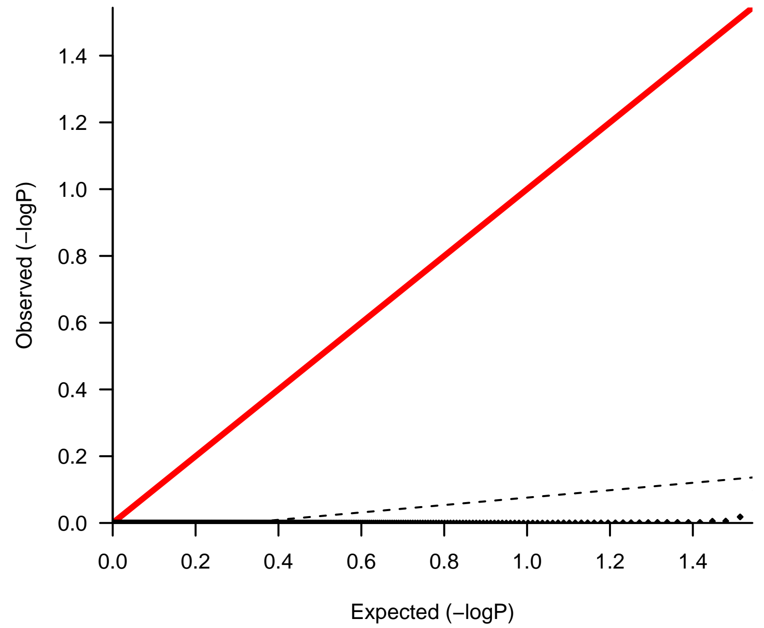

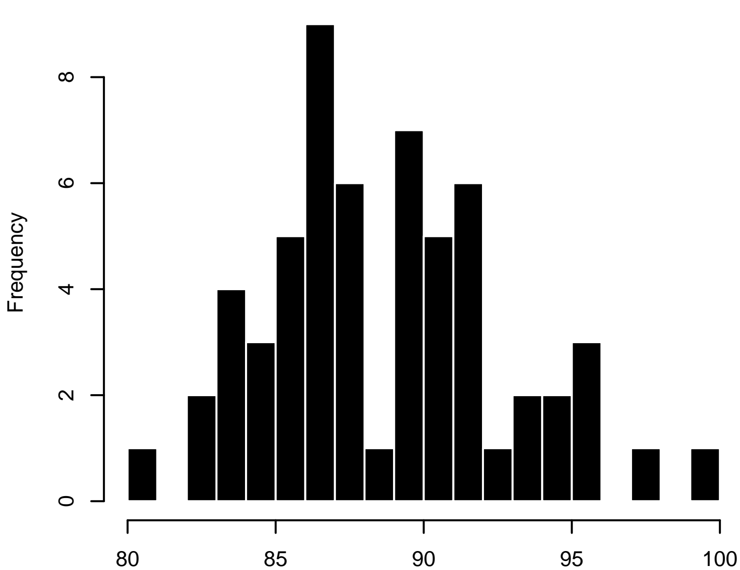

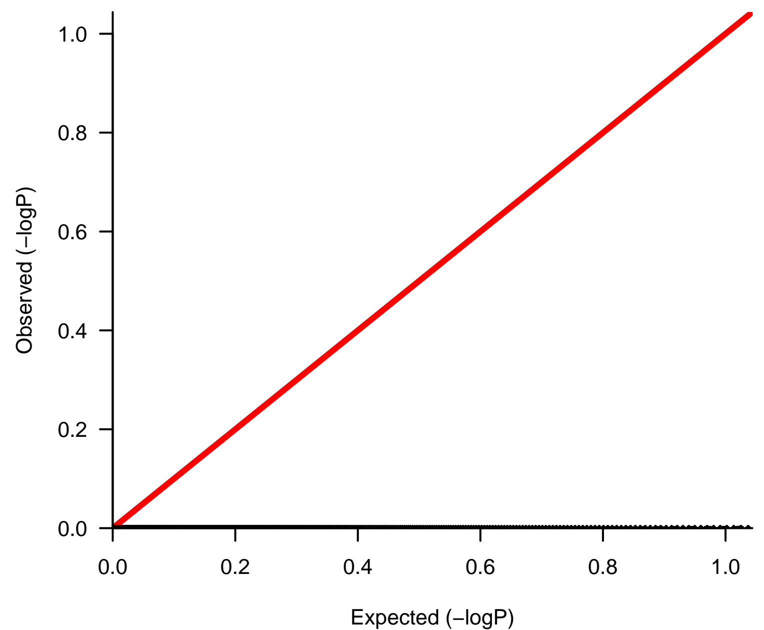

bioRxiv preprint doi: https://doi.org/10.1101/050203; this version posted October 5, 2017. The copyright holder for this preprint (which was not certified by peer review) is the author/funder, who has granted bioRxiv a license to display the preprint in perpetuity. It is made available under aCC-BY-NC-ND 4.0 International license.

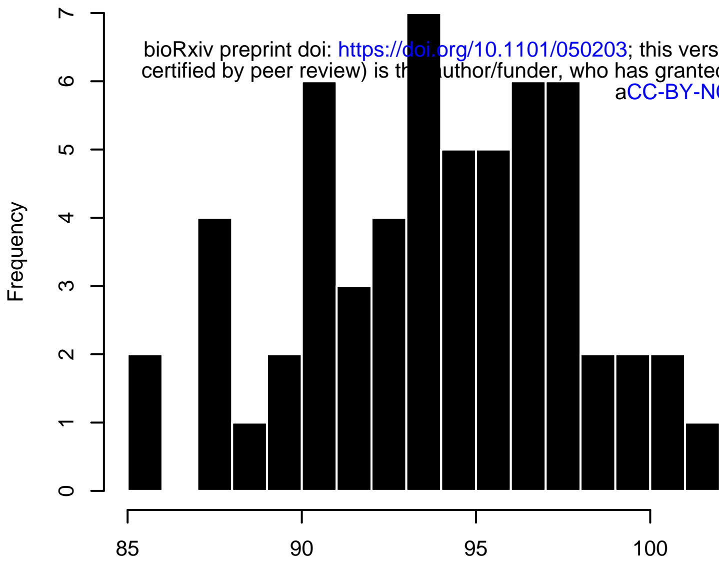

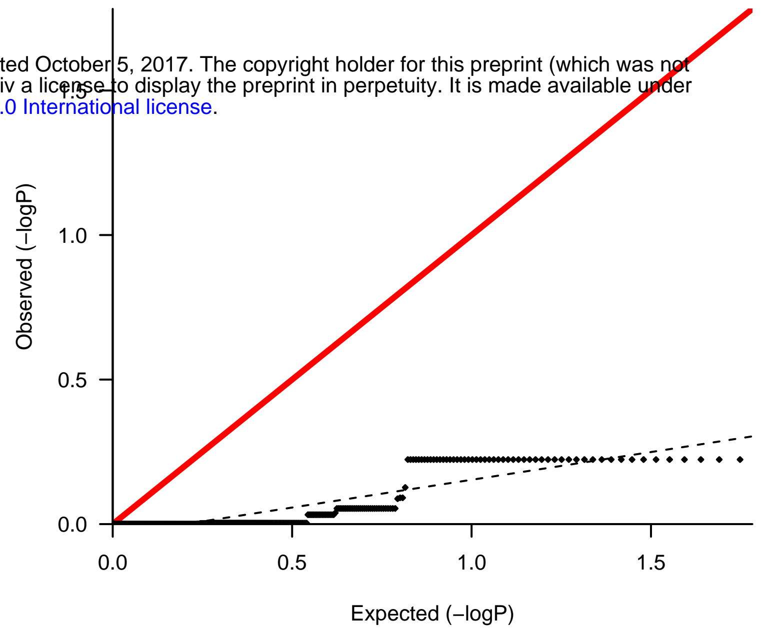

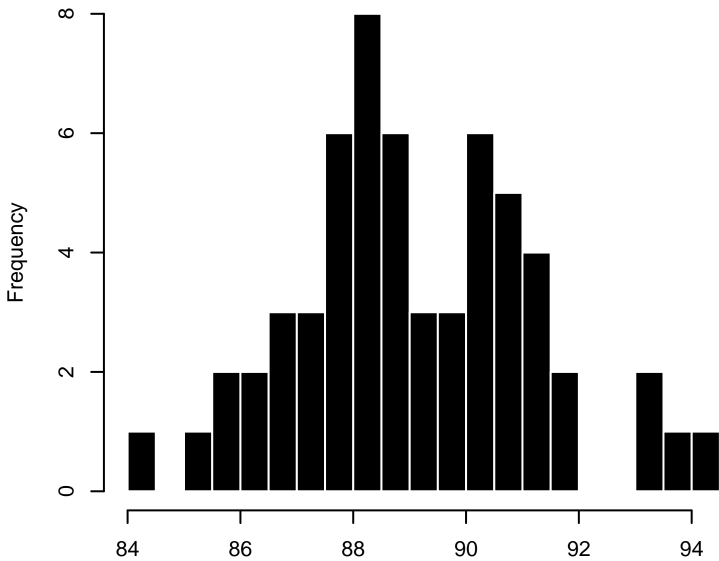

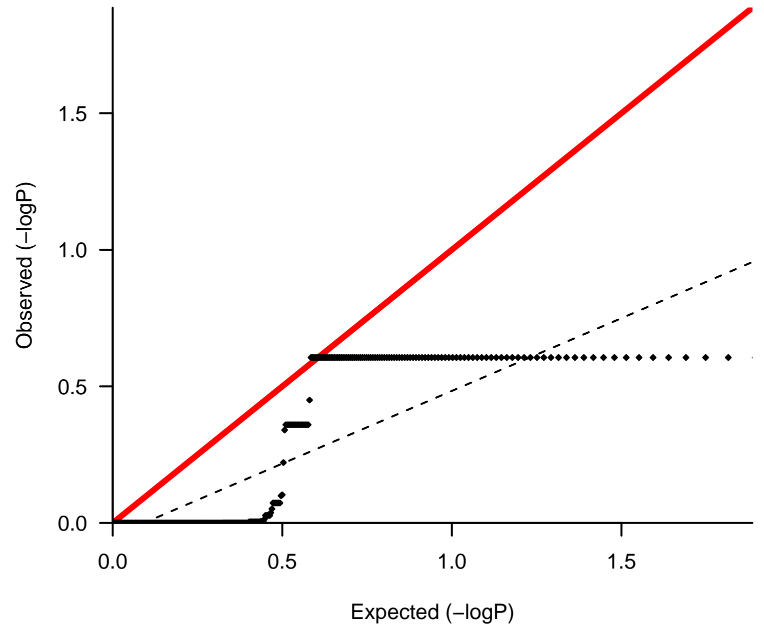

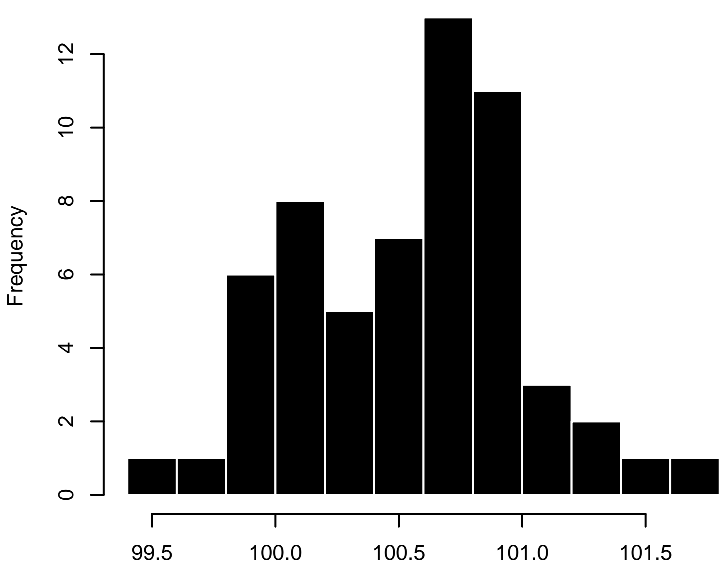

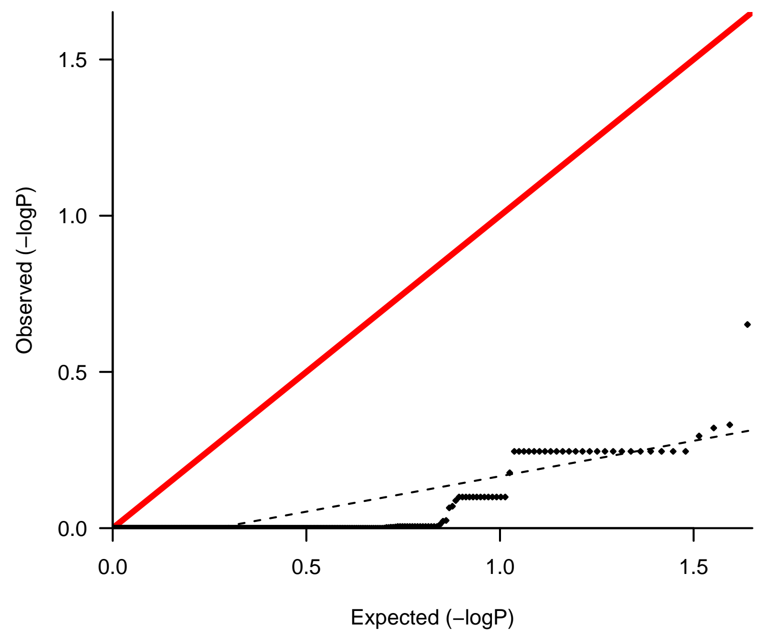

bioRxiv preprint doi: https://doi.org/10.1101/050203; this version posted October 5, 2017. The copyright holder for this preprint (which was not certified by peer review) is the author/funder, who has granted bioRxiv a license to display the preprint in perpetuity. It is made available under aCC-BY-NC-ND 4.0 International license.

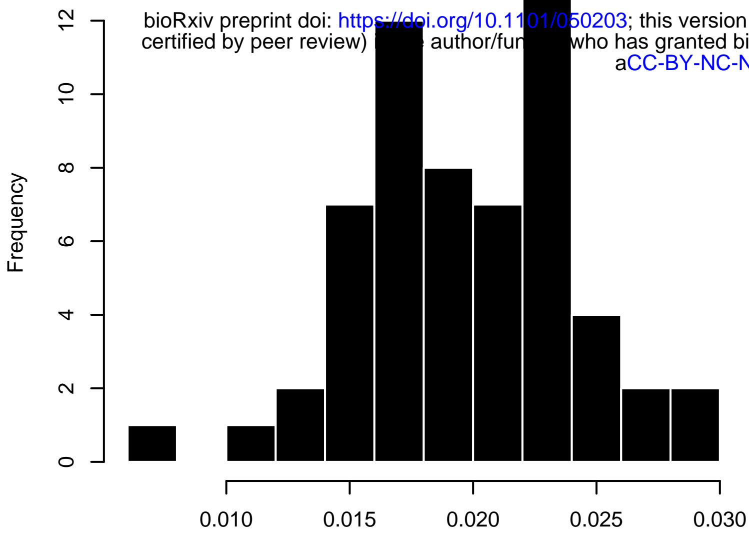

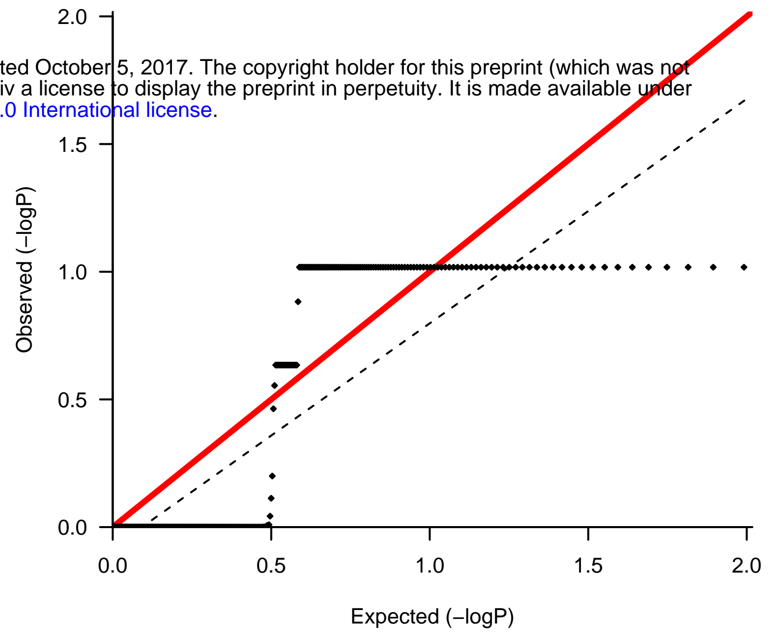

bioRxiv preprint doi: https://doi.org/10.1101/050203; this version posted October 5, 2017. The copyright holder for this preprint (which was not certified by peer review) is the author/funder, who has granted bioRxiv a license to display the preprint in perpetuity. It is made available under aCC-BY-NC-ND 4.0 International license.

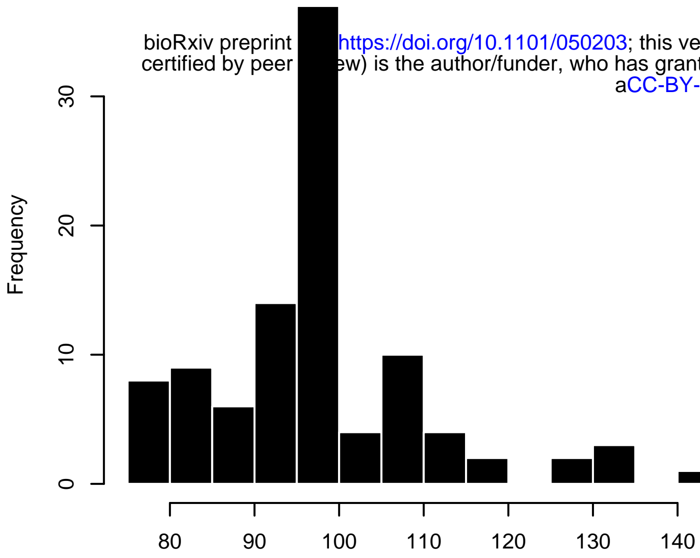

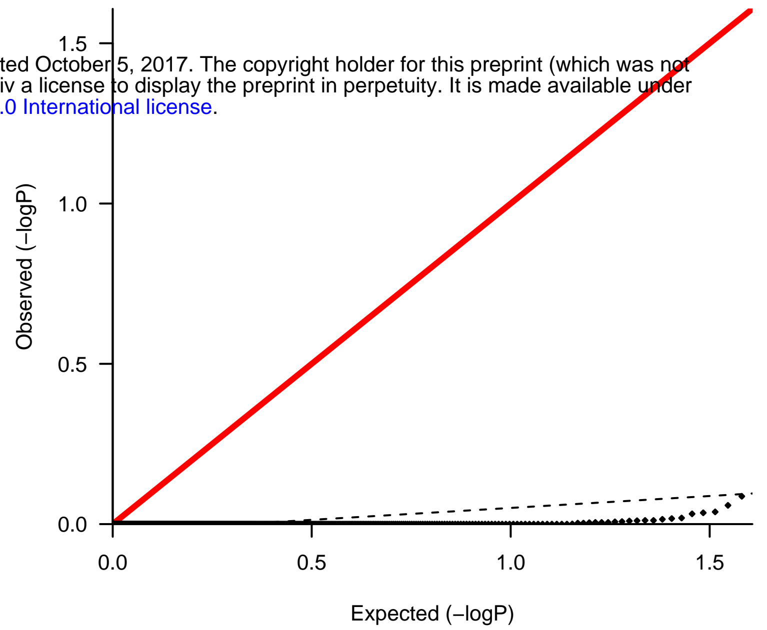

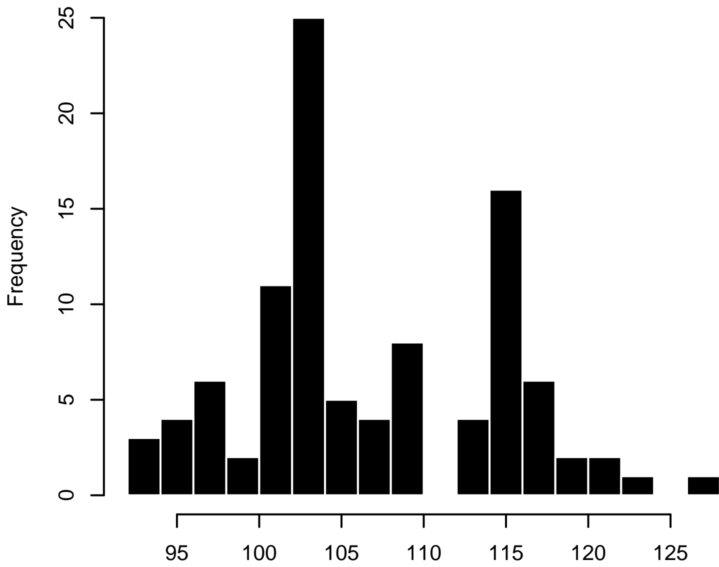

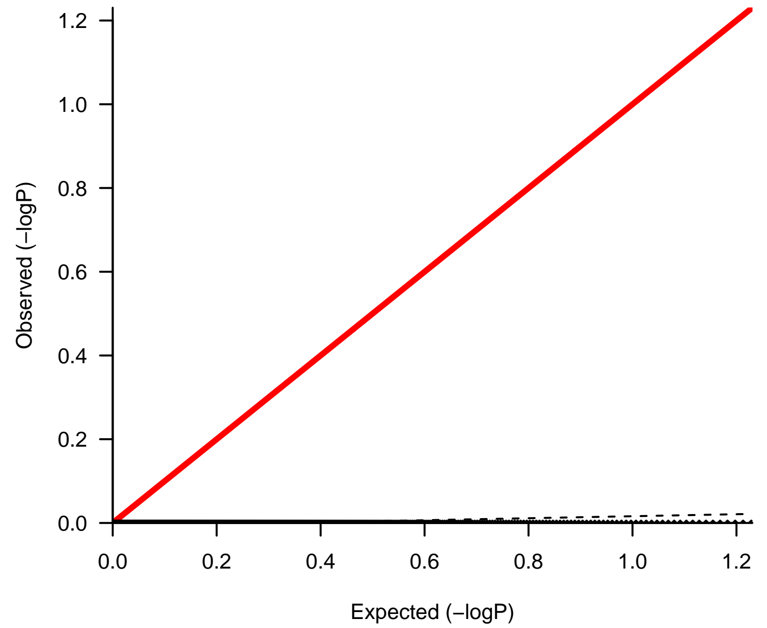

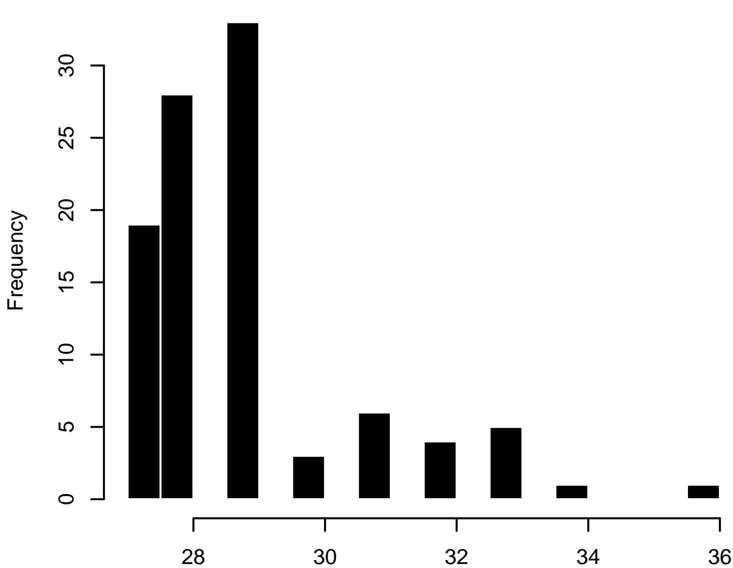

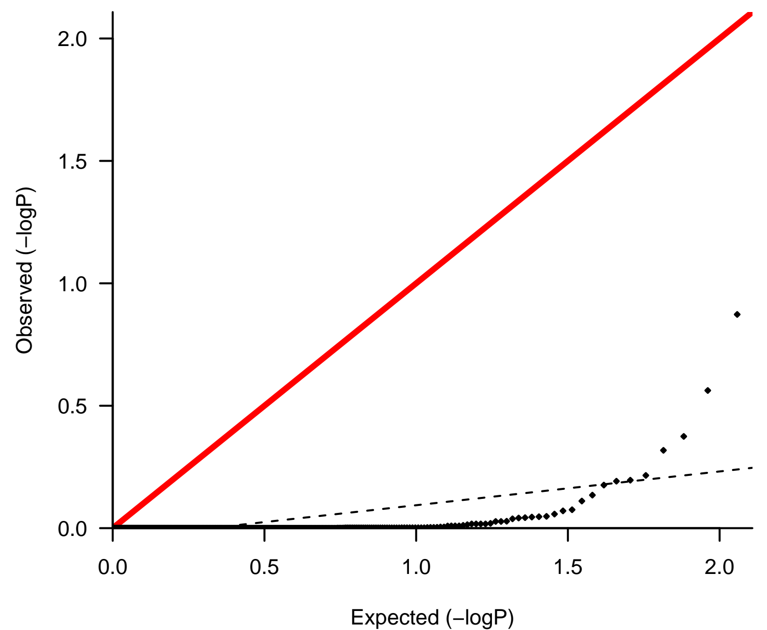

bioRxiv preprint doi: https://doi.org/10.1101/050203; this version posted October 5, 2017. The copyright holder for this preprint (which was not certified by peer review) is the author/funder, who has granted bioRxiv a license to display the preprint in perpetuity. It is made available under aCC-BY-NC-ND 4.0 International license.

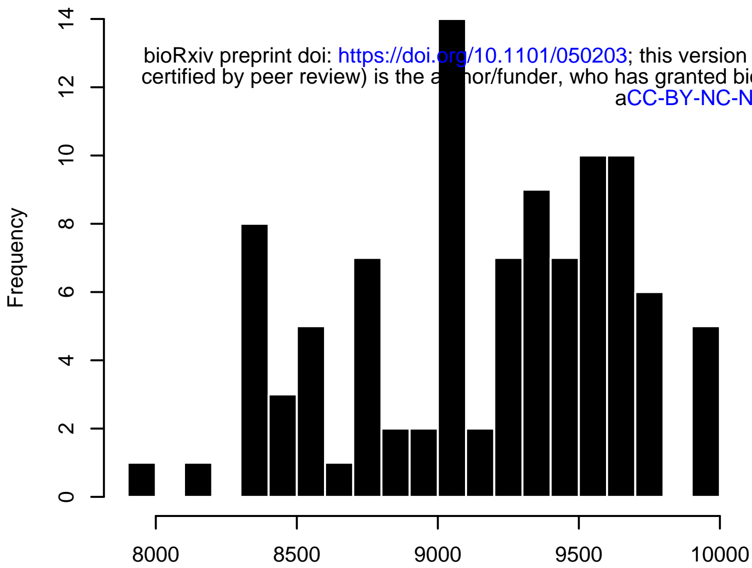

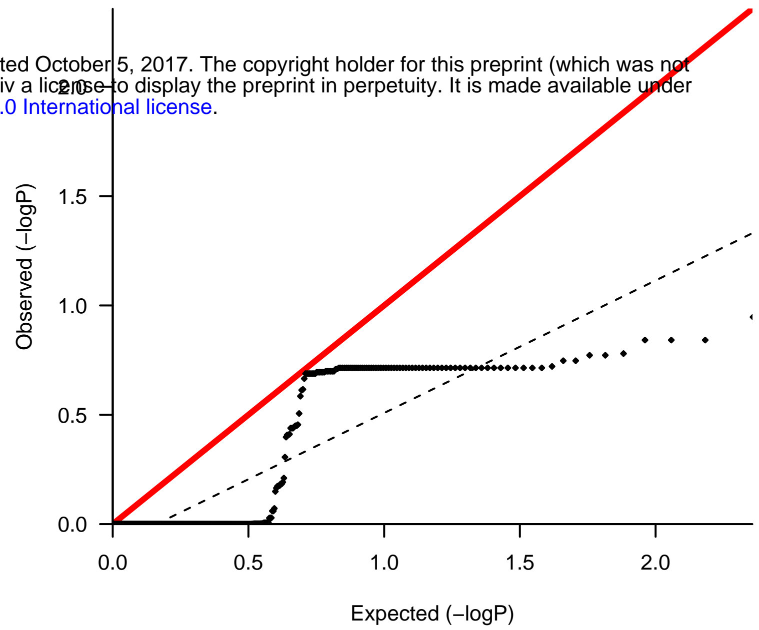

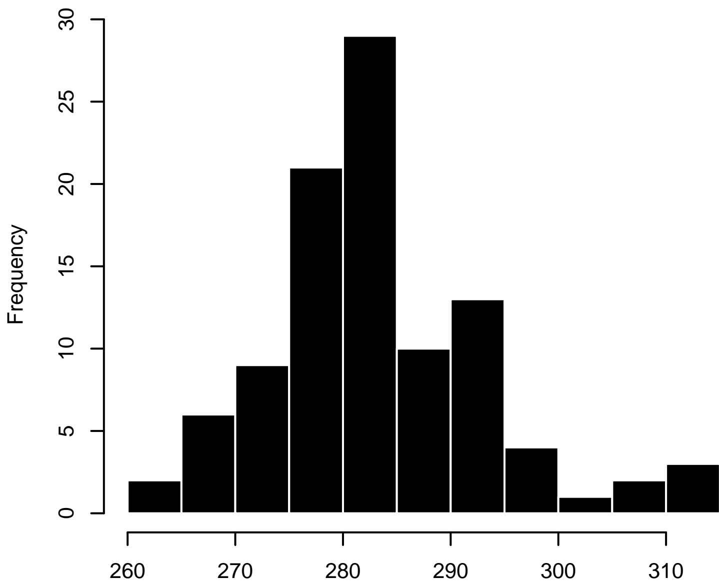

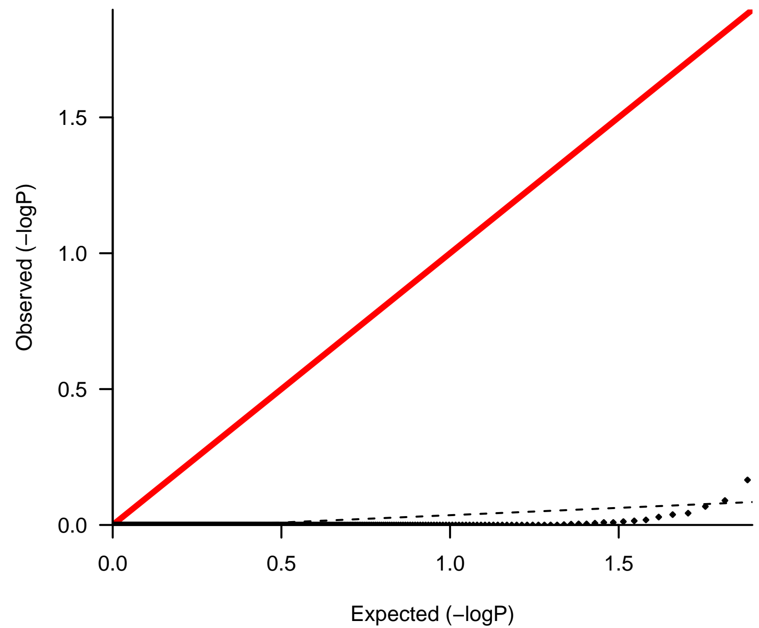

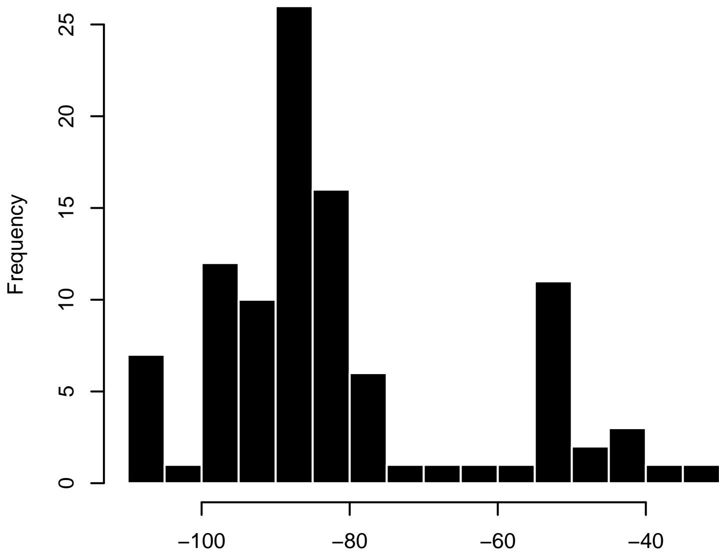

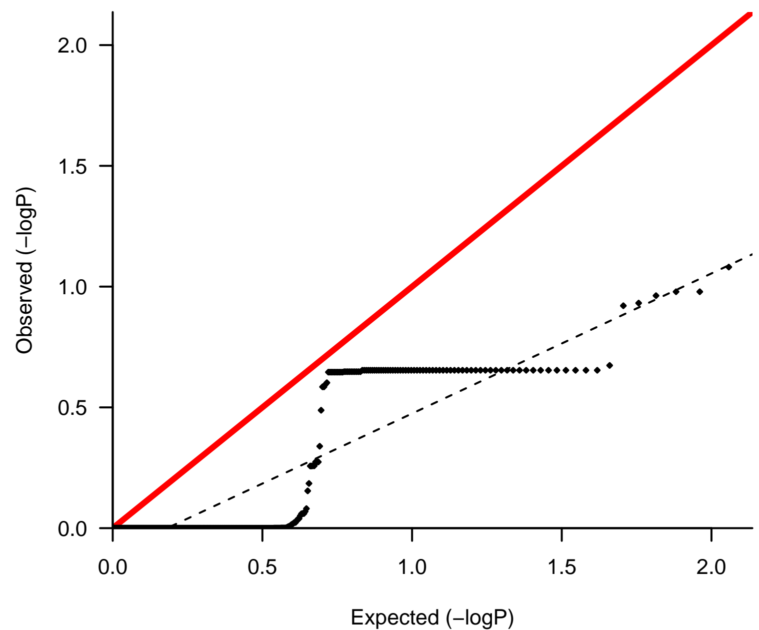

bioRxiv preprint doi: https://doi.org/10.1101/050203; this version posted October 5, 2017. The copyright holder for this preprint (which was not certified by peer review) is the author/funder, who has granted bioRxiv a license to display the preprint in perpetuity. It is made available under aCC-BY-NC-ND 4.0 International license.

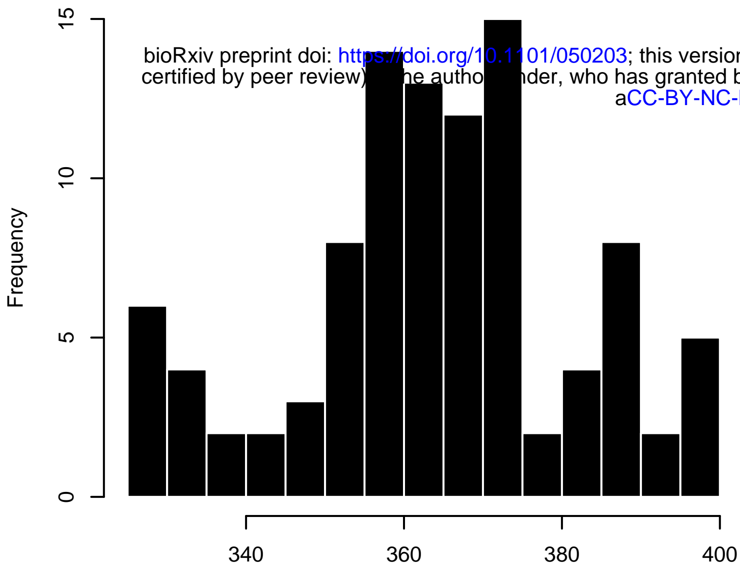

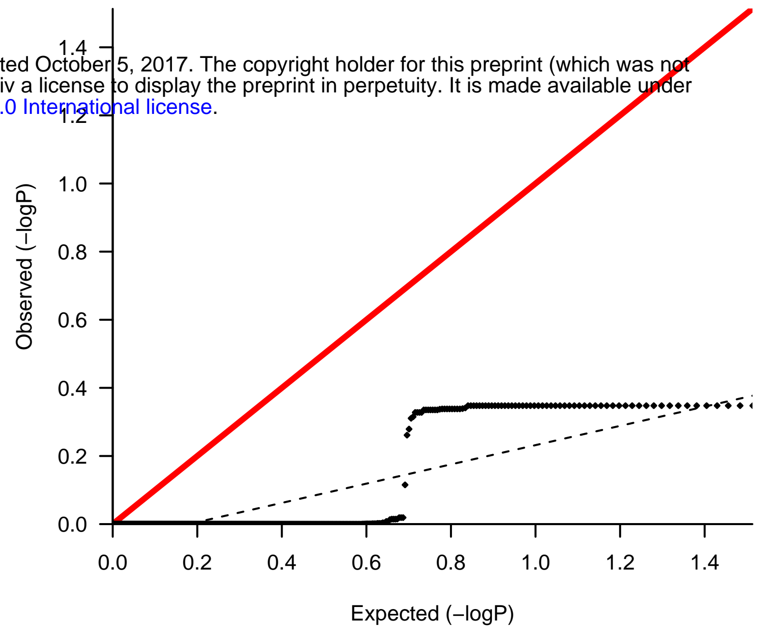

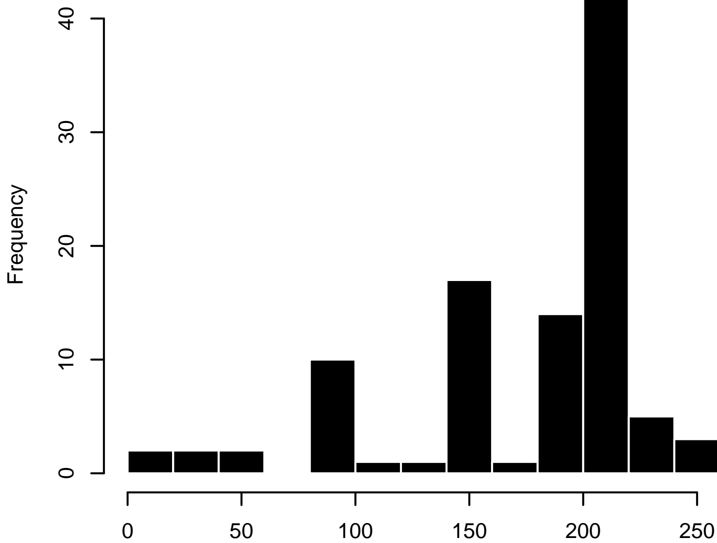

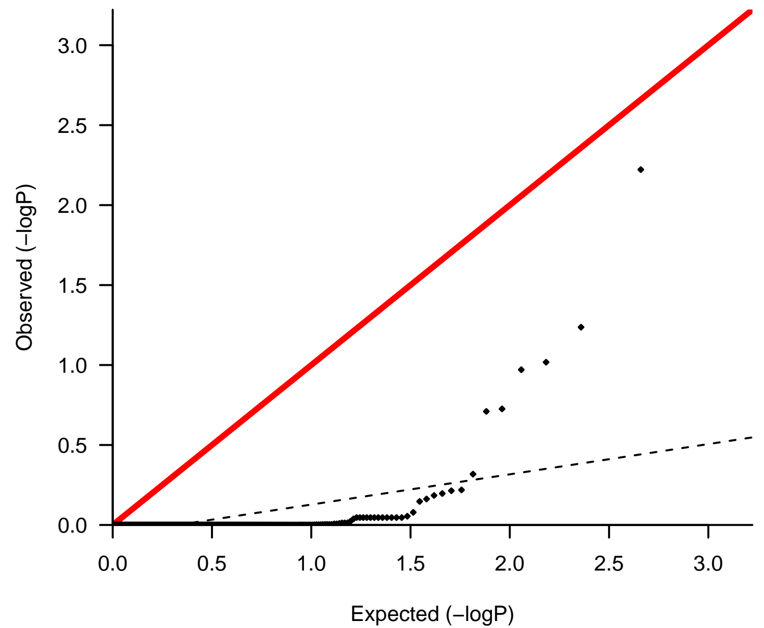

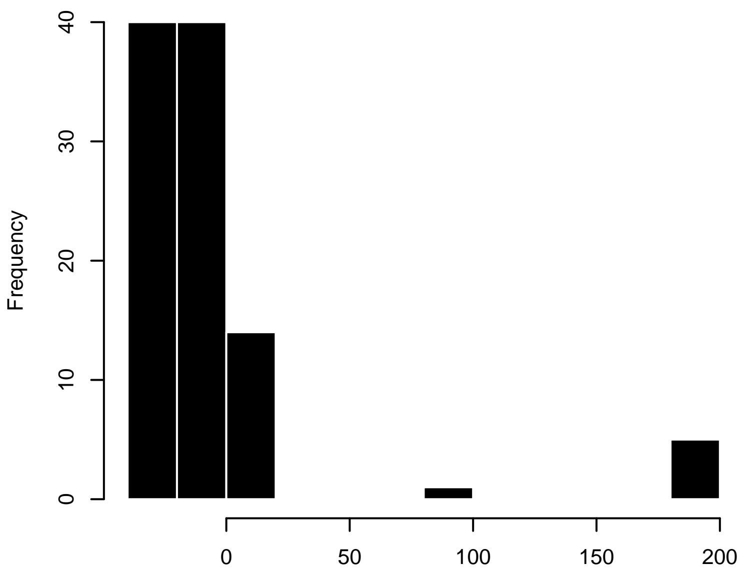

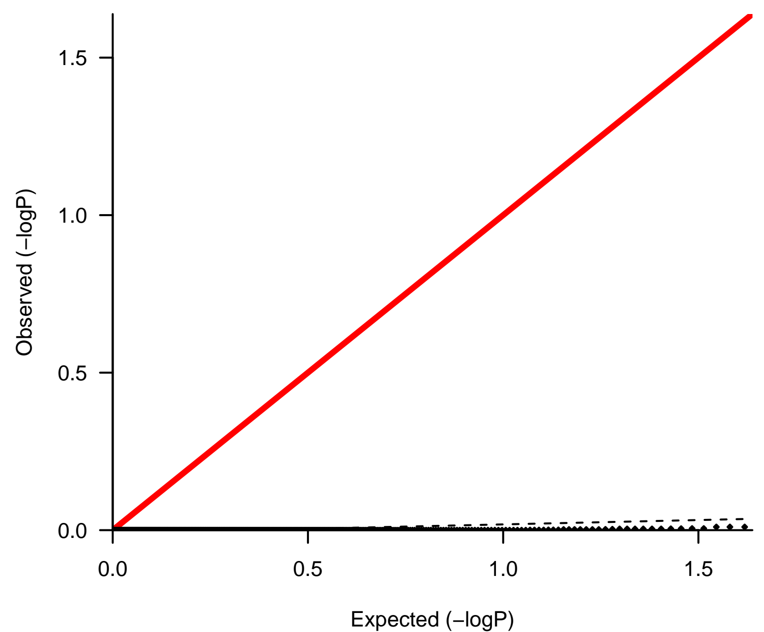

bioRxiv preprint doi: https://doi.org/10.1101/050203; this version posted October 5, 2017. The copyright holder for this preprint (which was not certified by peer review) is the author/funder, who has granted bioRxiv a license to display the preprint in perpetuity. It is made available under aCC-BY-NC-ND 4.0 International license.

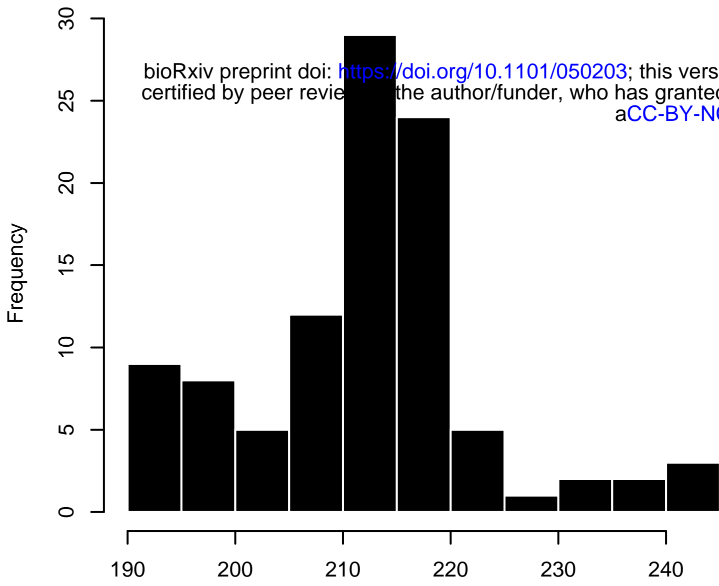

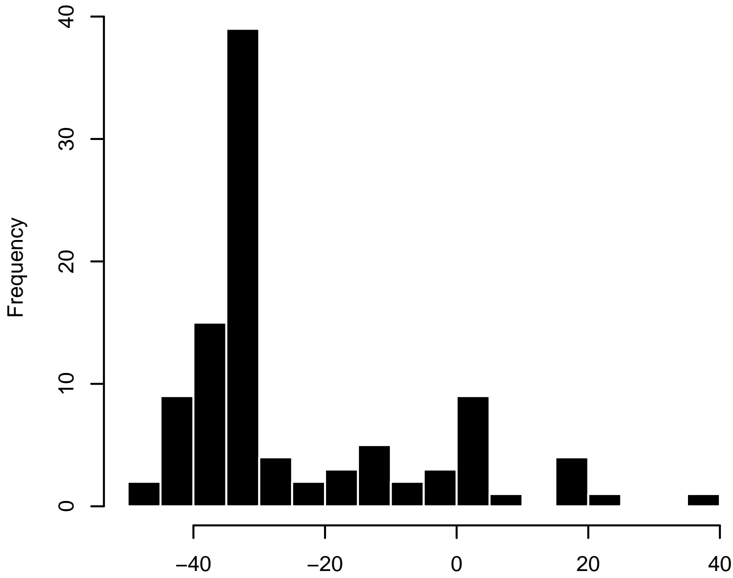

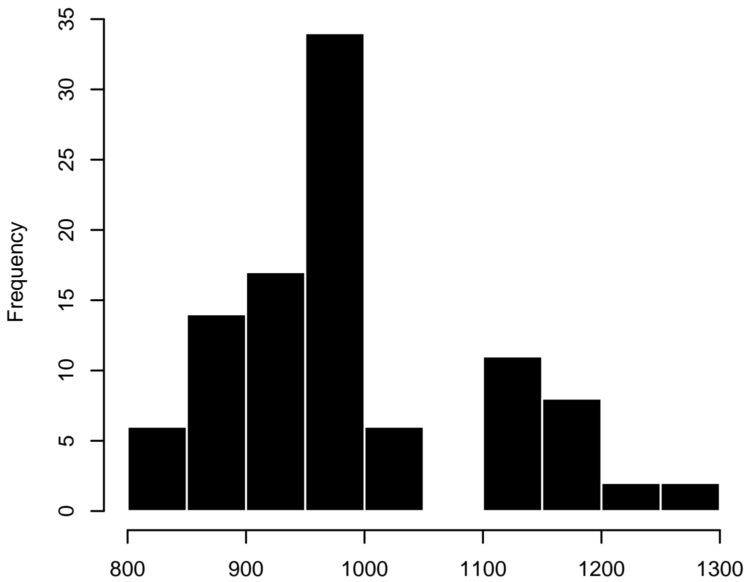

bioRxiv preprint doi: https://doi.org/10.1101/050203; this version posted October 5, 2017. The copyright holder for this preprint (which was not certified by peer review) is the author/funder, who has granted bioRxiv a license to display the preprint in perpetuity. It is made available under aCC-BY-NC-ND 4.0 International license.

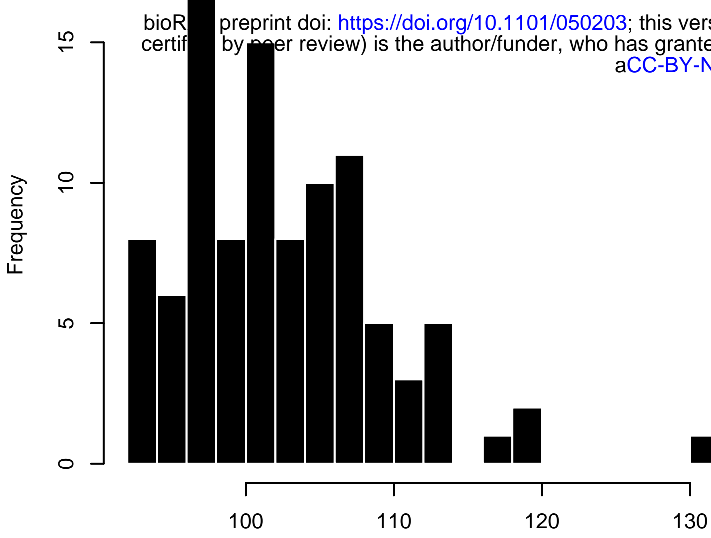

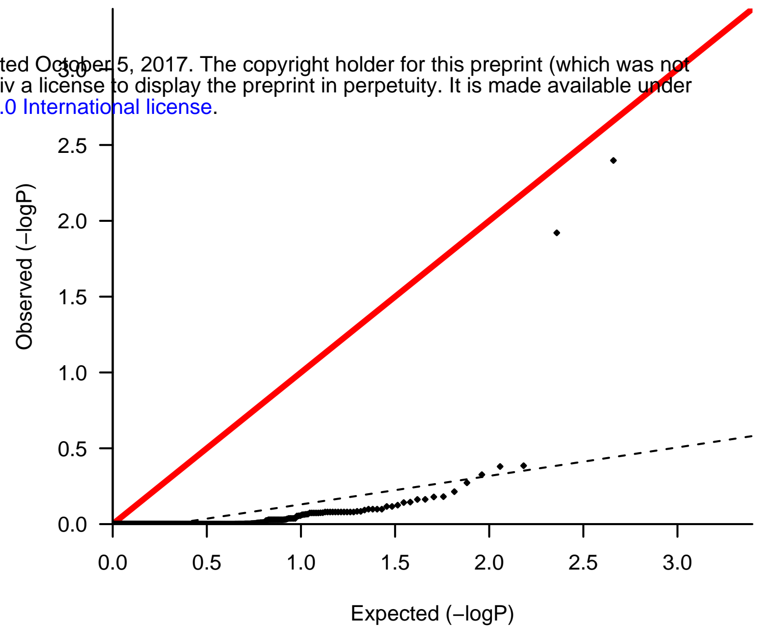

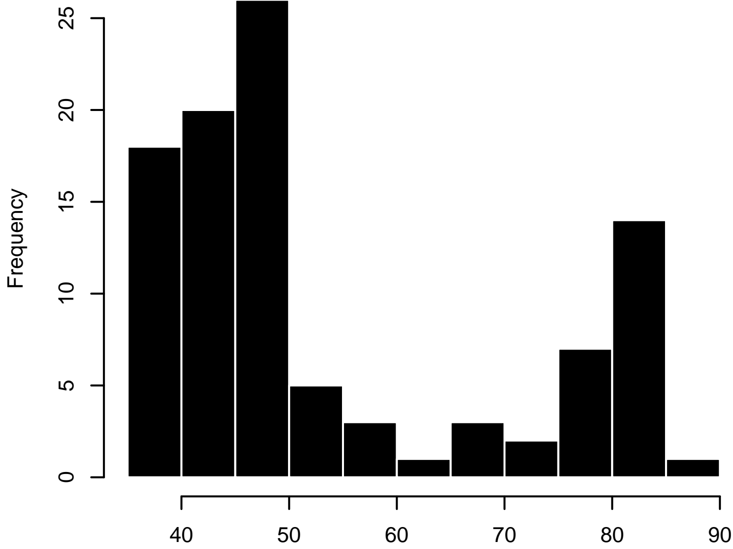

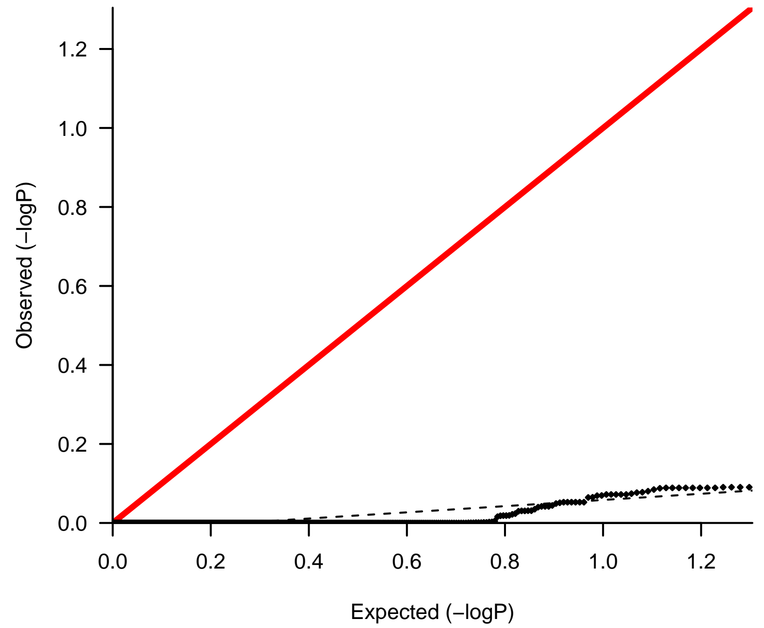

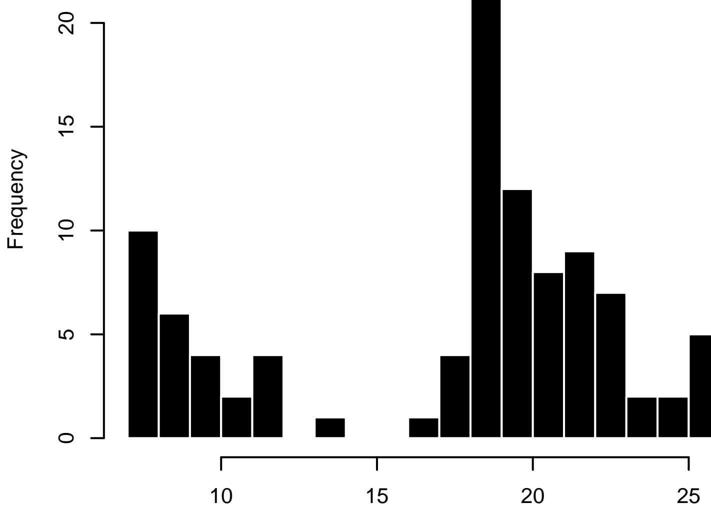

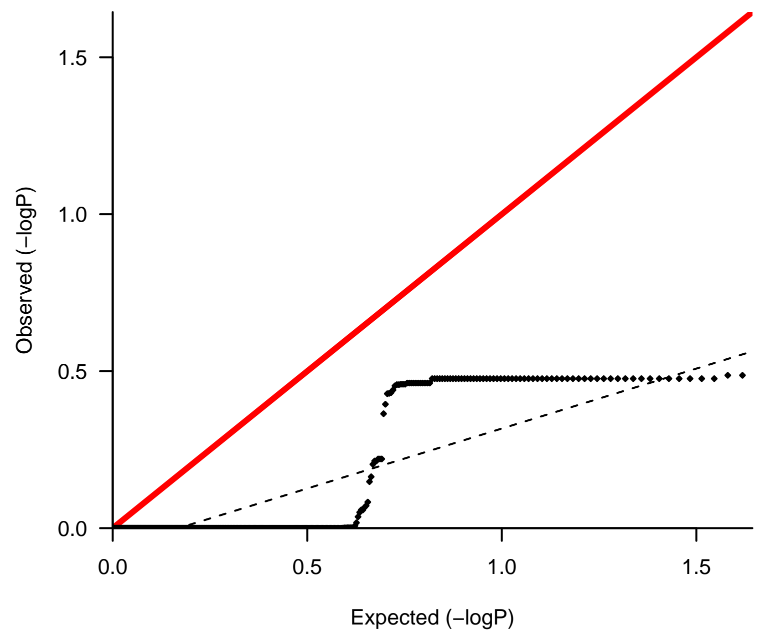

bioRxiv preprint doi: https://doi.org/10.1101/050203; this version posted October 5, 2017. The copyright holder for this preprint (which was not certified by peer review) is the author/funder, who has granted bioRxiv a license to display the preprint in perpetuity. It is made available under aCC-BY-NC-ND 4.0 International license.

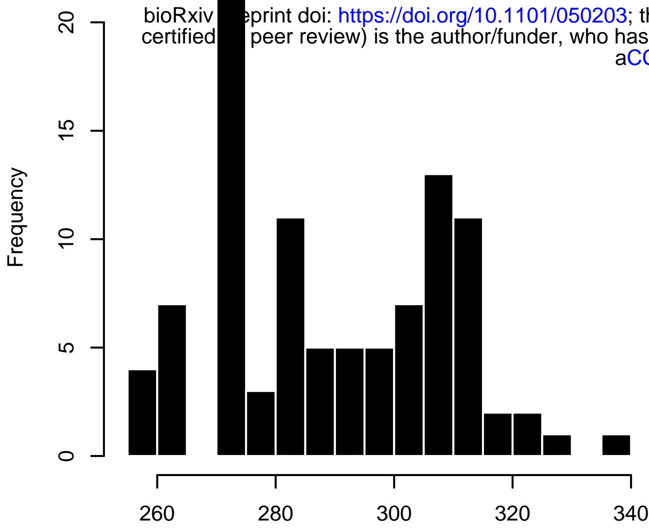

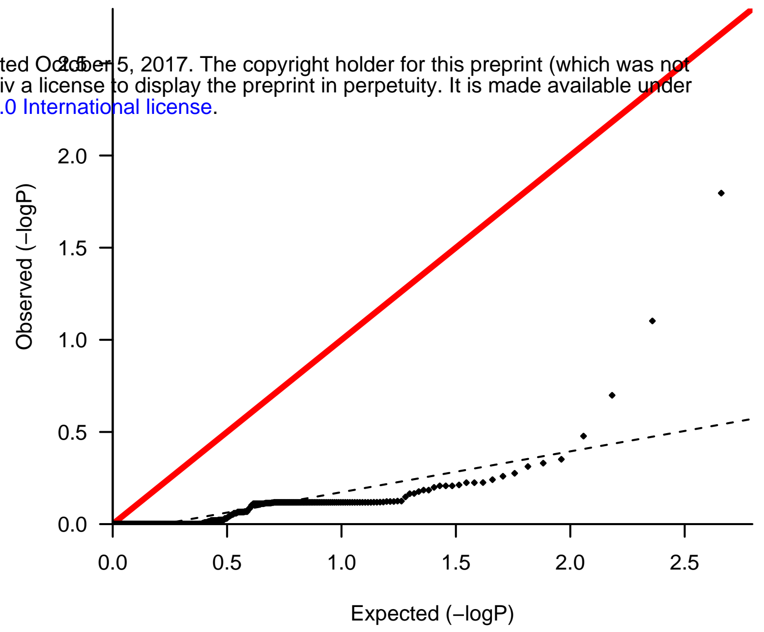

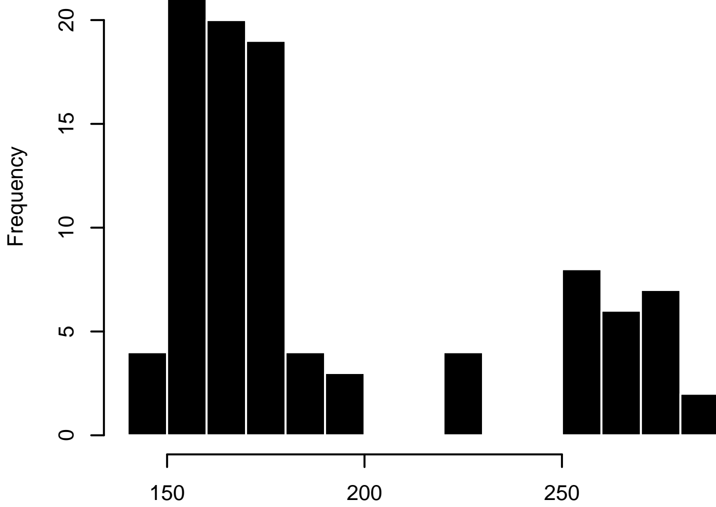

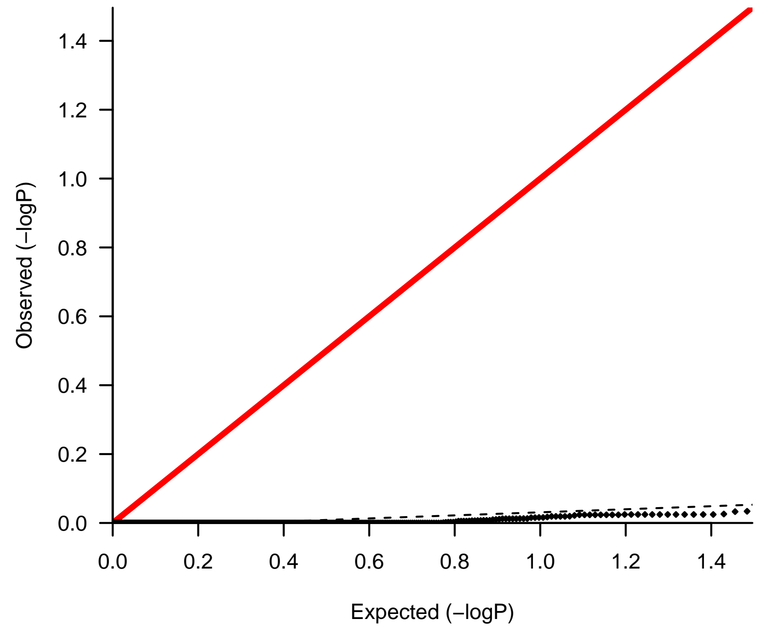

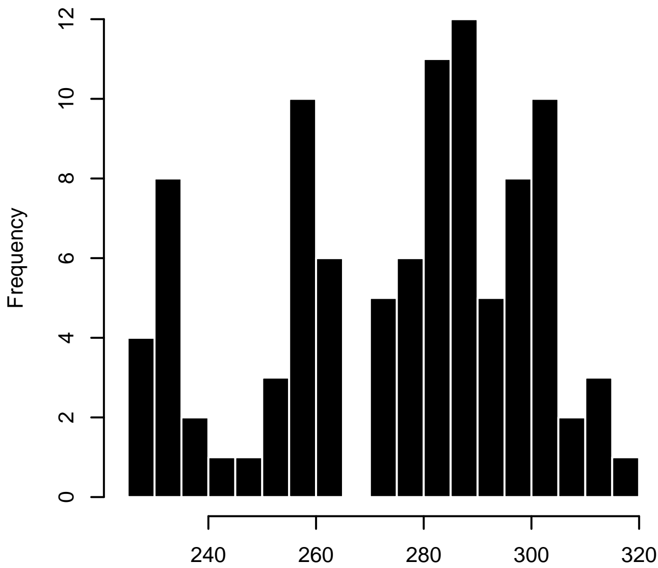

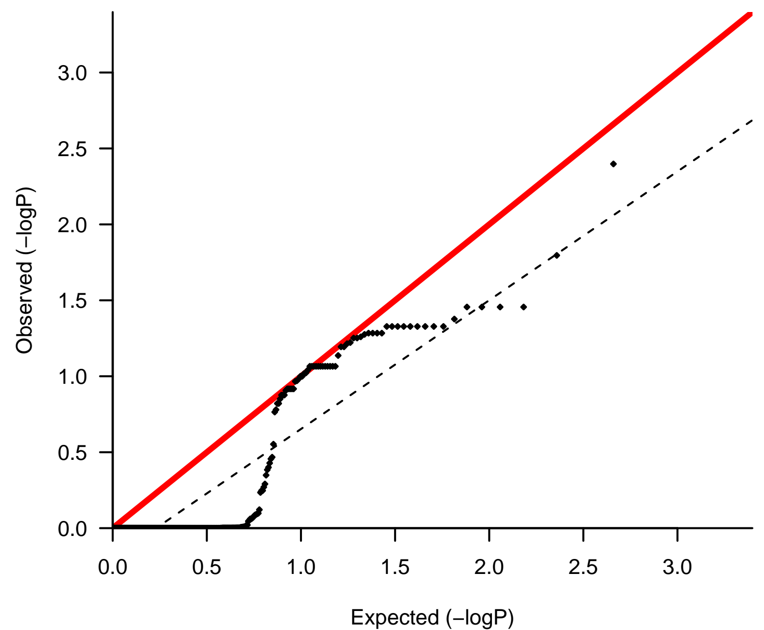

bioRxiv preprint doi: https://doi.org/10.1101/050203; this version posted October 5, 2017. The copyright holder for this preprint (which was not certified by peer review) is the author/funder, who has granted bioRxiv a license to display the preprint in perpetuity. It is made available under aCC-BY-NC-ND 4.0 International license.